Design of Macromolecular Anti-cancer Drug Delivery Systems using Molecular Dynamics Simulation

by

Negin Razavilar

A thesis submitted in partial fulfillment of the requirements for the degree of

Doctor of Philosophy

in

Chemical Engineering

Department of Chemical and Materials Engineering
University of Alberta

© Negin Razavilar, 2015

Abstract

In recent years, the application of self-associating block copolymer based drug delivery systems has attracted increasing attention as nano-sized carriers for the encapsulation and the controlled delivery of water insoluble drugs. Most of the drug formulations are based on the "trial and error" method with no specific library of polymer and drug combination. This is simply because in the context of drug formulation and drug delivery from polymeric micelles, many factors are necessary to study such as drug-polymer intermolecular interactions, release kinetics, polymer compatibility with human cells, etc. Computer simulation that can help design such polymeric drug delivery systems will enable researchers to make educated decisions on choosing a particular polymeric carrier for a given drug, avoiding time consuming and expensive trial and error based formulation experiments.

In the present thesis, we reported the use of molecular dynamics (MD) simulation to calculate the self-diffusion coefficients of a hydrophobic drug molecule in a series of micelle-forming PEO-*b*-PCL block copolymers with different structures and PCL block lengths in the presence of water molecules. MD analysis techniques like velocity auto-correlation functions, and squared displacement values along x, y and z axis provided useful atomistic details to understand the molecular origin of the diffusivity observed for drug molecules. Based on the evidence of reported work, intermolecular specific interactions between drug and different blocks of block copolymers all play important roles in the self-diffusion of drug

molecule (CuB) in block copolymers. Additionally, water concentration, polymer swelling and wriggling motion of polymer chains affect the diffusivity of water molecules. The computed radius of gyration (Rg) of the PCL block confirmed that the PCL block tends to exhibit a higher degree of swelling than the PEO block. The understanding of relative contributions of the inter molecular interactions between drug and polymer can help us to customize the performance of drug carriers by engineering the structure of block copolymers to achieve a desired drug self-diffusion.

Preface

Most of the research conducted for this thesis including the introduction is already published in scholarly research journals, led by Professor Phillip Choi at the University of Alberta, with Professors Anthony Young and Fakhreddin Jamali being the lead collaborators at the University of Alberta. I designed, with the assistance of Dr. Phillip Choi, the technical simulation methods discussed in all chapters. The data analysis in all chapters is my original work, as well as the literature review in introduction.

Dedication

To my parents who have sacrificed so much for me

To my beloved sister who is truly an angel and has been my motivation at difficult times

To my young aunt who recently passed away from cancer

To my other young aunt who passed away

And finally

To my lovely grandparents

Acknowledgements

I would like to take this opportunity and thank my academic supervisors Dr. Phillip Choi and Dr. Fakhreddin Jamali. I greatly appreciate Dr. Choi's technical feedback about my work which has always helped me to become a better researcher. During my PhD studies, I learned a lot about troubleshooting as well as technical material in the field of polymer and molecular dynamics simulations which I am sure will help me a lot in my future career. I would like to thank Dr. Jamali for his support throughout my research and helping me better understand pharmacokinetics and the technical subjects related to the field of Pharmacy. I would also like to thank him for letting me participate in the weekly journal club sessions held at the Faculty of Pharmacy and Pharmaceutical Sciences which helped me expand my field of knowledge beyond chemical engineering subjects. I would like to also acknowledge Dr. Anthony Young for providing support and insightful criticism to review my work. I am thankful to Dr. Yadollah Maham for giving me the opportunity to become his teaching assistant and learn more about chemical Engineering thermodynamics at the University of Alberta. I am also thankful to other faculty members, who served as committee members either on my candidacy and defense exams.

I would also like to thank Dr. Diwen Zhou, a former postdoctoral fellow in our research group who helped me better understand molecular dynamics and Gromacs software.

I am also thankful to my former supervisor, Dr. Mohammadreza Mehrnia who helped me finish our book: “Application of Chemical Engineering in Pharmaceutics” despite his very busy schedule at Tehran University. Also, I would like to thank my aunt, Malihe Razavilar, and my dear friends in Canada: Negar Malek, Leslie & Paul Precht, Maryam & Leila Zargarzadeh, Leily Mohammadi and Vida Moayedi for their ongoing support and kindness. The fun time that I spent with my dearest friends during weekends and holidays was most valuable.

My special thanks go to my beloved sister, Negar Razavilar for her constant encouragement, kindness and care. Although she is busy with her PhD studies and research activities, she has always dedicated her time to me and helped me manage stressful situations throughout my studies. Her beautiful and precious nature makes me believe that great human beings in our world still do exist and motivates me to become a better person. I am thankful for all the support provided by my parents throughout my life in Canada. They have always guided me and taught me to become a stronger individual.

The financial assistance (funding, and scholarships) provided by my supervisor, Natural Sciences and Engineering Research Council of Canada (NSERC), Faculty of Graduate Studies and Research (FGSR), Graduate Students Association (GSA) and Chemical & Materials Engineering (CME) department, and my parents is gratefully acknowledged.

Table of Contents

List of Tables

List of Figures

Nomenclature

Critical Micelle Concentration	CMC
Cucurbitacin B	CuB
Femtosecond	fs
Food and Drug Administration	FDA
Hydrogen Bond	H-bond
Lennard Jones	LJ
Molecular Dynamics	MD
Nanometers	nm
Picosecond	ps
Poly (ethylene oxide)-b-Poly (ε caprolactone)	PEO-b-PCL
Velocity Auto Correlation Function	VACF
Nano Second	ns
Radius of Gyration	R_g

Van der Waals	VdW
Mean Square Displacement	MSD

1. Cucurbitacins and cancer treatment

1.1. Introduction

A large number of Cucurbitacins have been isolated from different plant species belonging to plant families other than Cucurbitaceae during the last decades. Although the roots and the fruits of plant species belonging to Cucurbitaceae are very bitter, they have been used as folk medicines in some countries because of their pharmacological activities such as anti-inflammation and anticancer effects. Cucurbitacins wide range of pharmacological activities first attracted attention in the 1960s [1]. Natural and semi-synthetic Cucurbitacins show promising anticancer activities through several mechanisms [2-4]. Cancer is responsible for 12% of the world's mortality. Several treatments have been used to fight cancer including surgery, and radio- and/or chemo-therapy. Side-effects, toxicity and drug resistance have been the main concern when chemotherapy is an option [1-5]. Therefore, there has been a growing interest in the use of herbs as a promising source of more efficient therapeutic anticancer drugs. The most significant mechanisms with regard to the

anti-cancer behavior of Cucurbitacins are their ability to modify mitochondrial trans-membrane potential and transcriptional activities via nuclear factors or genes.

Although Cucurbitacins sound promising for cancer treatment, they are naturally hydrophobic. In other words, once they are administered into a cancer's patient body, they are eliminated due to their low solubility in blood stream [6]. Therefore, in order to obtain longer resident times for Cucurbitacins, effective drug carriers are needed to carry hydrophobic drugs and increase their solubility and residence time in the blood stream. Some polymer micelles have shown promising effects on the poor water solubility of Cucurbitacin drugs after administration [7,8].

1.2. Block copolymer micelles

Polymer micelles improve the water solubility of Cucurbitacin drugs due to their amphiphilic structure. Amphiphilic block copolymers consist of hydrophilic and hydrophobic blocks that can spontaneously self-associate in aqueous solutions above a threshold concentration, the critical micelle concentration (CMC), and form micelles. These nano-sized micelles have a unique core-shell structure that the core is made of hydrophobic blocks surrounded by hydrophilic blocks. In general, the hydrophobic block interacts with hydrophobic drugs and the hydrophilic shell provides stealth properties. Polymeric drug carriers at this scale (<200 nm) cannot be detected by the immune system and escape from renal excretion (elimination by kidney) due to their size which is always larger than 10 nm. Polyethylene oxide-b-

polycaprolactone (PEO-b-PCL) is the most common amphiphilic polymer used as a drug carrier. The reason is that the PEO block has stealth property which minimizes interactions between drug and cell membrane and polycaprolactone block is biodegradable, biocompatible and hydrophobic which can interact with hydrophobic drugs and act as a reservoir for hydrophobic drugs as well.

Polymeric micelles are considered to be one of the most promising drug delivery systems in the field of cancer treatment for several reasons: the hydrophobic micelle core is considered as an excellent host to incorporate and stabilize anticancer drugs, which are mostly hydrophobic. Nano-sized micelles and their stealth properties induced by the hydrophilic shell of polymeric micelles could result in efficient accumulation of the nano-sized drug carrier at the tumor site due to the enhanced permeation and retention (EPR) effect [9]. Penetration of micelle drug carriers into the tumor tissue is also facilitated by their small size. In addition, the flexibility of the core/ shell structure in polymeric micelles and the attachment of targeting ligands [10,11,12] enables us to fine tune these nano-scale drug carriers for optimal properties.

In recent studies a lot of emphasis has been made on micelles consisting of poly ethylene oxide-b-polyesters, polyD,L-lactide and polycaprolactone, polyethylene oxide-b-polypropylene oxide and polyethylene oxide-b-polyamino acid block copolymers. Higher number of functional groups in the hydrophobic block enable stronger drug-polymer interactions. The hydrogen bonds formed between hydrophobic anticancer drugs and the functional groups in the micelle-forming block

copolymer provide the basis for drug solubilization and stabilization in polymer micelles.

Polymeric micelles based on PEO-b-polypropylene oxide, PEO-b-polyesters and PEO-b-polyamino acids have been shown to successfully increase the water solubility of a number of clinically important hydrophobic drug molecules such as DOX, PTX and amphotericin B. Perhaps one of the most successful examples for the application of polymeric micellar formulations to increase drug-water solubility is the formulation of PTX in PEO-*b*-PDLLA micelles, a technique invented by Xichen Zhang and later developed by Burt et al., which have increased PTX solubility in aqueous solutions up to 5000-fold [13,14,15,16].

Another example is the increase in water solubility of DOX up to 12,000-fold with the application of PEO-*b*-PDLLA micelles [17]. Compatibility between the hydrophobic core of micelles and the entrapped hydrophobic drug molecule is very important and helps us determine the final drug loading capacity of a polymeric micellar system for a given anticancer drug. For example, DOX was chemically linked to the hydrophobic block of PEO-*b*-polyAsp in order to entrap more DOX molecules inside the hydrophobic core of PEO-*b*-polyAsp- DOX micelles [18]. Other examples on the importance of compatibility between hydrophobic block and anticancer drug molecules are provided and shown by Kwon et al. on the encapsulation of amphotericin B in polymeric micelles consisting PEO-*b*-polyAsp derivatives, in which the modifications of the hydrophobic core chemical structure

resulted in an increase in the level of encapsulated drug and drug loading capacities [19].

Modifications of the chemical structure of the micelle-forming block copolymer and the physicochemical properties of the core/shell forming blocks are possible in order to obtain instant, sustained, or delayed drug release processes for specific drug delivery requirements. If one considers to avoid water penetration into the polymeric micelles, the hydrophobicity and crystallinity of the hydrophobic core could be enhanced which eventually would lead to a delayed mode of drug release from the carrier [20,21,22]. As an example, polymeric micelles that have glassy or crystalline cores under body temperature (37°C), micelle core structures that are cross-linked polymers or as mentioned before strong hydrogen bonds between drug and hydrophobic block in the micelle core can all be used to retard the micelle dissociation, drug diffusion and the overall rate of drug release from the micellar carrier [23,24,25-27].

According to other anti-cancer studies that were conducted on tumor bearing mice, PEO-b-P(Asp)-DOX with different molecular weights of PEO chains (12,000 and 5000 g.mol-1), and free DOX, were used for 24 h after intravenous injection [28]. Higher levels of conjugated DOX were, however, required for an equal antitumor activity in comparison to free DOX drug molecules used for cancer treatment. Administration of higher concentrations of anticancer drug was allowed due to the lower toxicity of micelle-forming polymer–DOX conjugates in comparison to free drug (almost 20-times increase in maximum tolerable dose), which resulted in a

much higher therapeutic index for PEO-b-P(Asp)-DOX in [29] tumor-bearing animal models [30].

One of the most effective ways to lower the rate of drug release from polymer micelles is to increase the number of hydrogen bonds formed between hydrophobic drug and core forming block. Lee et al. studied the loading capacity of functionalized hydrophobic blocks of PEO-b- PDLLA (including carboxyl groups) micelles and the effect of functionalized hydrophobic block on the release of papaverine [31]. A significant increase in drug loading and decrease in drug release rate was shown with an increase in the level of free carboxylic groups on the polymeric backbone, which was due to the increasing interactions between the loaded drug and the core-forming block.

Polymeric micellar carriers have been considered ideal carriers for drug delivery so far due to their unique properties and special architecture. Hydrophilic brush-like polymer structures on the micellar surface along with the small size of micelles (10 – 100 nm) result in better protection for polymeric micellar drug delivery systems against recognition and uptake by RES, which will result in longer blood circulation times and higher accumulation of the carrier in selective tissues such as tumour or inflammation sites. Polymeric micelles offer a higher drug loading capacity and a more stable entrapment of hydrophobic drugs in comparison to colloidal delivery systems that mostly have not been able to retain their drug content in blood stream. Moreover, the stability of the micelles could be enhanced by modifying the core-shell chemical structure. For example, ester groups present in the structure of

polymer backbone could result in surface erosion, a type of degradation that occurs at the surface of micelle where excess amount of water is present, which in turn will affect micelle stability and residence time in the blood stream. Different approaches are taken in literature to address the issue of micelle instability and premature drug release such as: Chemical modification of the polymer structure in the micellar core (e.g., attachment of hydrophobic structures [32], addition of drug compatible moieties [19,33,34], chemical core crosslinking [35,36] and partial crystallisation of the micellar core [37].

Other hydrophobic drugs have attracted a lot of attention these days in the field of selective drug delivery from polymeric micelles and it is only a matter of time before other polymeric micellar formulations enter the stage of clinical evaluations. However, the therapeutic knowledge necessary for the delivery of different hydrophobic anticancer drugs has not been fully explored and limited information on the therapeutic efficacy of polymeric micellar formulations for therapeutic agents is available [38-40].

Research for the development of targeted drug delivery has led studies to the second generation of polymeric micellar carriers. Examples of these micelles are: nano-carriers decorated with different ligands, such as glyco-polymers and peptides or micelles covered with bio adhesive polymers on their surface. All the mentioned micelles are developed to enhance the targeting efficiency of the micelle carrier [41,42,11,12,43-50]. Modification of the surface of polymeric micelles has shown

progress in enhancing the recognition of drug carriers by selective tumor cells leading to improved drug delivery [43,44,46].

pH-responsive polymeric micelles are designed that can respond to changes in pH and release their drug content in specific organs or intracellular environments. For example, the acidic condition in the environment surrounding the tumor cells could trigger micelle degradation and cause drug release in the acidic environment [51-53].

1.3. Design of polymeric drug delivery systems

1.3.1. Polymer-drug compatibility

The degree of drug- polymer compatibility in polymeric drug delivery micelles can affect many things such as: stability of the micelle, drug encapsulation efficiency and drug release kinetics [54,55]. The term "compatibility" is related to material having comparable structure or intermolecular forces. Usually the term "like dissolves like" in chemistry signifies this concept. In order to design effective drug formulations, one must have the knowledge of polymer-drug compatibility. The degree of the drug-polymer compatibility can be quantified using the Flory-Huggins interaction parameter (χ). The smaller the χ value, more compatible the drug is with the block copolymer made up of the micelle and hence higher the predicted amount of drug solubilisation. This interaction parameter has been used to describe the different levels of solubilisation of several hydrophobic drugs in polymeric drug delivery

systems [55-60]. The Flory-Huggins interaction parameter (χ) is calculated based on the enthalpy of mixing for all components in the system according to the following equation:

$$\Delta \mathbf{H_m} = \boldsymbol{\chi}\, \mathbf{RT}\boldsymbol{\varphi_1}\boldsymbol{\varphi_2} \tag{1-1}$$

where $\Delta H_m$is the enthalpy change for mixing, χ is the Flory-Huggins interaction parameter, R is the universal gas constant and φ_i is the fractional volume of component i. Here, the enthalpy change of mixing can be calculated computationally using molecular dynamics simulation as demonstrated by Patel et al. [61]. The effect of block-copolymer structure and PCL (polycaprolactone) block length on the Flory-Huggins interaction parameter (χ) was studied. Longer PCL block contributed to more negative interaction parameters which corresponded to higher drug-polymer compatibility. The roles of polar and non-polar interactions between hydrophobic drugs such as Cucurbitacine B and polyethylene oxide-b-polycaprolactone were studied as well.

1.4. Thesis scope

In the concept of drug release from block copolymer micelles drug diffusion from micelles plays an important role. In micron-sized systems, the relationship between diffusion and release kinetics is known and has been extensively studied by many

authors mentioned in Chapter 2. However, the mentioned relation in nano-sized polymeric micelles is unknown and yet needs to be developed.

In this thesis, we calculated the diffusion coefficient of drug molecules (Cucurbitacine B) in nano-sized systems using molecular dynamics simulation. The first objective is to review drug release models in micro-sized drug delivery systems and to discuss the shortcomings of these models to predict drug diffusion coefficients in nano-sized drug delivery systems (micelles). The second objective is to compute the diffusion coefficient of Cucurbitacine B in pseudo-micelle environments using molecular dynamics simulation. The effect of block copolymer structure and water concentration on drug diffusion coefficient is discussed as well as intermolecular interactions between drug and polymer. The third objective is to study the role of intermolecular interactions between drug and hydrophobic blocks of polymers as well as the effect of hydrophobic block length on drug diffusivity. Finally, the last objective is to discuss the drug diffusion mechanism in polymer with different structures and block lengths by calculating the drug's diffusion activation energy. In the final chapter, the major conclusion along with future outlook is provided.

2. In-vitro Modelling of the Release Kinetics of Micron and Nano-sized Polymer Drug Carriers[1]

2.1. Introduction

Polymers have been used as drug carrier systems for several decades. Some polymers used in practice are biodegradable [62-66] while others are not. Examples of degradable and non-degradable polymers are shown in Figure 2-1. Since non-degradable polymers cannot be easily eliminated from the patient's body upon the consumption of the drugs, biodegradable polymers are mostly used. However, polymers that exhibit long degradation time (longer than the time scale of the drug

[1] A version of this chapter has been published. Razavilar, N., Choi, P. In-vitro modelling of the release kinetics of micron and nano sized polymer drug carriers, Int. J. Drug Delivery, 2013, (5) 362-378.

release) are usually considered as “non-degradable” from the drug kinetics perspective as the molecular weights of such polymers do not change during the release process. Figure 2-1 and Figure 2-2 show a few “non-biodegradable” and biodegradable polymer structures that are commonly used as drug delivery systems. Figure 2-3 (a) and (b) show the drug carrier systems in which the drug is encapsulated by polymer in a spherical geometry. Different geometries (e.g., cylindrical) can be used but they exhibit different release kinetics even though the same polymer is used. The effect of the device geometry on drug release kinetics will be discussed later. Since such systems are usually micron-sized, continuum models are found suitable for describing the corresponding kinetics. Figure 2-3 c) shows a carrier system that is made up of polymeric micelles. In fact, this type of carrier system has become quite popular in recent years as such nanometer-size systems offer longer circulation times [67-70]. Such micelles are formed from individual amphiphilic polymer chains that spontaneously form nano-sized aggregates in selective solvents (water in the case of drug delivery systems) above a threshold concentration called the critical micelle concentration (CMC). This is due to the good solubility of one and poor solubility of the other block of the copolymer in the selected solvent [71]. These polymeric micelles are usually tens of nanometers in size. They are characterized by their unique core-shell structure, in which the core is composed of hydrophobic blocks that are surrounded by a palisade of hydrophilic blocks. Generally, the hydrophobic core acts as a micro reservoir for the solubilization of hydrophobic drugs while the hydrophilic shell provides stealth properties. However, their release

kinetics differs significantly from that of the micron-sized carriers and it is conceivable that continuum models may not be applicable.

Figure 2-1. Chemical structures of "non-biodegradable" polymers used for drug delivery. The first structure from the left is urethane links and the second structure is polydimethylsiloxane.

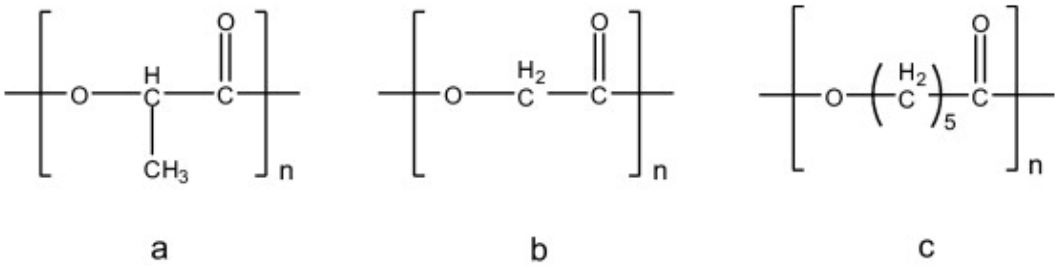

Figure 2-2. Chemical structures of biodegradable polyesters: (a) polylactide, (b) polyglycolide and (c) polycaprolactone.

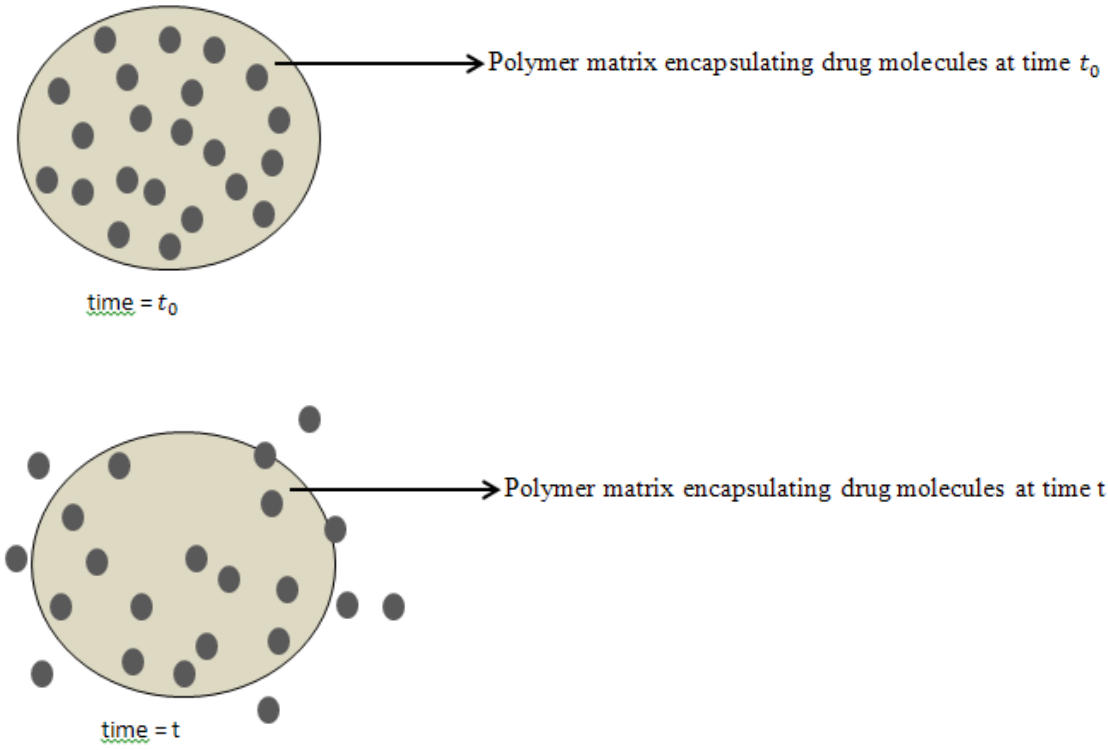
Polymer matrix encapsulating drug molecules at time t_0
time = t_0
Polymer matrix encapsulating drug molecules at time t
time = t

a)

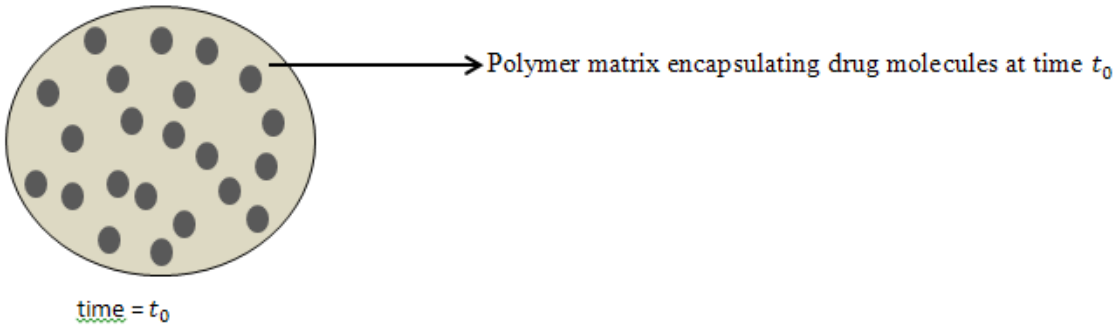
Polymer matrix encapsulating drug molecules at time t_0
time = t_0

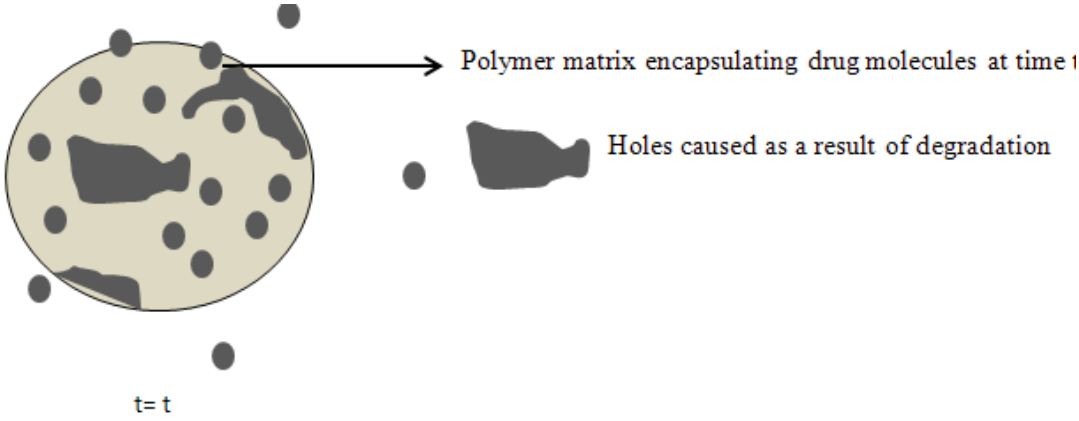
Polymer matrix encapsulating drug molecules at time t
Holes caused as a result of degradation
t= t

b)

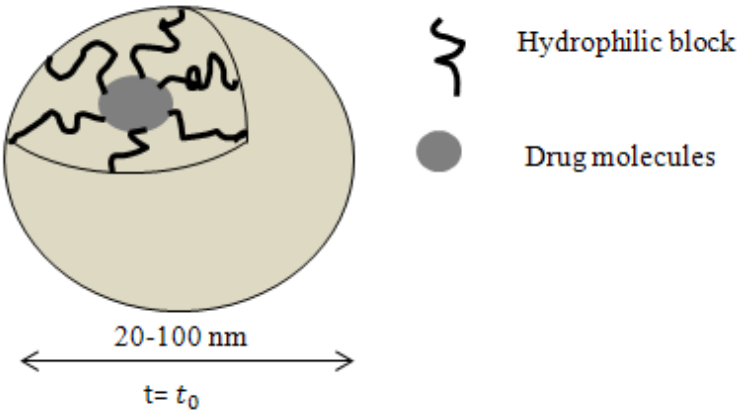
Hydrophilic block
Drug molecules
20-100 nm
t= t_0

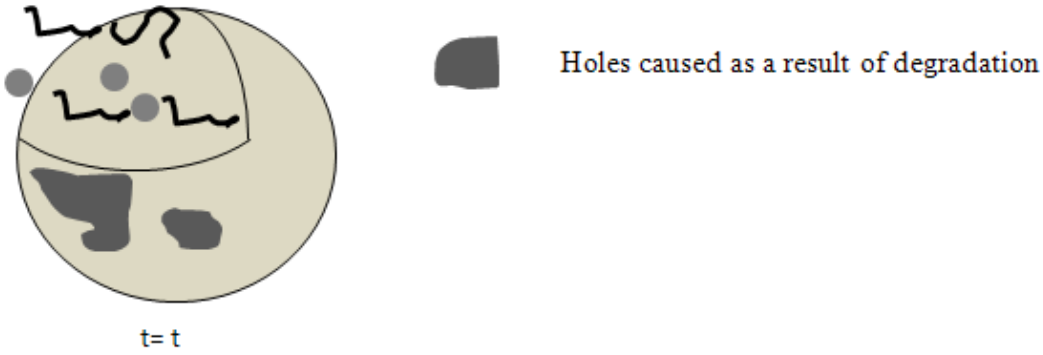

c)

Figure 2-3. Schematic representation of a) micron-sized non-biodegradable polymer, b) micron-sized biodegradable polymer and c) nano-sized polymeric micelle system.

Obviously, the chemical structure of the polymer used in the aforementioned carriers will play a significant role in determining the total amount of drug released over a given period of time (i.e., release profile) which will in turn affect the *in vivo* pharmacokinetics parameters (e.g., clearance, half-life, etc.). All of the aforementioned polymer carrier systems can be administered via oral or intravenously. Recently, a great deal of attention has focused on the development of controlled release drug delivery systems that are administrated intravenously. It is desirable to have the total concentration of drug last longer in the bloodstream so that multiple dosages for patients are not required. When comparing single dose to multiple dose administration of drugs, a single dose has been proven to be a more cost-effective alternative so far.

It is worth noting that the decrease in drug concentration in blood is attributed to two factors: distribution of the drug to targeted and non-targeted tissues and elimination of the drug by kidney or metabolism. The distribution of the drug to the tissues occurs at a much faster rate compared to its elimination process. Figure 2-4 shows a typical drug concentration vs. time curve from a pharmacokinetic experiment on micron-sized polymer drug carriers. During the distribution process, the concentration of the drug in bloodstream decreases considerably because a high percentage of the drug distributes to different tissues. Later, equilibrium in the drug concentration will then be established between the tissues and the blood stream.

The elimination process occurs to micron-sized carriers. However, if the polymer carrier systems have sizes in the range of 10 nm – 400 nm, the elimination rate can be significantly decreased [67-70]. Obviously, the most ideal situation is that the carriers are only distributed to the target tissues and there is no elimination. Regardless micron-sized or nano-sized carriers, it is obvious that drugs exhibiting required diffusivity in the polymer are most desirable. The intent of this review paper is to discuss different in-vitro mathematical models as well as their usages and limitations.

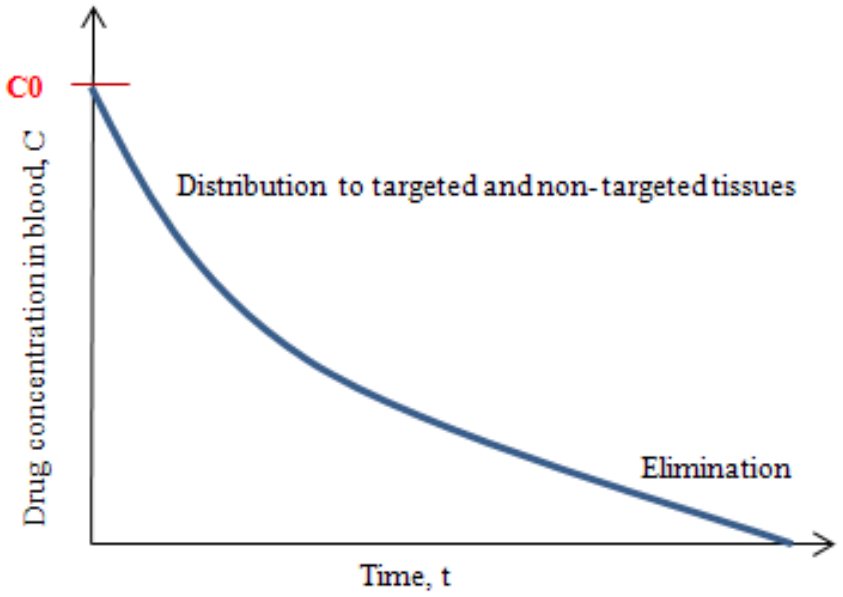

Figure 2-4. A typical drug concentration profile in blood after intravenous administration of drug. The drug concentration is at the highest level shortly after the intravenous injection at t~0 (C_0) and decreases during the distribution and elimination phases. The distribution phase includes distribution of drug to targeted and non-targeted tissues.

2.2. Continuum Models for Micron-Sized Carriers

Continuum models were first developed to describe the release kinetics of drug encapsulated in a micron-sized polymer film. Such models are essentially developed for in vitro environment by including various effects such as concentration gradient, swelling, and degradation of polymer. Later, researchers developed micron-sized continuum models to describe kinetics of drug encapsulated in devices with different geometries such as thin films, spheres and cylinders. Three types of micron-sized drug carriers will be discussed and they are non-biodegradable, swollen, and biodegradable polymers.

The advantages and disadvantages of micron-sized continuum models used to describe drug delivery kinetics will be discussed respectively for thin films, spheres and cylinder geometries for each drug delivery device in the following sections.

2.2.1. Non-Biodegradable Polymeric Carriers

As mentioned, mathematical models developed for this type of polymers are essentially used for biodegradable polymers exhibiting long times for complete degradation. In other words, the degree of degradation is negligible relative to the release time scale. With these types of polymers, water molecules tend to diffuse into these systems causing swelling which results in diffusion of drug molecules out through the swollen polymer matrix. Five decades ago, Professor Higuchi was the

first one to lay the foundation for quantitative analysis of drug release from polymer matrices. He proposed a simple thin film model based on a pseudo-steady state assumption for the release of drug from an ointment using simple mass balance concept and Fick's laws.

2.2.1.1. Higuchi Model for Non-Reservoir Polymeric Carriers

Higuchi treated the drug release problem as a steady state, one dimensional diffusion process. Based upon Fick's first law [72], the rate of diffusion of drug R_t (mole/s) for a non-biodegradable and non-swelling polymer matrices [73] is given by the following expression:

$$\mathbf{R_t} = -\mathbf{SD}\frac{\mathbf{dC}}{\mathbf{dx}} \tag{2-1}$$

S is the cross sectional area (m^2); D is the diffusion coefficient of the drug in the polymer matrix (m^2/s); C is the concentration of the drug and x is the distance from solvent-matrix interface (Figure 2-5).

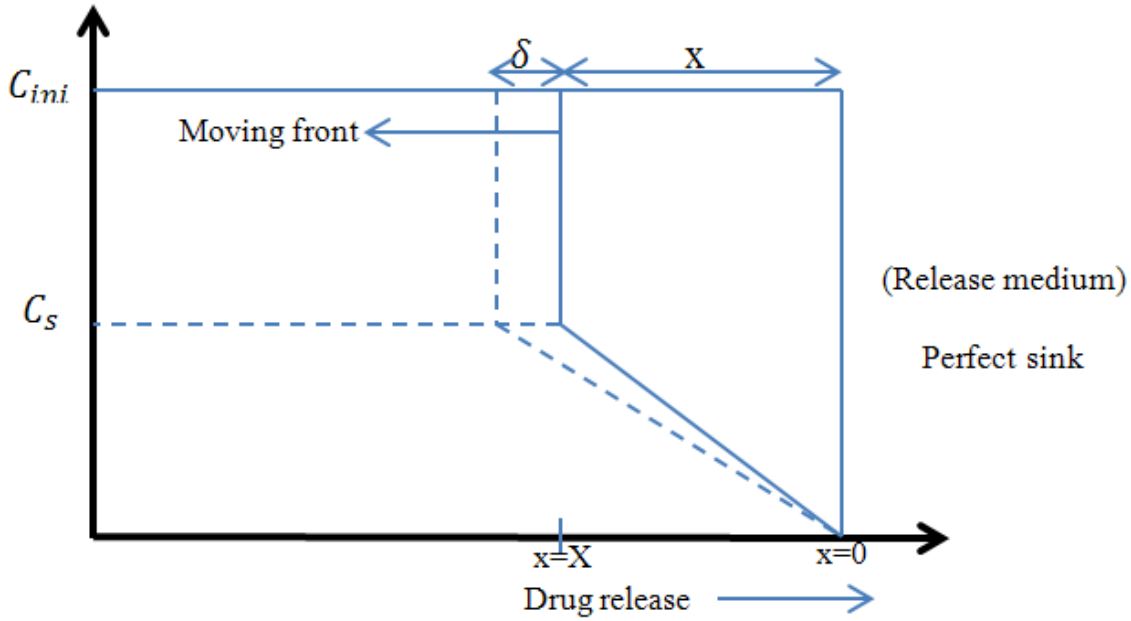

Figure 2-5. Schematic presentation of the drug concentration-distance-profile after exposure to perfect sink conditions. $C_{ini}(C_0)$ is the initial drug concentration in the polymer matrix which is much higher than C_s the solubility concentration of the drug in the matrix. X represents the distance from the matrix-medium interface, δ is the thickness of the thin film.

The boundary conditions are:

$C=\mathbf{C_b K}$ at x=0 (2-2)

$C=\mathbf{C_s}$ at x= X (2-3)

C_b is the drug concentration in the release media and C_s is the solubility concentration of the drug in the matrix. C is the drug concentration in the polymer matrix. Perfect sink condition is assumed which implies that the concentration of drug in the polymer matrix is much higher than the drug concentration at the matrix-medium interface (C_bK). K is the matrix-to-medium partition coefficient. The initial drug concentration inside the polymer matrix is much higher than its solubility

concentration (by a factor of 10 or more). According to this assumption is takes a very long time for the excess amount of the drug concentration to dissolve at a distance x from the films surface. Therefore, the drug concentration at a distance "x" from the film at any time remains almost constant which results in pseudo steady state condition. In order to solve Fick's law to obtain the diffusion coefficient we must know how the concentration profile of the drug looks like. One solution is to assume a linear concentration profile for the drug. Therefore we have:

$$\mathbf{R_t = SD\frac{(C_S - C_bK)}{X(t)}} \tag{2-4}$$

In order to solve the above equation we have:

$$\mathbf{R_t = \frac{dM_t}{dt} = \frac{d}{dt}\{\left[C_0 - \frac{1}{2(C_s + C_bK)}\right] SX(t)\}} \tag{2-5}$$

where C_0 (C_{ini}) is the total drug concentration and M_t is the total amount of drug released at any time t. After substituting R_t in the above equation and the followed by a series of integration, the final equation is written as:

$$\mathbf{M_t = S[D(C_s - C_bK)(2C_0 - C_s - C_bK)t]^{1/2}} \tag{2-6}$$

It is assumed that the initial drug concentration is higher than its solubility concentration in the polymer matrix. Also, under sink conditions it is assumed that the drug concentration in the release medium is almost zero which means that: $C_b \sim 0$. When $C_s \ll C_0$:

$$\mathbf{M_t = S[2DC_sC_0t]^{1/2}} \tag{2-7}$$

The above equation can also be further simplified to the following form:

$$\mathbf{M_t = k\sqrt{t}}, \qquad \mathbf{where\ k = S\sqrt{2DC_sC_0}} \tag{2-8}$$

It is obvious that total mass of drug released follows "square root of time" dependence.

In all the above equations K is the partition function of the drug between the membrane and the reservoir.

For the non-core-shell carriers with different geometries as shown in Figure 2-6, the mass of drug released shows much more complicated time dependence. Roseman and Higuchi proposed the following implicit equations. Here, the term implicit signifies that M_t cannot be isolated on the left hand side of the equation [74,75].

For spherical carriers:

$$\frac{\mathbf{M_t}}{\mathbf{M_\infty}} - \frac{\mathbf{3}}{\mathbf{2}}\left[\mathbf{1} - \left(\mathbf{1} - \frac{M_t}{M_\infty}\right)^{\mathbf{2/3}}\right] = -\frac{\mathbf{3D}}{\mathbf{R^2}}.\frac{\mathbf{C_s}}{\mathbf{C_0}}.\mathbf{t} \tag{2-9}$$

For cylindrical carriers:

$$\frac{M_t}{M_\infty} + \left(\mathbf{1} - \frac{M_t}{M_\infty}\right)\mathbf{ln}\left(\mathbf{1} - \frac{M_t}{M_\infty}\right) = \frac{\mathbf{4}D}{R^2}.\frac{C_s}{C_0}.t \tag{2-10}$$

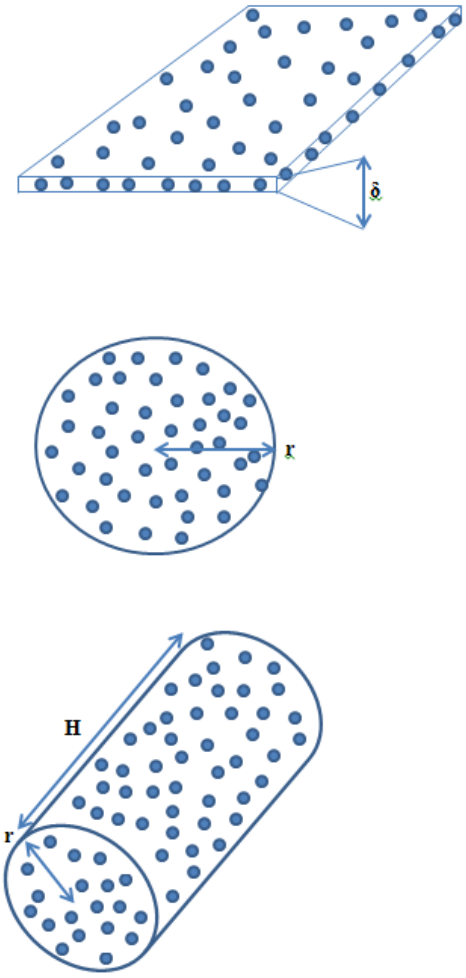

Figure 2-6. Thin film, spherical and cylindrical geometries used to model drug release from non-reservoir devices (devices without a core-shell structure).

If the initial concentration of the drug in the polymer matrix is homogeneously distributed at a value below the solubility concentration of the drug (C_0), and the perfect sink conditions are still applied at the surface of the thin film, the drug concentration at a distance "x" from the surface of the thin film cannot be considered constant anymore and will vary with respect to time. In this case, Fick's second law for one dimensional isothermal drug transport should be solved [76]:

$$\frac{\partial C}{\partial t} = D\frac{\partial^2 C}{\partial x^2} \tag{2-11}$$

The solution to Fick's second law with the above assumptions for thin film is [77,78]:

$$\frac{M_t}{M_\infty} = 4\left(\frac{Dt}{\delta^2}\right)^{\frac{1}{2}}\left\{\pi^{-\frac{1}{2}} + 2\sum_{n=1}^{\infty}(-1)^n \, ierfc\frac{n\delta}{2\sqrt{Dt}}\right\} \tag{2-12}$$

The second term in brackets vanishes at small times therefore:

$$\frac{M_t}{M_\infty} = 4\left(\frac{Dt}{\delta^2\pi}\right)^{\frac{1}{2}} \tag{2-13}$$

The above equation is accurate for $\frac{M_t}{M_\infty} \leq 0.6$ (short time release). According to the above equation which is obtained by using a pure "Fickian diffusion" approach; the release of drug again shows $t^{1/2}$ dependence. The same relation between fractional drug release and time was obtained according to Higuchi's approach discussed earlier. Therefore, the principal result is a square root time dependence of the drug transport. For thin films at long times, we have:

$$\frac{M_t}{M_\infty} = 1 - \frac{8}{\pi^2}\exp\left(-\frac{\pi^2 Dt}{L^2}\right), L = \delta \tag{2-14}$$

In another study, the release rate of an anti-Parkinson drug from degrading polymer (PLGA matrix) was studied. During the time of the experiment, which was exactly 4 days, the changes in the volume of the polymer matrix was negligible; therefore, the polymer microspheres were considered as non-biodegradable implants. In their study, their experimental results showed a good fit with the following solution of Fick's second law of diffusion:

$$\frac{M_\infty - M_t}{M_\infty} = \frac{6}{\pi^2} \sum_{n=1}^{\infty} \frac{1}{n^2} \exp\left(-\frac{n^2 \pi^2}{R^2} Dt\right) \quad (2\text{-}15)$$

where M_t and M_∞ are the cumulative amounts of drug at time *t* and infinity; R is the radius of the sphere and D is the diffusion coefficient. This model assumes perfect sink condition, the polymer matrix is considered to be a sphere and that the drug is distributed homogeneously initially. From the above equation, it is obvious that the amount of drug released at any time does not depend on polymer molecular weight and volume during the course of experiment.

For spheres at short times after solving the above equation we have [79]:

$$\frac{M_t}{M_\infty} = 6\left(\frac{Dt}{\pi r^2}\right)^{\frac{1}{2}} - \frac{3Dt}{r^2}, \qquad \frac{M_t}{M_\infty} < 0.4 \quad (2\text{-}16)$$

For spheres at long times,

$$\frac{M_t}{M_\infty} = 1 - \frac{6}{\pi^2} \exp\left(-\frac{\pi^2 Dt}{r^2}\right), \qquad \frac{M_t}{M_\infty} > 0.6 \quad (2\text{-}17)$$

For cylinders at short times,

$$\frac{M_t}{M_\infty} = 4\left(\frac{Dt}{\pi r^2}\right)^{\frac{1}{2}} - \frac{Dt}{r^2}, \qquad \frac{M_t}{M_\infty} \leq 0.4 \quad (2\text{-}18)$$

For cylinder at long times,

$$\frac{M_t}{M_\infty} = 1 - \frac{4}{(2.405)^2} \exp\left(-\frac{(2.405)^2 Dt}{r^2}\right), \qquad \frac{M_t}{M_\infty} > 0.6 \quad (2\text{-}19)$$

Here, only radial diffusion is considered.

2.2.1.2. Higuchi's Model for Reservoir Polymer Carriers

The reservoir (or core-shell) structure is one that the drug molecules are in the core of the structure and are surrounded by a layer of polymer. This structure can also be prepared in different geometries as shown in Figure 2-7.

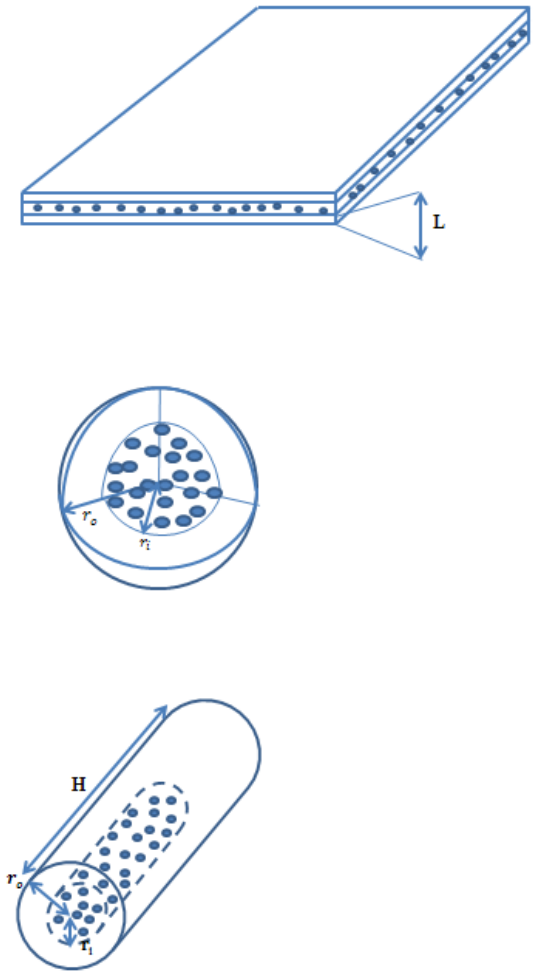

Figure 2-7. Common reservoir (core-shell type) structures encapsulating drug molecules for drug delivery.

Higuchi's assumption is used again here; the released drug in the shell is rapidly replaced by the excess amount of drug available in the core of the reservoir. This is in line with Higuchi's assumption that initial drug concentration is much higher than the solubility concentration of the drug in the polymer which means the drug concentration will not change as a function of time within the shell of the reservoir. Assuming perfect sink conditions, equations to describe the kinetics of drug release have been obtained for different geometries shown in Figure 2-7 [79].

For thin films,

$$\boldsymbol{M_t = \frac{SDKC_s}{L}.t} \tag{2-20}$$

For spheres,

$$\boldsymbol{M_t = \frac{4\pi DKC_s r_o r_i}{r_o - r_i}.t} \tag{2-21}$$

For cylinders,

$$\boldsymbol{M_t = \frac{2\pi HDKC_s}{\ln(\frac{r_o}{r_i})}.t} \tag{2-22}$$

Perfect sink conditions are again provided in the surrounding bulk fluid. In the following models, $C_0 \ll C_s$. Furthermore, there is no drug excess in the core which means that the released drug molecules are not replaced and the drug concentration at the inner membrane's surface decreases with time. For thin film

$$\boldsymbol{\frac{M_t}{M_\infty} = 1 - \exp\left(-\frac{ADKt}{VL}\right)} \tag{2-23}$$

For spheres,

$$\frac{M_t}{M_\infty} = 1 - \exp\left(-\frac{3r_0 DKt}{(r_i)^2 r_0 - (r_i)^3}\right) \quad (2\text{-}24)$$

For cylinders,

$$\frac{M_t}{M_\infty} = 1 - \exp\left[-\frac{(r_i H + r_0 H + 2r_i r_o)DKt}{(r_i)^2 H(r_0 - r_i)}\right] \quad (2\text{-}25)$$

Applications of the above mentioned models for both non-reservoir and reservoir types drug delivery devices to analyze experimental data have been reported by Siepmann et al. [79].

2.2.2. Analytical Solutions

Higuchi's model does have some limitations that are mainly due to the initial assumptions made to simplify the mathematical description of the systems. For example, the initial concentration of the drug should be at least 10 times higher than the solubility concentration of the drug in the matrix to ensure that the pseudo steady state condition applies. This assumption is not possible for drugs with high aqueous solubility which leads to the failure of Higuchi's model with an error more than 11% compared to the exact solution for the system [75]. In this case in practice we will not have a linear concentration profile anymore and the drug concentration at a distance "x" from the thin film surface will change with respect to time and will dissolve in the medium; therefore, Fick's second law will apply and the concentration profile of drug is a Gaussian function (normal probability distribution)

which could be obtained by solving Fick's one dimensional law of diffusion for unsteady-state conditions:

$$\frac{\partial f}{\partial t} = D\frac{\partial^2 f}{\partial x^2} \qquad -\infty < x < +\infty, t > 0 \qquad (2\text{-}26)$$

The only assumption here is that the diffusion coefficient is not a function of the drug concentration. Initial condition is specified as: f(x, t=0) =$f_0(x)$. The function "f" is "concentration" as a function of x and t.

The solution for the above equation is:

$$f(x,t) = \int_{-\infty}^{+\infty} f_0(x')\{\frac{1}{\sqrt{4\pi Dt}} e^{-\frac{(x'-x)^2}{4Dt}}\}dx' \qquad (2\text{-}27)$$

If we use the "Dirac Delta" function for f_0 we obtain:

$$f(\Delta x, \Delta t) = \frac{1}{\sqrt{4\pi D\Delta t}} e^{-\frac{(\Delta x)^2}{4D\Delta t}} \qquad (2\text{-}28)$$

Where $\Delta x = x - x_0$.

As we can see in the above equation, the concentration profile of such a case is a Gaussian function that is not linear at all.

2.3. Swelling Non-Reservoir Polymeric Carriers

One major assumption of all of the aforementioned models is that the polymer matrix does not swell. However, in reality, swelling does take place in many polymer

carriers. Almost all oral drug delivery carriers are non-reservoir, non-biodegradable but swell. These carriers are usually prepared by compressing a powder mixture of a hydrophilic polymer and drug into tablets.

2.3.1. Power Law Model

Peppas et al. modified Higuchi's model in order to consider the polymer swelling kinetics. According to equation (2-14), the first 60% of the fractional drug release can be explained by multiplying a constant by the square root of time. A simple and comprehensive equation can be used to model such drug release process which is called the power law [80]:

$$\frac{\mathbf{M_t}}{\mathbf{M_\infty}} = \mathbf{at^n} \qquad (2\text{-}29)$$

In the above equation "a" is a constant which incorporates the structural and geometric characteristics of the drug delivery device and "n" is the release exponent which is indicative of the drug delivery mechanism. The power law is a very useful equation that was proposed by Ritger and Peppas at 1985. This model is not derived from solutions of Fick's laws and is recognized as a semi-empirical equation.

Case I and Case II drug release extremes have been studied by Alfrey et al [81]. Here, Case I refers to a Fickian diffusion process where the penetrant mobility is much slower than the segmental relaxation rate while Case II refers to a case where the penetrant mobility is much higher than the segmental relaxation rate. Case II applies to polymer matrices that swell. When the exponent is between 0.5 and 1 for a thin

film, the process is called anomalous transport. In order to better understand the different mechanisms of drug transport through polymer matrices during swelling, the swelling interface number has been used to describe the balance between drug release and solvent (water) penetration into the polymer matrix:

$$\boldsymbol{S_W = \frac{\vartheta \delta_t}{D}} \tag{2-30}$$

Where ϑ is the velocity of the polymer-moving front which depends on the solvent (water) diffusivity, D is the drug diffusion coefficient and δ_t is the thickness of the swollen gel layer.

According to the above equation if the drug diffusion coefficient is much lower than that of the solvent (water) ($S_W \gg 1$), solvent penetration will control the release pattern (i.e., swelling controlled transport). If the drug diffusion coefficient is much higher than the solvent (water) mobility ($S_W \ll 1$), drug diffusion will control the release pattern.

In the power law equation, we can see that if the exponent is 0.5 for a thin film the process is Fickian or Case I transport as mentioned before. On the other hand, if the exponent is 1, for a thin film the process, it is Case II transport that involves swelling of the polymer matrix and water uptake. For other geometries different exponent values corresponding to different drug release mechanisms and they can be found in literature [82,83 81,82]. A list of different values for "n" is shown in Table 2-1 for different geometries. One should be cautious about using the values in Table 2-1

because there are several assumptions used in the power law such as: perfect sink conditions and drug release at short time (60% of the drug is released)

Table 2-1 Values of the exponent "n" for the power law equation

Geometry	Case I Fickian diffusion	Anomalous transport	Case II swelling controlled transport
Thin film	n = 0.5	$0.5 < n < 1.0$	n = 1.0
cylinder	n = 0.45	$0.45 < n < 0.89$	n = 0.89
sphere	n = 0.43	$0.43 < n < 0.89$	n = 0.83

The well-known power law expression was used in a study to describe the drug release from simple swellable and erosion matrix systems in which degradation is confined to a thin surface layer of the polymer matrix [84 83]. In their study, the exponent (n) was used for the interpretation of the release mechanism from polymeric controlled drug release systems [85 84].

Swelling and degradation of polymer matrices were studied in chitosan-polycarbophil complexes and hydroxy propyl methyl cellulose containing a simple mixture of chitosan and polycarbophil powders [86 85]. The drugs used in this study were hydrochlorothiazide and ketoprofen. According to this study, the chitosan–polycarbophil complex showed good swelling with low degradation and slower drug release compared to the other matrices containing different polymer material. The segment mobility in different polymer types affected the drug release kinetics during

swelling. The power law was used to explain the drug release kinetics and different values for the exponent (n) were obtained.

Obviously, the power law has its own limitations:

1. The power law model still requires the model system to be in the perfect sink conditions. When a large volume of fluid surrounds a drug carrier, this assumption holds. Otherwise, the bulk concentration of drug would not be negligible.

2. Although different values for "n" are specified here. For different geometries, the power law still lacks the ability to model pharmaceutically relevant geometries. As mentioned before, different parameters in the power law are used for thin films, spheres and cylinders which are usually not the exact geometries used for drug delivery devices in experiments.
3. An insight to the underlying mechanism for drug release cannot be obtained by using the power law equation.
4. Only one dimensional diffusion behavior is considered in the power law model.

2.3.2. Other Swelling Models

Mathematical modeling of swelling controlled polymeric systems presented by Lee [87 86] suggested that both swelling and mass erosion could be modeled using the same type of diffusion equations. Lee [88 87] considered time-dependent diffusion coefficients defined as:

$$\mathbf{D_t} = \boldsymbol{D_i} + (\boldsymbol{D_\infty} - \boldsymbol{D_i})[\mathbf{1} - \mathbf{exp}(-\boldsymbol{kt})] \quad (2\text{-}31)$$

D_i = initial drug diffusion coefficient.

D_∞ = drug diffusion coefficient in the swollen polymer after long time.

The model equation was solved for a Non-reservoir type system where Higuchi' assumption fails; $C_0 \leq Cs$:

$$\frac{\boldsymbol{M_t}}{\boldsymbol{M_\infty}} = \mathbf{1} - \sum_{\boldsymbol{n=0}}^{\infty} \frac{\mathbf{8}}{\mathbf{(2n+1)^2\pi^2}} \mathbf{exp}\{-(\boldsymbol{n} + \mathbf{0.5})^2\boldsymbol{\pi}^2(\frac{\boldsymbol{D_\infty t}}{\boldsymbol{l^2}} + \frac{\boldsymbol{D_\infty}}{\boldsymbol{kl^2}}[\mathbf{1} - \mathbf{exp}(-\boldsymbol{kt})])\} \quad (2\text{-}32)$$

The analytical solution when Higuchi's assumption holds; $C_0 > Cs$:

$$\frac{\boldsymbol{M_t}}{\boldsymbol{M_\infty}} = \frac{\mathbf{1}}{(\frac{\boldsymbol{C_0}}{\boldsymbol{C_s}})\mathbf{erf}(\boldsymbol{\gamma})} \frac{\mathbf{2}}{\boldsymbol{\pi}^{\mathbf{1/2}}} [\frac{\boldsymbol{D_\infty t}}{\boldsymbol{l^2}} - \left(\mathbf{1} - \frac{\boldsymbol{D_i}}{\boldsymbol{D_\infty}}\right)\frac{\boldsymbol{D_\infty}}{\boldsymbol{kl^2}}[\mathbf{1} - \mathbf{exp}(-\boldsymbol{kt})]]^{\frac{\mathbf{1}}{\mathbf{2}}} \quad (2\text{-}33)$$

where

$$\boldsymbol{\pi}^{\mathbf{1/2}}\boldsymbol{\gamma}\,\mathbf{exp}(\boldsymbol{\gamma}^{\mathbf{2}})\,\mathbf{erf}(\boldsymbol{\gamma}) = \frac{\boldsymbol{C_s}}{\boldsymbol{C_0 - C_s}} \quad (2\text{-}34)$$

Siepmann and coworkers [89-92] developed a mathematical model to describe drug release from dissolving HPMC matrices. The "sequential layer" model considers

diffusion, swelling, and polymer dissolution simultaneously. In the model, they considered transport both in the radial and the axial directions. The drug and water diffusion is based on Fick's second law for cylindrical devices with concentration dependent diffusivities:

$$\frac{\partial C_k}{\partial t} = \frac{\partial}{\partial r}\left(D_k \frac{\partial C_k}{\partial r}\right) + \frac{DK}{r}\frac{\partial C_k}{\partial r} + \frac{\partial}{\partial z}\left(DK \frac{\partial C_k}{\partial z}\right) \tag{2-35}$$

where C_k is the concentration of the diffusion speciesD_k is the diffusion coefficient of the diffusion species. The diffusion coefficients of water and drug are estimated according to the free volume theory:

$$D_1 = D_{1eq} \exp\left(-\beta_1\left(1 - \frac{C_1}{C_{1eq}}\right)\right) \tag{2-36}$$

$$D_2 = D_{2eq} \exp\left(-\beta_2\left(1 - \frac{C_2}{C_{2eq}}\right)\right) \tag{2-37}$$

where $D_{1eq}$and D_{2eq} are the diffusion coefficient of water and drug in the equilibrium swollen state of the system, $\beta_1$and $\beta_2$are dimensionless constants and $C_{1eq}$is the water concentration in the equilibrium-swollen state of the system.

The reptation model is used to explain polymer dissolution [93-95]. In this model, a dissolution rate constant is considered (k_{diss}) which quantitatively characterizes a constant dissolution velocity per unit area:

$$M_{Pt} = M_{P0} - k_{diss} A_t t \tag{2-38}$$

where M_{Pt} and M_{P0} are the dry matrix masses at times t=t and t=0. A_t is the system surface area at time t. Other models accounting for polymer dissolution have been summarized in a review article by Narasimhan [93] .

Figure 2-8 shows the important parameters one needs to consider before developing a mathematical model for in-vitro drug release kinetics.

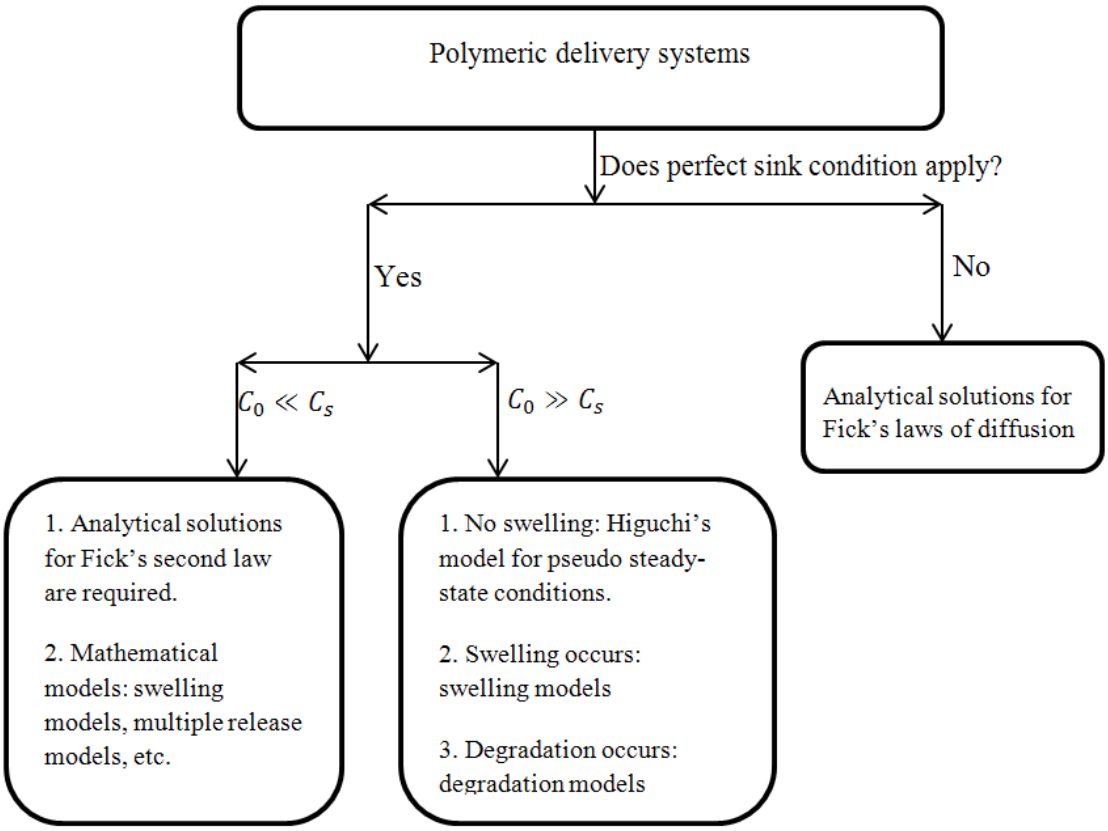

Figure 2-8. Important steps that are needed to consider before using or developing mathematical models to describe in-vitro drug release kinetics.

2.4. Biodegradable Non-Reservoir Polymeric Carriers

Modeling degradation processes is obviously more challenging than all of the models described in the previous sections simply because such degradation models need to take the hydrolysis reaction into account as such reactions change the polymer structure, molecular weight and properties. The penetration of water molecules into the polymer matrices triggers hydrolysis reaction. As a result, degradation occurs which leads to the formation of monomers and oligomers that create pores or holes in the bulk structure of polymers. Depending on the type of polymer, two types of erosion behavior can happen: surface erosion and bulk erosion. In bulk degradation, the volume of the polymer decreases and degradation occurs when enough water concentration becomes available for polymer chains by diffusion. On the contrary, in surface degradation the volume of the polymer does not change and only polymer chains at the surface are broken due to the reaction between water and ester groups. This type of degradation happens much faster than bulk degradation and the degradation rate does not depend on the water concentration at the surface.

Figure 2-9 illustrates both bulk and surface erosions.

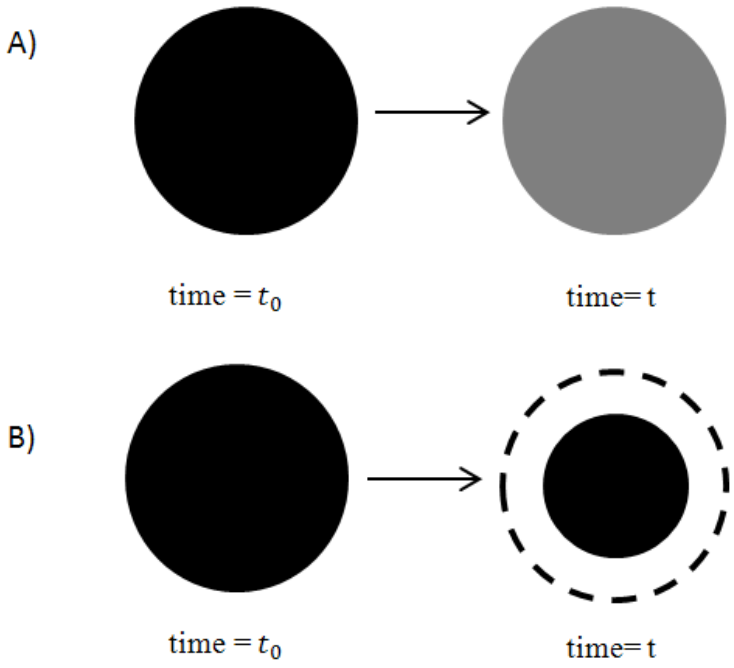

Figure 2-9 Illustration of bulk eroding matrix polymer (A) and surface eroding matrix polymer (B)

2.4.1. Models

In the following paragraphs we will introduce the major mechanistic models developed for drug release from degrading polymer matrices. In these models, the underlying mechanism of drug release is not clear. However, empirical models have been also developed to describe drug release from degrading polymer matrices based upon the assumption that the drug release process obeys zero order kinetics. Such models somewhat similar to the power law model lack the ability to give the drug release mechanisms.

Hopfenberg [96] developed an empirical model from drug release from eroding polymers by assuming that the overall release process is controlled by a single zero order process. This overall process considers a combination of dissolution, swelling, and polymer chain scission. A general mathematical equation was derived, which is valid for thin films, cylinders, and spheres:

$$\frac{M_t}{M_\infty} = 1 - \left[1 - \frac{K_0 t}{C_0 a}\right]^n \quad (2\text{-}39)$$

where n = 3, 2 and 1 for spheres, cylinders and thin films, respectively. Here, *a* is the radius of the sphere or cylinder or half thickness of thin film. C_0 is the initial drug concentration in the system. K_0 is the equilibrium rate constant which has the units of concentration per time for a zero order kinetic process. This constant depends on the solution temperature, ionic strength and surface area of the matrix. Since in this model the drug release kinetics controls the overall kinetics, this model cannot be used for bulk eroding surfaces. This model can only be applied to surface eroding systems.

During the course of degradation, the polymer molecular weight and mass change as a function of time that in turn causes the drug diffusivity as well. Therefore, in this process, the drug diffusion coefficient can no longer be considered as constant. For this purpose the following equation was used to determine the diffusion coefficient:

$$D_{Mw} = D_0 + \frac{k}{Mw} \quad (2\text{-}40)$$

If the degradation kinetics is described by a first order process (e.g., PLGA), *Mw* of the polymer at a given time is approximated by:

$$\boldsymbol{M_{w,t} = M_{w,0}\exp(-k_{deg}t)} \quad (2\text{-}41)$$

where $M_{w,0}$is the initial polymer molecular weight, $k_{deg}$is the first order degradation rate constant.

By incorporating the time dependence of molecular weight into Crank's [77] diffusion model and Koizumi's [97] model, one yields the following kinetics equation:

$$\boldsymbol{\frac{M_t}{M_\infty} = 1 - \frac{6}{\pi^2}\left(\sum_{n=1}^{\infty}\frac{1}{n^2}\exp\left(-\frac{Dn^2\pi^2 t}{r^2}\right)\right.} \quad (2\text{-}42)$$

The above model can also be used when the drug initial concentration is smaller than its solubility concentration in the system.

For Koizumi's model:

$$\boldsymbol{Q = 4\pi a^2\left[\sqrt{2(C_0 - C_s)C_s Dt} + \frac{4C_s}{9a}\left\{\frac{C_s}{(2C_0 - C_s)} - 3\right\}Dt\right]} \quad (2\text{-}43)$$

where *a* is the radius of a spherical particle.

The above equations can only be used for bulk degradation cases because the degradation kinetics controls the overall kinetics. As mentioned before, surface

erosion is considered when the drug diffusion controls the overall kinetics of the release process.

One assumption in the models described in the "non-biodegradable polymers" sections is that the polymer matrix loaded with drug molecules is considered to be homogeneous. When degradation occurs to the polymer matrix, the matrix will become heterogeneous in terms of the distribution of the molecular weight of the polymer chains and pores created on the surface of matrices. This obviously will affect the diffusivity of drug. If we consider other species such as water and acid being released during the course of polymer degradation, this adds complexity to the required mathematical models. In particular, the diffusion coefficient of drug becomes a function of time and position in the matrix as well. These models are called "models of multiple release mechanisms" which were studied by Himmelstein and co-workers [98,99]. Others [100] developed a model for thin film geometries to describe the drug release from surface erodible polymer matrices. Their model assumes perfect sink conditions and no changes in the total volume of the matrix. The following expression is used to describe this model:

$$\frac{\partial C_i}{\partial t} = \frac{\partial}{\partial x}\left[D_i(x,t)\frac{\partial C_i}{\partial x}\right] + \vartheta_i \quad i = A, B, C, E \tag{2-44}$$

C_i and D_i are the concentration and the diffusivity of species i, and ϑ_i is the net sum of the degradation and synthesis of species i, and x is the space variable. In order to consider the effect of the degradation process on the diffusion coefficient, the

diffusivity of all species is related to the extent of polymer hydrolysis according to the following expression:

$$\mathbf{D_i} = \mathbf{D_{i,0}}\,\mathbf{exp}\left[\frac{\mu(C_{D,0}-C_D)}{C_{D,0}}\right], \quad \mathbf{A, B, C, E} \tag{2-45}$$

$D_{i,0}$ is the diffusion coefficient of species i when the polymer is not hydrolyzed, $C_{D,0}$ and C_D are the concentration of species i at time zero and t respectively, and μ is a constant.

Charlier et al.[101] also developed a model for bulk eroding PLGA films. Assuming first-order polymer chain cleavage kinetics,

$$\frac{dM}{dt} = -kM \tag{2-46}$$

$$M = M_0 e^{-kt} \tag{2-47}$$

where $M_0$is the initial polymer molecular weight, k is the degradation rate constant. With:

$$\frac{D}{D_0} = \frac{M_0}{M} \tag{2-48}$$

$$D = D_0 e^{-kt} \tag{2-49}$$

where D_0 is the drug diffusion coefficient before degradation.

Finally, an expression for drug release is obtained:

$$Q = S^2\sqrt{\frac{2C_0C_sD_0(e^{kt}-1)}{k}} \tag{2-50}$$

where C_0 is the initial drug concentration, C_s is the drug solubility in the matrix, S is the surface area of the film exposed to the medium. At short times, the above equation becomes Higuchi's equation:

$$\mathbf{Q = S\sqrt{C_0 C_s D_0 t}} \tag{2-51}$$

In other words, at short times, drug release is diffusion based and at long times, the drug release is affected by polymer degradation.

Heller and Baker [102] developed a model that applies to bulk eroding polymers that undergo hydrolysis and are solubilized by conversion to small, water-soluble molecules. The Higuchi model was used as a basis:

$$\mathbf{\frac{dM_t}{dt} = \frac{A}{2}\left(\frac{2PC_0}{t}\right)^{\frac{1}{2}}} \tag{2-52}$$

where P is the permeability of the polymer to the drug, A is the surface area for both sides of the film and C_0 is the initial drug concentration in the polymer. According to Higuchi's model, the drug permeability was assumed to be constant but during degradation the drug permeability changes with respect to time:

$$\mathbf{\frac{P}{P_0} = \frac{\text{Initial number of bonds}}{\text{Number of remaining bonds}} = \frac{N}{N-Z}} \tag{2-53}$$

The bond cleavage order was assumed to be first order as shown in the following equation:

$$\mathbf{\frac{dZ}{dt} = K(N - Z)} \tag{2-54}$$

where K is the first order rate constant.

After integration and substituting back into Higuchi's equation, it yields:

$$\frac{dM_t}{dt} = \frac{A}{2}\left[\frac{2P_0 \exp(Kt) C_0}{t}\right]^{\frac{1}{2}} \quad (2\text{-}55)$$

It should be noted that factors such as polymer crystallinity, pH of the release medium, and physical size of the matrix also affect hydrolysis reactions [103,104].

2.5. Nano-Sized Polymeric Carriers

In general, nano-scale (10 – 200 nm) polymer drug carriers are in the form of micelle. And they tend to be stable (no degradation and/or dissolution in blood stream) relative to the time scale associated with the drug release process. From a modeling perspective, such block copolymers can be modeled as non-biodegradable systems even though they are biodegradable. In fact, many studies of micellar carriers showed that drug encapsulated by micelles releases completely before the degradation of the block copolymers takes place [105].

Owing to the length scale of the micelles, continuum models obviously lack the ability to describe the kinetics of drug release as the concentration of the drug in the micelle fluctuate significantly and it is not appropriate to assign a concentration profile (as what is done for continuum models) to such systems. Nevertheless, there are a few authors who have made the attempt to describe drug release from micelles using continuum models discussed before. For example, E. Khodaverdi et al. [106] have carried out an experimental in-vitro release of naltrexone hydrochloride from

block copolymer micelles at 37 °C under perfect sink conditions. They observed that the amount of drug released is related to the square root of time. Higuchi's diffusion model was used to describe the release process. Sutton et al., [107] have applied the technique of continuum model to study the whole micelle. In particular, the authors treated the micelle as a sphere (see Figure 2-10) and applied Higuchi's model for short time releases from the micelle (less than 75 hours):

$$\boldsymbol{S\frac{dQ}{dt} = -4\pi a^2 D\frac{dc}{da}} \tag{2-56}$$

where

S: surface area

D: diffusion constant of drug in polymer matrix.

C: concentration of drug in radial distance.

A: distance from the center of the sphere.

Assuming that the release process is pseudo-steady state, they obtained:

$$\boldsymbol{C_0\left(a_0^3 + 2a'^3 - 3a_0a'^2\right) + C_s\left(4a'^2a_0 + a_0^3 \ln\frac{a_0}{a'} - a_0^3 - a_0^2a' - 2a'^3\right) = 6DC_sa_0t} \tag{2-57}$$

where C_s is the solubility of the drug in the permeating fluid:

a_0: radius of the spherical core of the micelle.

a': distance of moving front from the center of the core at time t.

C_0: drug loading concentration.

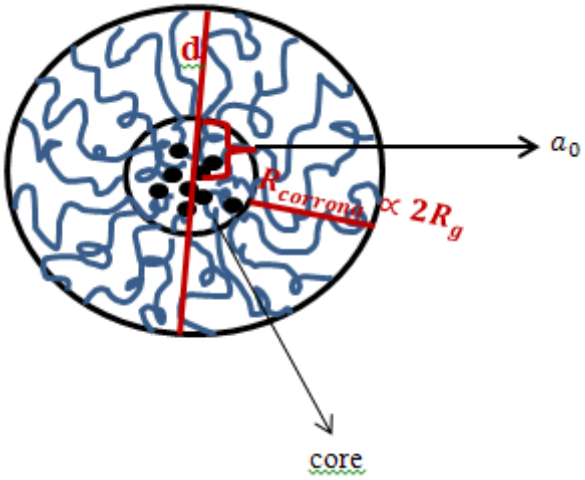

Figure 2-10. Schematic illustration of DOX loaded in a diblock copolymer micelle with the same corona block PEG and two different core blocks polyD,L-lactide or polycaprolactone. d, hydrodynamic diameter of the micelle; 2Rg, PEG, thickness of corona.

The fractional drug release is given by:

$$\frac{\mathbf{M(t)}}{\mathbf{M_\infty}} = \mathbf{1} - [(\frac{\mathbf{a'}}{\mathbf{a_0}})^{\mathbf{3}} + \mathbf{1/2}\,\frac{\mathbf{C_s}}{\mathbf{C_0}}((\frac{\mathbf{a'}}{\mathbf{a_0}}) + (\frac{\mathbf{a'}}{\mathbf{a_0}})^{\mathbf{2}} - \mathbf{2}\left(\frac{\mathbf{a'}}{\mathbf{a_0}}\right)^{\mathbf{3}}\Big)] \quad (2\text{-}58)$$

where

M (t): Mass of drug released at time t.

M_∞ = Mass of drug released as the time approaches infinity.

$$\mathbf{a_0} = \frac{\mathbf{d}}{\mathbf{2}} - \mathbf{R_{corrona}}$$

In the above equation, a' is a function of time, t. The dynamic light scattering technique was used to measure d, and radius of gyration was used to find $R_{corrona}$. After calculating a_0 and knowing the ratio of $\frac{C_S}{C_0}$, the value of a'can be estimated by fitting the experimental data (fractions of drug released at each time) into the above equation. The diffusion coefficient was obtained by substituting the value for a' into equation (2-58). As mentioned earlier, the above equations are valid for short time drug release from micelles. At long times, polymer degradation happens which causes the rest of the drug molecules to be released from the micelle as well. For long time release, the following Higuchi model is used:

$$\frac{\mathbf{M(t)}}{\mathbf{M(\infty)}} = \mathbf{P}\left[\mathbf{1} - \frac{\mathbf{6}}{\boldsymbol{\pi}^{\mathbf{2}}}\mathbf{exp}\left(\frac{-\boldsymbol{\pi}^{\mathbf{2}}\mathbf{Dt}}{\mathbf{a_0^2}}\right)\right] \quad (2\text{-}59)$$

where P is the fraction of drug released at infinite time which was obtained by the extrapolation of the fraction of drugs released at the longest times of the measurements.

If one examines critically what has been done to model the release kinetics from micelles, it seems that most of these authors have missed some important points here. As mentioned, the first Higuchi model was used for kinetics of short time release from the micelle. According to the assumption in Higuchi's steady-state release model the concentration profile for the drug was assumed to change linearly with the distance from the solvent-polymer interface. Due to the very small size of the micelles (20 – 100 nm in diameter) one cannot assume that the concentration of drug at any distance from the core changes. From a practical point of view, such concentrations could be considered as constant throughout the micelle at any distance from the micelle core. In addition, according to the authors' assumption, pseudo-steady state conditions apply. Such conditions apply when the initial concentration of the drug loaded onto the polymer is much higher than the solubility concentration of the drug in solvent. Therefore, the concentration of drug at any distance from the solvent-polymer interface should remain almost constant with respect to time. Given the size of the micelle core which is very small, the concentration of the drug loaded in the core cannot be much higher that the drug solubility in the solvent. In other words, an excess amount of drug in the polymer core does not exist. Therefore, the pseudo-steady state assumption here fails.

Finally, another assumption here is that the micelle is "spherical". However, other geometries do exist (e.g., rod-like micelles). Therefore, Higuchi's model for sphere would not be valid.

2.5.1. Molecular Modeling

As mentioned, use of continuum models for micelles is not suitable. In this regard, molecular dynamics (MD) simulation is probably the most suitable approach for studying the dynamics of the drug release process. The essence of MD simulation is that every atom in a molecular system is treated as a classical particle and the Newton's equation of motion is solved under certain conditions (e.g., constant temperature, constant pressure, etc.). Analysis of the resultant trajectory (e.g., positions and velocities of the atoms as a function of time) will yield thermodynamic and transport properties of interest. Since MD is a relatively mature simulation technique, there exist many excellent references on the topic [108,109]. In the context of drug release studies, MD can be used for two purposes. One is to simulate the micelle environment and calculate the corresponding flux of the drug molecules while the other is to calculate the diffusion coefficients of drug molecules diffusing in micron thick polymer films. In terms of simulating micelles at the atomistic level, it is very expensive simply because a micelle normally contains more than 100,000 atoms (it contains tens of block copolymers, tens of drug molecules and tens of thousands water molecules). Therefore, certain level of coarse graining is needed to reduce the number of atoms in the system, thereby reducing computational costs

(Figure 2-11). For example, several scientists [110-112] have developed a coarse-grain (CG) model for simulating phospholipids. Phospholipids have a hydrophilic head due to negatively charged phosphate groups and maybe other groups and their tail is hydrophobic due to lipids. Therefore, they have a high tendency to aggregate and form micelles in water, somewhat similar to the behavior of block copolymers in water. According to Klein and coworkers' method, one way to simulate the micelles is to represent each monomer in a block copolymer as a single spherical unit.

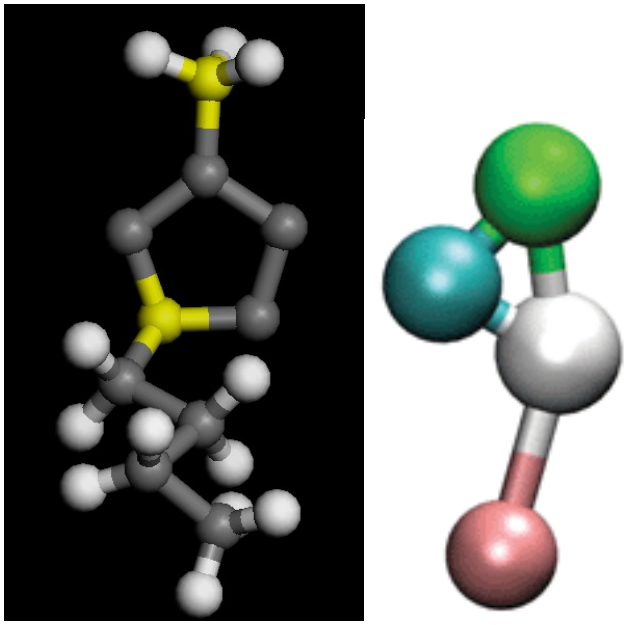

Figure 2-11. Schematic presentation of an "all atom" model on the left and a coarse-grained model on the right. According to the figure on the right, each sphere color represents a specific monomer inside the blocks of a block copolymer. These spheres represent larger groups of atoms. In the "all atom" model each atom is presented with the same gray color.

By using this representation, both non-bonded and bonded interaction potentials are defined slightly different from all-atom simulations [113,114]. The Harmonic potential used to describe the bonds between monomers is defined as:

$$\mathbf{U_{bond}(r_{ij}) = (k_b/2)(r_{ij} - r_0)^2} \tag{2-60}$$

where r_0 is the equilibrium bond distance. Another bonded potential is defined as:

$$\mathbf{U_{bend}\left(\theta_{ijk}\right) = k_\theta\left[1 - \cos\left(\pi - \theta_{ijk}\right)\right]} \tag{2-61}$$

where k_θ is adjusted until the bond angle is correct (comparable with all-atom simulation parameters). Regarding the non-bonded interaction potential, the approach is slightly different. Obviously, one cannot use the same non-bonded interaction parameters obtained from the all-atom models to model interactions between larger groups of atoms. The Lennard-Jones potential functions differ from those of various atom pairs with wider potential wells in the case of the CG method. And such CG non-bonded interaction potentials are usually tested by comparing the computed density using such potentials with the corresponding experimental values. In addition, the radial distribution function of the block copolymer obtained from the all-atom method could be used as a reference. The non-bonded parameters σ and $\in$ are adjusted to reproduce the first peak position and height of the radial distribution function. The non-bonded interaction potential function for CG atom pairs is described as follows:

$$\mathbf{U\left(r_{ij}\right) = \left(\frac{15}{4}\right) \in \left[\left(\frac{\sigma}{r_{ij}}\right)^9 - \left(\frac{\sigma}{r_{ij}}\right)^6\right]} \tag{2-62}$$

Water molecules present in the micelles are considered to be a spherical and symmetric site called "W" which has LJ (6-4) interactions with each other and is made of "three" water molecules:

$$\mathbf{U}(\mathbf{r_{ij}}) = \left(\frac{\mathbf{15}}{\mathbf{4}}\right) \in [(\frac{\boldsymbol{\sigma}}{\mathbf{r_{ij}}})^{\mathbf{6}} - (\frac{\boldsymbol{\sigma}}{\mathbf{r_{ij}}})^{\mathbf{4}}] \quad (2\text{-}63)$$

To determine the diffusivity of drug molecules through the micelle, one method is to the Einstein relation. For this purpose, one needs to obtain the mean square displacement (MSD) of the center-of-mass of individual drug molecules from the MD trajectory [113]. In the long time limit of normal diffusion, where the slope of the logarithmic plot of mean square displacement versus time (becomes constant, the center of mass diffusion coefficients is calculated from the Einstein relation [115]:

$$\mathbf{D} = \frac{\mathbf{1}}{\mathbf{6}} \lim_{\mathbf{t}\to\infty} \frac{\mathbf{d}}{\mathbf{dt}} \langle |\mathbf{R(t)} - \mathbf{R(0)}|^{\mathbf{2}} \rangle \quad (2\text{-}64)$$

where R(t) and R(0) are vectors of displacement at time t and t=0.

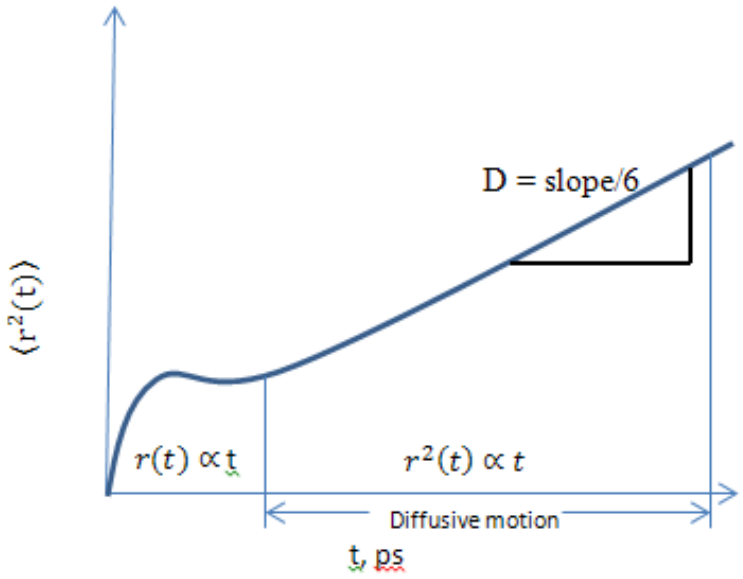

Figure 2-12. A schematic plot of mean square displacement vs. time. The slope of the plot at long times is related to the diffusion coefficient according to Einstein's relation.

Molecular dynamics simulation can also be used to calculate the drug diffusivity in micron thick polymer films. This is useful, as the drug release profile requires knowledge of the drug diffusivity. This is true for all the continuum models previously discussed. The challenge here is to obtain reliable diffusivity. The situation becomes more complicated when the polymer matrix degrades. This is because when degradation takes place, the diffusion at short times is considered to be Fickian diffusion and at long times, it is time dependent.

Recently, Berhane et al., [116] applied the MD technique to calculate diffusion coefficient of a drug namely 5-aminosalicyclic acid in a polymer thin film and found that the resultant value ($5.7\times 10^{-6} cm^2/s$) yielded an accurate prediction of the drug

release from the delivery system (root mean square error of 5%). The release profile was validated using experimental data from in vitro dissolution experiments. One noteworthy point here is that the computation only used 3 hours of computational times. In another study, the diffusion coefficient of Nifedipine in phospholipid bilayer was calculated using an all atom molecular dynamics simulation [117]. In addition to the diffusion coefficient, the authors were able to gain insight into the detailed interactions between the drug molecule and the membrane. Experimental permeability values and computed diffusion coefficients were compared in literature [118] to investigate the diffusion coefficient of Theophylline and Aspirin molecules in PVA membranes. Both experimental and simulation data showed that Aspirin exhibited lower diffusivity than Theophylline due to stronger intermolecular interactions between Aspirin and PVA membrane. Many researchers have emphasized on the advantages of using molecular dynamics simulations to avoid experimental estimation of diffusivity that is usually time-consuming and expensive. For example, to design a gel for a specific drug delivery application, Dutta et al., [119] used molecular dynamics simulations to calculate the cross-linking density of polymers which affect swelling and release of drug molecules. The authors specifically emphasized the advantage of molecular dynamics simulation over continuum modeling and experimental methods as molecular dynamics directly addresses the intermolecular interactions between drug and polymers which are crucial for designing the gels of interest.

2.6. Summary

Continuum in vitro drug release models such as Higuchi's model, various variations of it and other complex mathematical models were discussed. When the initial drug concentration in a polymer carrier is lower than its solubility concentration, Higuchi's model tends to fail with an error of about 11% compared to the exact solution of the diffusion equations. This occurs when drug is highly soluble in the aqueous solution. Although the power law is a more comprehensive model for describing drug release kinetics, it still has its own limitations and one of them is not able to provide the release mechanism.

Improvements to the continuum models in fact have been very useful for obtaining the fractional drug release profile vs. time that is commonly done in experimental studies. These models are normally used to investigate a proper "fit" for the experimental measurements of drug release. In all the major in vitro drug release models, knowledge of the drug diffusivity in the polymer carrier is important to determine the fractional drug release profile. In this regard, molecular dynamics simulation is a powerful tool for estimating the required diffusivity. The molecular level simulation can provide information about the underlying mechanism for drug release from polymer matrices.

If drug release occurs in a nano-sized micelle, none of the discussed continuum models could describe the kinetics of drug release accurately. For such small

systems, molecular dynamics simulation is a powerful tool to study the motion of molecules under certain conditions of temperature, pressure and system size. Measurement of drug diffusivity in the micelle environment is obviously not a trivial task. The microscopic diffusivity of drug molecules can be calculated using Einstein's equation.

3. Foundations of Molecular Dynamics Simulation

As mentioned in Chapter 2, continuum models are not suitable for describing the drug release kinetics of a nano-sized system and molecular dynamics (MD) simulation should be used. However, there are some limitations of the method. And that is the size of the systems that the technique can handle. Since MD generates position and velocity of each atom in a system as a function of time, it requires a significant amount of computation and memory. Such simulations can take up days to weeks depending on the size of the system. Therefore, the practical limit on such simulations is systems that contain only a few thousands atoms.

In this chapter, we will discuss the MD method used in the thesis to study polymeric drug delivery systems under constant temperature and pressure conditions. A complete discussion about molecular dynamics method could be found in [120-123].

3.1. Introduction

Molecular dynamics simulation is a popular method used to study the motion of atoms and molecules under a particular set of conditions. State variables are used to determine conditions in a molecular dynamics simulation such as:

N= number of atoms

P= pressure

T= temperature

And the method can be used for systems having the following boundary characteristics:

1. Open systems
2. Closed systems
3. Periodic systems

The third type of boundaries (periodic) is used to simulate bulk systems which will be discussed later. We are always interested in obtaining information about the macroscopic information of a system. The macroscopic information is based on averaging microscopic properties over many microstates over a long period of time. Microstates are obtained by either a classical approach where Newtonian mechanics applies or a quantum approach where quantum mechanics applies. In the classical mechanics approach, the total energy of the system is presented as:

$$\mathbf{H}\,(\mathbf{p},\mathbf{q}) = \mathbf{K}(\mathbf{p}) + \mathbf{V}(\mathbf{q}) \tag{3-1}$$

where H, the Hamiltonian (i.e., the total energy of a system) is a function of position and velocity of the particles made up of the system. K is the kinetic energy and V is the potential energy of system. The microstates of the system are specified by positions and velocities of all atoms. A "phase space" is created by the collection of positions and velocities of atoms in a classical mechanic approach. However according to the quantum mechanics approach, an operator $\widehat{H}$ is used to obtain the "phase space":

$$\widehat{\mathbf{H}} = \sum_{\mathbf{i=1}}^{\mathbf{N}} \frac{-\hbar^2}{\mathbf{2m_i}} \left(\frac{\partial^2}{\partial \mathbf{x_i^2}} + \frac{\partial^2}{\partial \mathbf{y_i^2}} + \frac{\partial^2}{\partial \mathbf{z_i^2}} \right) + \widehat{\mathbf{V}} \tag{3-2}$$

The term in the parenthesis is called the Laplacian. The time independent Schrödinger equation for wave function:

$$\widehat{\mathbf{H}}\boldsymbol{\varphi}_\mathbf{n} = \mathbf{E}\boldsymbol{\varphi}_\mathbf{n} \tag{3-3}$$

Here, φ_n is called the wave function which describes the phase space on a quantum mechanics approach. When the operator $\widehat{H}$ acts on a certain wave function φ, and the result is proportional to the same wave function φ and the proportionality constant, E, is the energy of the state n. It is too complex and time consuming to solve the above equation for Avogadro number of particles in the system; therefore, we use statistical mechanics [120-123]. Statistical mechanics is the application of probability theory to study behavior of a large number of particles at thermodynamic

equilibrium. It provides a framework for relating the microscopic properties of individual atoms and molecules to the macroscopic or bulk properties of materials.

Microscopic information $\xrightarrow{statistical\ mechanics}$ Macroscopic information	
Classical, quantum	***thermodynamic properties***

Molecular dynamics simulation (MD) is a method that uses classical mechanics to generate microstates or phase spaces. Molecular dynamics allows the study of all kinds of properties such as time dependent properties. In statistical mechanics, an average value is defined as an average taken over large number of microstates of systems considered simultaneously. An experimentally observable quantity corresponds to this average. Suppose that we have a large system and each microstate is visited with equal probability. The observed property A is given by the following equation:

$$\boldsymbol{A_{observable}} = \frac{\mathbf{1}}{\boldsymbol{N}} \sum_{\boldsymbol{\nu=1}}^{\boldsymbol{N}} \boldsymbol{A_\nu} \qquad (3\text{-}4)$$

where N is the number of measurements of A. A_ν is the value of A during ν^{th} measurement.

$$\boldsymbol{A} = \sum_{\boldsymbol{\nu}} [\frac{\mathbf{1}}{\boldsymbol{\nu}} (\#\ \boldsymbol{of\ times\ state\ \nu\ is\ observed})]\ \boldsymbol{A_\nu} = \sum_{\boldsymbol{\nu}} \boldsymbol{P_\nu A_\nu} = \langle \boldsymbol{A} \rangle \qquad (3\text{-}5)$$

where $\langle A \rangle$, is the ensemble average, a collection of microstates that are consistent with the thermodynamic state of the system. According to the ergodic hypothesis, the ensemble average mentioned above should be equal to the time average obtained from a MD simulation if the simulation is carried out for a long time [122]. This hypothesis simply states that if one allows the system to evolve in infinite time so that the system passes through all possible states, the time average should not depend on the initial configuration of atoms. The following equation describes the time average $\bar{A}$ for a thermodynamic property A:

$$\bar{A} = \lim_{\tau \to \infty} \frac{1}{\tau} \int_0^{\infty} A(t) dt \tag{3-6}$$

3.2. Equations of Motion

The dynamic behavior of molecules in a MD simulation is based on classical Newton's second law of motion:

$$\mathbf{F} = \mathbf{ma} = \mathbf{m} \frac{\mathbf{dv}}{\mathbf{dt}} = \mathbf{m} \frac{\partial^2 \mathbf{r}}{\partial t^2} \tag{3-7}$$

where in the above equation r is the position; F is the force acting on each atom; m is the mass of an atom; and a is acceleration. The force can be obtained from the potential energy, U(r), which is also a function of position of atoms in the system. The force is defined as:

$$\boldsymbol{F} = -\frac{\partial U(r)}{\partial r} \tag{3-8}$$

The collection of all potential energy equations is called “force field” which is a combination of functions describing two types of interactions between atoms: bonded interactions and non-bonded interactions.

3.3. Force Field

The function which describes the potential energy uses a set of parameters which is referred to as the “force field” [124]. The force field function can be generated based on either experimental work or on assumptions and approximations to solve the Schrodinger equation theoretically. The most common assumption is the “Born-Oppenheimer” approximation that ignores the electronic motions and describes the energy of the system as a function of the nuclear coordinates only. This assumption is based on the fact that the nuclear mass is much greater than the electronic mass. Based on the mentioned approximation we should solve the Schrodinger equation to obtain the potential energy surfaces which correspond to the potential energy of the system. Another method to obtain the potential energy is to rely on experimental work which describes the energy in terms of functions including several parameters. An example of a force field representing non-bonded and bonded interactions is the following:

$$\boldsymbol{V(R)} = \sum_{\boldsymbol{bonds}} \boldsymbol{k_r}(\boldsymbol{r}-\boldsymbol{r_0})^2 + \sum_{\boldsymbol{bonds}} \boldsymbol{k_\theta}\,(\boldsymbol{\theta}-\boldsymbol{\theta_0})^2 + \sum_{\boldsymbol{dihedrals}} \frac{\boldsymbol{V_n}}{\boldsymbol{2}}[\boldsymbol{1} + \boldsymbol{\cos(n\varphi-\gamma)}] + \sum_{\boldsymbol{i>j}}\left(\frac{\boldsymbol{A_{ij}}}{\boldsymbol{R_{ij}^{12}}} - \frac{\boldsymbol{B_{ij}}}{\boldsymbol{R_{ij}^{6}}}\right) + \sum_{\boldsymbol{i>j}} \frac{\boldsymbol{q_i q_j}}{\boldsymbol{4\pi\varepsilon R_{ij}}} \quad (3\text{-}9)$$

The first term in the above equation is referred to as the bonds stretching term; the second term is the bond bending term and the third term is the torsions. The fourth term is the Van der Waals interactions between two atoms and the last term is referred to as the Coulomb potential. A great deal of research has been done to modify the force fields to represent systems closer to reality. For example, in the CFF force field, parameters were modified to extend its applicability in the field of zeolites and organic polymers. The result was called the PCFF force field [125,126]. The COMPASS (Condensed-phase Optimized Molecular Potentials for Atomistic Simulation Studies) [127] force field was developed later to extend the applicability of PCFF force field to condensed phase applications. The non-bond parameters were re-parameterized and optimized to fit the condensed-phase properties. It has been shown that the COMPASS force field is able to predict accurate structural, conformational, cohesive, and other physical properties for a wide range of polymers and molecules [127]. Rigby has demonstrated that liquid density for a variety of substances with complex molecular structures could be reproduced by COMPASS force field [128]. In this thesis, we are studying the effect of polymer dynamics on drug and water diffusivity; therefore, the COMPASS force field was suitable. The COMPASS force field describes the total potential energy of the system according to the following equation:

$$\boldsymbol{E_{total} = E_b + E_\theta + E_\varphi + E_\tau + E_{cross} + E_{vdw} + E_Q} \quad (3\text{-}10)$$

The first five terms in the above equation describe the short-range intra-molecular interactions which correspond to bond stretching (b), bond bending angle (θ), torsion angle (φ), Wilson-out of plane-angle (τ), and cross coupling terms (E_{cross}). These cross-coupling terms help us achieve higher accuracy. They include combinations of two or more short-range interaction terms (e.g., bond-bond, bond-angle and bond-torsion) that would predict vibration frequencies and structural variations associated with the conformational changes. The last two terms of the above equation describe the non-bonded interactions which correspond to the Lennard Jones (LJ) 9-6 function for the dispersive interactions and Coulombic function for electrostatic interactions. Quadratic polynomials are used in the COMPASS force field to describe the bond stretching and bond bending angle terms:

$$\boldsymbol{E_b = \sum_b [k_2 (b - b_0)^2 + k_3 (b - b_0)^3 + k_4 (b - b_0)^4]} \quad (3\text{-}11)$$

$$\boldsymbol{E_\theta = \sum_\theta [k_2 (\theta - \theta_0)^2 + k_3 (\theta - \theta_0)^3 + k_4 (\theta - \theta_0)^4]} \quad (3\text{-}12)$$

where b_0 and θ_0 are equilibrium bond lengths and bond bending angles respectively. Torsion angle between four atoms is described by a three term Fourier expansion as following:

$$\boldsymbol{E_\varphi = \sum_\varphi [k_1 (1 - cos\varphi) + k_2 (1 - cos2\varphi) + k_3 (1 - cos3\varphi)]} \quad (3\text{-}13)$$

According to Wilson et al. [129] an out-of-plane angle or improper torsion coordinate arises when the local molecular structure is made of four atoms with three valence

bonds formed to one center atom. The expression describing improper torsion angle (τ) is shown in the equation (78):

$$\boldsymbol{E_{\tau} = \sum_{\tau} k_2\, \tau^2} \tag{3-14}$$

The $E_{cross}$is made of six terms which is a combination of the four types of intramolecular interactions mentioned above:

$$\boldsymbol{E_{cross} = \sum_{b,b'} k(b - b_0)(b' - b_0') + \sum_{\theta,\theta'} k(\theta - \theta_0)(\theta' - \theta_0') + \sum_{b,\theta} k(\theta - \theta_0)(b - b_0) + \sum_{b,\varphi}(b - b_0)[k_1(1 - cos\varphi) + k_2(1 - cos2\varphi) + k_3(1 - cos3\varphi)] + \sum_{\theta,\varphi}(\theta - \theta_0)[k_1(1 - cos\varphi) + k_2(1 - cos2\varphi) + k_3(1 - cos3\varphi)] + \sum_{\theta,\theta,\varphi} k(\theta - \theta_0)(\theta' - \theta_0')cos\varphi} \tag{3-15}$$

Dispersion interactions in a molecule are described by LJ-9-6 function along with repulsion interactions caused by the overlapping electron clouds (Pauli repulsion), which is also referred to as Van der Waals (VdW) interactions:

$$\boldsymbol{E_{vdw} = \sum_{i,j} \epsilon_{ij}[2(\frac{\sigma}{r_{ij}})^9 - 3(\frac{\sigma}{r_{ij}})^6]} \tag{3-16}$$

where σ is the intermolecular distance at equilibrium and ϵ_{ij} is the interaction strength. A 6th-order combination rule [130] is used for unlike atom pairs to calculate the off-diagonal parameters:

$$\boldsymbol{\sigma = (\frac{(r_i^0)^6 + (r_j^0)^6}{2})^{\frac{1}{6}}} \tag{3-17}$$

$$\boldsymbol{\epsilon_{ij} = 2\sqrt{\epsilon_i . \epsilon_j}\left(\frac{(r_i^0)^3 . (r_j^0)^3}{(r_i^0)^6 . (r_j^0)^6}\right)} \tag{3-18}$$

The Coulombic function is used to describe the electrostatic interaction energy (E_Q) as shown in the following equation:

$$\mathbf{E_Q} = \sum_{\mathbf{i,j}} \frac{\mathbf{q_i q_j}}{\mathbf{r_{ij}}} \quad (3\text{-}19)$$

Here $q_i$and q_j are the partial atomic charges on atoms i and j. The partial atomic charges of a molecule are calculated from the charge bond increment, σ_{ij} which describes the charge separation between two valence-bonded atoms i and j [127]. Therefore, the net partial atomic charge on atom i is considered to be the sum of all the charge bond increments as the following:

$$\mathbf{q_i} = \sum_{\mathbf{j}} \boldsymbol{\sigma}_{\mathbf{ij}} \quad (3\text{-}20)$$

Here, j represents all the atoms that are valence bonded with atom i.

3.4. Molecular Dynamics Algorithms

The goal of MD simulation as mentioned before is to generate microstates which are made of positions and velocities of all atoms in each time step. These microstates are obtained by integrating Newton's Second law of motion in time steps (Δt). For this purpose, the finite difference schemes are used. Given a set of initial positions (r_i) and velocities (v_i) at time t, the positions and velocities at time t+Δt are calculated. All atoms are assigned initial velocities according to the Maxwell-Boltzmann distribution at the temperature of interest. Forces on atoms are calculated by the distance-derivative of potential energy function as mentioned before. This force

calculation is the most time-consuming step in the process of obtaining microstates. Usually when integrating the equations of motion we would like to use the largest possible time step. At larger time steps we need to solve fewer equations of motions and use less memory. Obviously, shorter time steps would give us more accurate trajectories but we need more memory to solve the equations of motions. For systems with high temperatures where higher frequency of motion is obtained, we need to consider small time steps. The highest vibration frequency is considered to be around 10^{-14} s (10 femtosecond). If we are interested in creating up to 10 segments for each frequency we should have a time step with a size of about 1 femtosecond. We have used a time step of 1 femtosecond in this thesis.

Velocity Verlet algorithm along with Materials Studio software in this thesis was used to integrate equations of motion as explained in the next section. The Verlet algorithms [131] are the most widely used integration algorithms in the MD simulation. The Verlet algorithm uses positions, accelerations at previous time step to determine new positions. In the velocity Verlet algorithm, for given positions, velocities and accelerations at time t, we can compute:

$$\mathbf{r_i(t+\Delta t) = r_i(t) + v_i(t)\Delta t + \frac{f_i(t)}{2m_i}(\Delta t)^2} \quad (3\text{-}21)$$

$$\mathbf{a_i(t+\Delta t) = \frac{f_i(t+\Delta t)}{m_i}} \quad (3\text{-}22)$$

$$\mathbf{v_i(t+\Delta t) = v_i(t) + \frac{[f_i(t)+f_i(t+\Delta t)]}{2m_i}\Delta t} \quad (3\text{-}23)$$

Generally speaking every integration algorithm should have the following specifications:

1. Fast and require little memory

2. Allow use of a long time step

3. Duplicate classical trajectory as closely as possible

4. Obey energy and momentum conservation

5. Time-reversible

6. Require simple information and should be easy to program

Energy and momentum conservation are described as the following:

1. Conservation of Energy:

$$\mathbf{dH} = \sum_{\mathbf{i}}\left(\frac{\mathbf{dH}}{\mathbf{dp_i}}\mathbf{dp_i} + \frac{\mathbf{dH}}{\mathbf{dq_i}}\mathbf{dq_i}\right) \tag{3-24}$$

Where H is the Hamiltonian, P is momentum and q is position.

$$\frac{\mathbf{dH}}{\mathbf{dt}} = \sum_{\mathbf{i}}\left(\frac{\mathbf{dH}}{\mathbf{dp_i}}\dot{\mathbf{p}}_{\mathbf{i}} + \frac{\mathbf{dH}}{\mathbf{dq_i}}\dot{\mathbf{q}}_{\mathbf{i}}\right) = \sum_{\mathbf{i}}\left(\dot{\mathbf{q}}_{\mathbf{i}}\,\dot{\mathbf{p}}_{\mathbf{i}} - \dot{\mathbf{p}}_{\mathbf{i}}\dot{\mathbf{q}}_{\mathbf{i}}\right) = \mathbf{0} \tag{3-25}$$

2. Conservation of total linear momentum:

$$\mathbf{P} = \sum_{\mathbf{i}} \mathbf{p_i} \tag{3-26}$$

In equations of motion:

$$\dot{\mathbf{q}_i} = \frac{\mathbf{p_i}}{\mathbf{m_i}}, \dot{\mathbf{p}_i} = -\boldsymbol{m_i}\frac{\mathbf{d}\boldsymbol{v_i}}{\mathbf{dt}} = \mathbf{F_i} \quad (3\text{-}27)$$

Therefore, we have:

$$\frac{\mathbf{d}\boldsymbol{p_i}}{\mathbf{dt}} = \dot{\boldsymbol{p}}_{\boldsymbol{i}} = \boldsymbol{F_i} \quad (3\text{-}28)$$

In an isolated system, all forces cancel out; therefore, the total linear momentum is conserved. A MD global algorithm is shown in Figure 3-1.

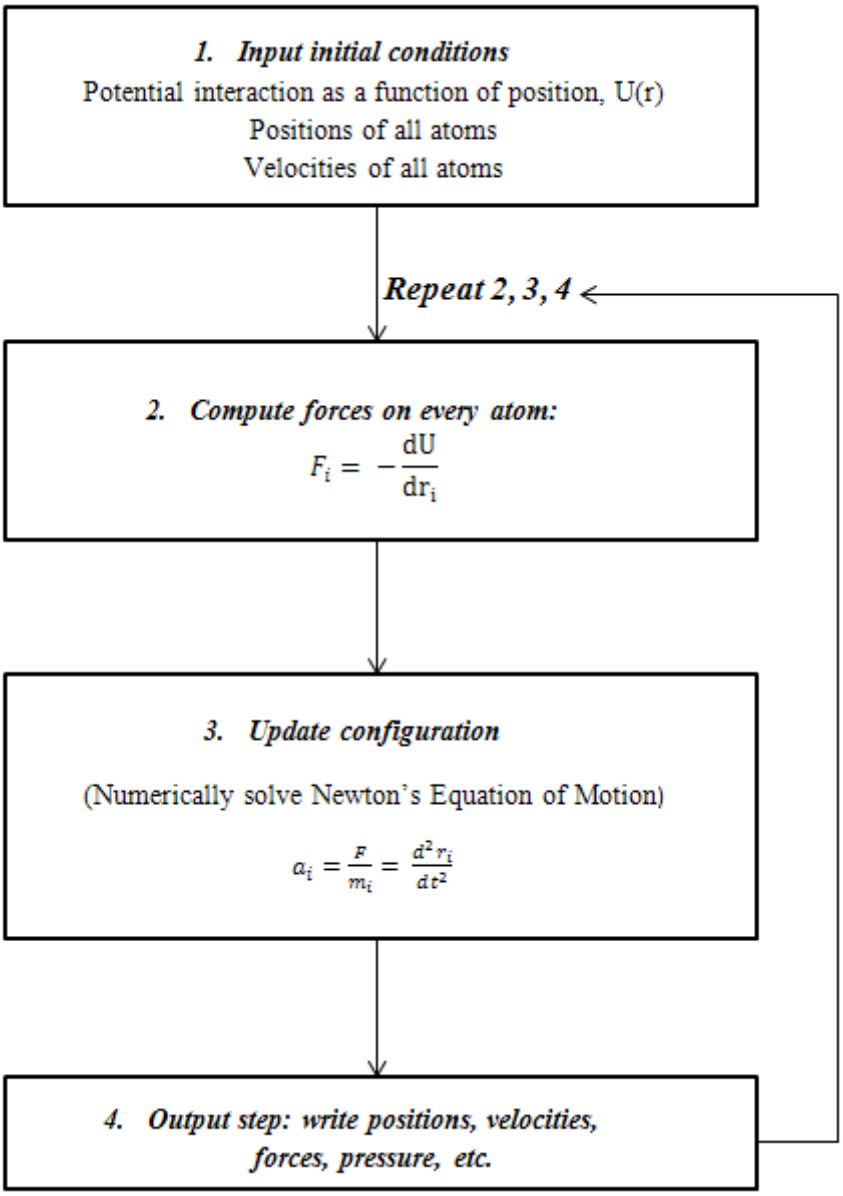

Figure 3-1 MD global algorithm

3.5. Molecular Dynamics in Various Thermodynamic Ensembles

An "ensemble" is the collection of all possible microstates that are consistent with the thermodynamic state of the system. Some examples of ensembles are: "microcanonical" and "canonical" ensembles. The "microcanonical" ensemble is the collection of all microstates with fixed N, V, and E; appropriate for a closed, adiabatic system. The "canonical" ensemble is the collection of all microstates with fixed N,V, and T; in this ensemble, the energy of the microstates can fluctuate; appropriate for a closed system in contact with a heat bath. The canonical ensemble better represents experimental systems where energy of the system changes due to heat exchange with its surroundings. Most common thermodynamic ensembles that represent the experimental conditions are canonical (NVT) or isothermal-isobaric (NPT) ensembles. In such systems, we are able to control either the temperature or pressure of the systems which is what is usually done in experiments. However, to fulfill this goal one would need to reformulate the Newton's equations of motion. This will be discussed in the following sections.

3.5.1. Thermal Coupling

The temperature in MD simulation can be controlled using one of the three options: Velocity re-scaling (Berendsen thermostat), Andersen thermostat, and the extended

Lagrangian form (Nose-Hoover thermostat). We can control a system's temperature by bringing it into contact with a heat bath. By doing so, the system and the bath particles collide with each other and exchange energy, and eventually come into thermal equilibrium with each other. In this situation, the probability of finding the system in a given momentum (p) state is given by the Maxwell-Boltzmann (M-B) distribution:

$$\mathbf{P(p)} = (\frac{\boldsymbol{\beta}}{\mathbf{2\pi m}})^{\frac{3}{2}} \mathbf{exp}\left[\left(-\frac{\boldsymbol{\beta p^2}}{\mathbf{2m}}\right)\right] \quad (3\text{-}29)$$

Thus, we see that the temperature of this system is the variance of this distribution, which is equal to mk_BT.

One way of mimicking the "thermalizing" effect of coupling the system to a heat bath is called the Anderson thermostat [132]. In this approach the coupling is modelled by stochastic thermal forces that act occasionally on randomly chosen particles, taking the system from one constant energy state to another. Between collisions, the dynamics of the system is microcanonical; in other words the total energy of the system between collisions remains constant. The number of collisions in each time interval or time step is decided by the following Poisson distribution:

$$\mathbf{P(t)} = \boldsymbol{\nu}\mathbf{e}^{-\boldsymbol{\nu}\mathbf{t}} \quad (3\text{-}30)$$

where, ν, is the collision frequency between the heat bath and atoms. After collision occurs the new momentum for the atom or molecule is chosen randomly from a

Maxwell-Boltzmann distribution at temperature T. In principal ν can be chosen however there is an optimal choice:

$$\boldsymbol{\nu = \frac{2a\kappa V^{1/3}}{3k_B N}} \tag{3-31}$$

where a, is a dimensionless constant, V is the volume, N is the number of particles, k_B is the Boltzmann constant and $\boldsymbol{\kappa}$ is thermal conductivity.

Another method to control the temperature of system is the Velocity-scaling procedure. This scheme works by scaling the velocities of particles at each time step in order to keep the system temperature constant. However, the natural fluctuations of kinetic energy of the system are suppressed by this method and hence realistic canonical trajectories are not produced. The stochastic methods work by adding a friction term to the Newton's equation of motion. This scheme generates an exactly defined canonical ensemble which is discussed here.

The extended system (ES) method (Nosé-Hoover thermostat) was introduced by Nosé [133,134] and subsequently reformulated by Hoover [135] to eliminate the time scaling so that the trajectories in real time and with evenly spaced time points can be obtained. This is one of the most widely used methods for performing canonical simulations that produces true canonical ensembles. Since this thermostat was used to control temperature in all the simulations described in the present thesis, we briefly review this thermostat algorithm. In this method, an additional (fictitious) degree of freedom to the real physical system is introduced to represent interaction of the system with heat bath. The heat bath mass is considered to be Q, and the magnitude

of this variable determines the coupling between the reservoir and the real system and hence influences the temperature fluctuations. The Lagrangian expression for the total system (heat bath+ real system) is given by:

$$\mathbf{L_{Nose}} = \sum_{\mathbf{i=1}}^{\mathbf{N}} \frac{\mathbf{m_i s^2 \dot{r}^2}}{\mathbf{2}} - \mathbf{U(r^N)} + \frac{\mathbf{Q}}{\mathbf{2}}\mathbf{\dot{s}^2} - \mathbf{(f+1)k_B T ln s} \qquad (3\text{-}32)$$

Where f+1 = 3N+1 is the degrees of freedom for the extended systems and T is the desired temperature. The parameter s represents an extra degree of freedom for the system. The third and fourth terms in the above equation represent the kinetic and potential energy for the heat bath. It is worth noting that when s=1 the original Lagrangian equation is recovered. Introducing the thermodynamic friction coefficient the equations of motion with an extra degree of freedom are recovered as the following:

$$\boldsymbol{\xi} = \mathbf{s}\dot{\mathbf{s}} = \frac{\mathbf{s^2\, p_s}}{\mathbf{Q}} \qquad (3\text{-}33)$$

p_s in the virtual system as a virtual variable is equivalent to the variable "p_i" in the real system.

$$\mathbf{\dot{r}_i} = \frac{\mathbf{p_i}}{\mathbf{m_i}}\,, \qquad \mathbf{Q} = \frac{\boldsymbol{\tau}_\mathbf{T}^\mathbf{2}\mathbf{. T_0}}{\mathbf{4\pi^2}}$$

where τ_T is the period of kinetic oscillations between reservoir and system and is directly related to the reference temperature.

$$\mathbf{\dot{p}_i} = -\frac{\partial \mathbf{U(r^N)}}{\partial \mathbf{r_i}} - \boldsymbol{\xi}\mathbf{p_i} \qquad (3\text{-}34)$$

$$\dot{\xi} = \frac{1}{Q}\left(\sum_{i=1}^{N} \frac{p_i^2}{m_i} - (f+1)k_B T\right) \quad (3\text{-}35)$$

If Q is high, the flow of energy between the physical system and the heat bath will be too slow and consequently, infinite Q corresponds to a NVE MD system where no energy exchange between the heat bath and physical system occurs. On the other hand, if Q is too low, then the energy fluctuations would be too high, causing equilibration problems. If the energy of the extended system is conserved, then the Nosé-Hoover thermostat reproduces the canonical ensemble of the real physical system in every respect.

3.5.2. Pressure Coupling

The physical meaning of pressure can be defined only when the system of interest is inside a container with a specific volume. The container in computer simulations is the unit cell which is subjected to periodic boundary conditions in order to reproduce the bulk system. This type of boundary conditions will be explained in the next section. In MD simulation, in order to control the pressure, the unit cell volume will become a variable which will change during the course of simulation. Constant pressure in an NPT simulation is achieved by the Parrinello-Rahman method. In the same spirit as the temperature coupling, the system can also be coupled to a "pressure bath."

GROMACS supports constant-pressure simulations using the Parrinello-Rahman approach [136], which is similar to the Nose-Hoover temperature coupling. With the

Parrinello-Rahman barostat, the box vectors as represented by the matrix b obey the matrix equation of motion:

$$\frac{db^2}{dt^2} = VW^{-1}\acute{b}^{-1}\left(P - P_{ref}\right) \tag{3-36}$$

V is the volume of the box and W determines the strength of coupling. The matrix P and P_{ref} are the current and reference pressure respectively. The equations of motion for the particles are also changed, just as for the Nose-Hoover coupling. We only show the Parrinello-Rahman modification here:

$$\frac{\mathbf{d^2 r_i}}{\mathbf{dt^2}} = \frac{\mathbf{F_i}}{\mathbf{m_i}} - \mathbf{M}\frac{\mathbf{dr_i}}{\mathbf{dt}} \tag{3-37}$$

$$\mathbf{M} = \mathbf{b^{-1}}\left[\mathbf{b}\frac{\mathbf{db'}}{\mathbf{dt}} + \mathbf{b'}\frac{\mathbf{db}}{\mathbf{dt}}\right]\mathbf{b'^{-1}} \tag{3-38}$$

The (inverse) mass parameter matrix (W^{-1}) determines the strength of the coupling, and how the box can be deformed. The size of the box also determines the coupling strength, and it is calculated automatically in GROMACS by obtaining the approximate isothermal compressibility β and the pressure time constant τ_p in the input file (L is the largest box matrix element):

$$\left(\mathbf{W^{-1}}\right)_{\mathbf{ij}} = \frac{\mathbf{4\pi^2 \beta_{ij}}}{\mathbf{3\tau_p^2 L}} \tag{3-39}$$

3.6. Periodic Boundary Conditions

Periodic boundary conditions are necessary to minimize edge effects in a finite system. The atoms of the system to be simulated are put into a space-filling box, which is surrounded by translated copies of itself (Figure 3-2). Thus there are no boundaries of the system; the artifact caused by unwanted boundaries in an isolated cluster is now replaced by the artifact of periodic conditions. In a crystalline system this type of boundary condition is desired (although motions are naturally restricted to periodic motions with wavelengths fitting into the box). However, if we are interested to simulate non-periodic systems, such as polymer melts, liquids or solutions, this type of boundary condition causes errors.

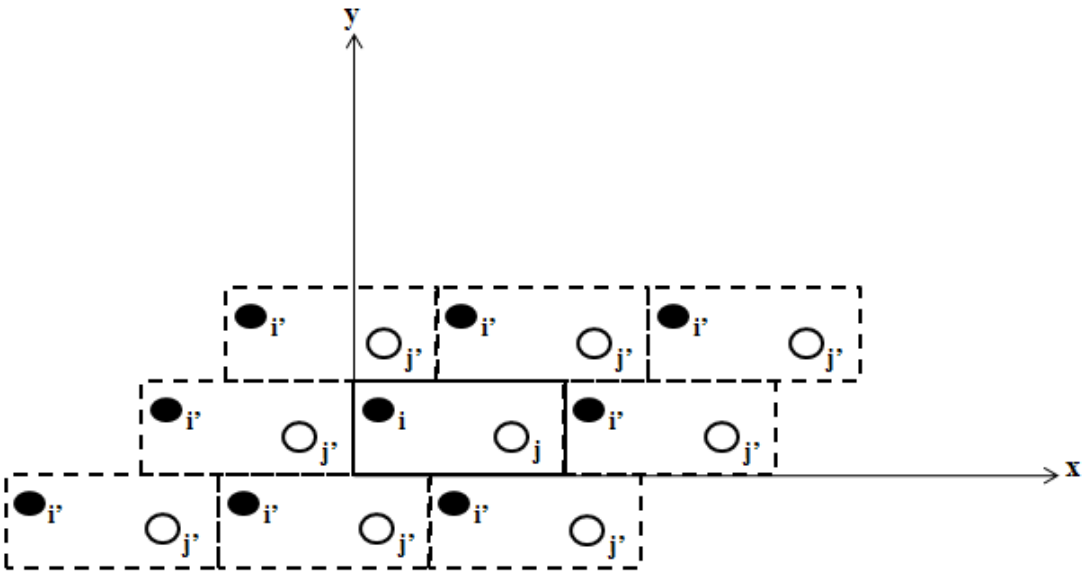

Figure 3-2 Periodic boundary conditions in two dimensions

The particles in the unit cell and the mirror images surrounding the unit cell are free to move in and out of each image cell. The number of particles per cell should remain constant in other words the number of particles moving out of one cell should be equal to the number of particles entering the same cell. The unit cell is defined by the three box vectors a, b, and c which should satisfy the following equations:

$$\mathbf{a_y = a_z = b_z = 0} \tag{3-40}$$

$$\boldsymbol{a_x > 0,\ \ b_y > 0,\ \ c_z > 0} \tag{3-41}$$

$$\mathbf{|b_x| \le \frac{1}{2}a_x,\ |c_x| \le \frac{1}{2}a_x,\ \ |c_y| \le \frac{1}{2}b_y} \tag{3-42}$$

For the calculation of the non-bonded interactions between two neighbor atoms the distance within a spherical volume around one atom in the unit cell is considered for calculations (short-range calculations). Sometimes this assumption causes errors due to neglecting important longer range electrostatic interactions between two atoms. In order to correct this problem the Ewald summation method is often used which will be discussed in the next section.

3.7. Ewald Summation

The Ewald summation method [137] was introduced in 1921 to consider the long-range electrostatic interactions between charged particles and their infinite periodic images surrounding the unit cell. In this method the distance between the charged particles in two periodic images are considered to be greater than the distance

considered for short-range calculations (in a cubic box with length L the distance is considered to be greater than half the box length, so the equation for N charged particles would be the following:

$$\mathbf{U_{electrostatic}} = \frac{\mathbf{1}}{\mathbf{2}}\sum_{\mathbf{n}}'\sum_{\mathbf{i=j=1}}^{\mathbf{N}}\left|\frac{\mathbf{q_i q_j}}{\mathbf{nL+r_{ij}}}\right| \quad (3\text{-}43)$$

The prime indicates that the self-interaction between particles i and j should not be considered when they are in the same periodic image. The equation mentioned here is convergent therefore we can transform the above equation into two convergent equations; the first one is the sum of short-ranged interactions which is treated with a simple cut-off and the second term is periodic which could be described as Fourier series. Therefore we have:

$$\mathbf{U_{ewald}} = \mathbf{U_r} + \mathbf{U_m} + \mathbf{U_0} \quad (3\text{-}44)$$

The second term is obtained by surrounding each point charge with a Gaussian distribution having an opposite sign and the same charge magnitude. Finally a compensating charge density is added to the second term to obtain the original value of potential which ends up forming the above equation. An interaction potential could be written as the sum over k vectors in space:

$$\mathbf{U_m} = \frac{\mathbf{1}}{\mathbf{2}}\sum_{\mathbf{k\neq 0}}\frac{\mathbf{4\pi}}{\mathbf{k^2}}\mathbf{e}^{\frac{\mathbf{-k^2}}{\mathbf{4\alpha}}}|\boldsymbol{\rho}(\mathbf{k})|^{\mathbf{2}} \quad (3\text{-}45)$$

Where α is the inverse length and ρ(k) is given by:

$$\boldsymbol{\rho}(\mathbf{k}) = \sum_{\mathbf{i=1}}^{\mathbf{N}}\mathbf{q_i}\mathbf{e}^{\mathbf{ikr}} \quad \mathbf{(3\text{-}46)}$$

The first term in the Ewald summation equation is calculated based on simple calculation of the Coulomb function except for the fact that the Gaussian distribution (erf$\left|\alpha(r_{ij}+nL)\right|$)considered in the second term should be subtracted from this term (Coulomb function):

$$\mathbf{U_r} = \frac{\mathbf{1}}{\mathbf{2}}\sum_{\mathbf{i\neq j}}^{\mathbf{N}} \frac{\mathbf{q_i q_j}}{\mathbf{r_{ij}}} \frac{\mathbf{erfc}(\boldsymbol{\alpha}|\mathbf{r_{ij}+nL}|)}{|\mathbf{r_{ij}+nL}|} \tag{3-47}$$

where erfc (x) = 1-erf(x) and erf (x) is defined as the following:

$$\mathbf{erf}(\boldsymbol{x}) = \frac{\mathbf{2}}{\sqrt{\boldsymbol{\pi}}}\int_{\mathbf{0}}^{\boldsymbol{x}} \boldsymbol{e}^{-r^2}\, \boldsymbol{dr} \tag{3-48}$$

And finally a self-interaction correction form is introduced:

$$\mathbf{U_0} = -\frac{\boldsymbol{\alpha}}{\sqrt{\boldsymbol{\pi}}}\sum_{\boldsymbol{i=1}}^{\boldsymbol{N}} \boldsymbol{q_i}^{\mathbf{2}} \tag{3-49}$$

4. Molecular dynamics study of the diffusivity of a hydrophobic drug Cucurbitacin B in pseudo polyethylene oxide-b-polycaprolactone micelle environments[2]

4.1. INTRODUCTION

In recent years, nano-sized block-copolymer micelles have been used extensively for the controlled delivery of hydrophobic drugs [138-153]. One major advantage of these nano-sized delivery systems is that they exhibit a long circulation time in the

[2] A version of this chapter has been published. Razavilar, N.; Choi, P. Molecular Dynamics Study of the Diffusivity of a Hydrophobic Drug Cucurbitacin B in Pseudo-poly(ethylene oxide-b-caprolactone) Micelle Environments. Langmuir. 2014, (30) 7798-7803.

blood stream. This is because their size makes it difficult for the liver and the kidney to remove them. Once polymer micelle is injected and exposed to water in the blood stream, water molecules start to diffuse into the micelle followed by the drug molecules diffusing out of the micelles until all drug molecules are exhausted. During this process, micelles are slightly swollen by the water but the structure is more or less intact because the critical micelle concentrations of the block copolymers used in practice are generally very low [154-156]. In the context of designing block copolymer from the drug release kinetics point of view, study of the *in-vivo* release kinetics (i.e., monitoring of the drug concentration in the blood stream upon delivery of the micelles) does not yield local release kinetics of the micelles. In fact, many concurrent physiological processes overshadow the local release kinetics. Therefore, *in-vitro* studies are frequently used for the block copolymer design purpose. Obviously, the effectiveness of a newly designed block copolymer still needs to be confirmed by *in-vivo* studies. In *in-vitro* studies, the amount of drug released from micelles to water over a period of time is monitored. In the case of the drug being encapsulated by a polymer thin film with micron thickness, continuum kinetic models are typically used to fit such experimental data to understand the underlying diffusion mechanism [157-159]. Such approach has also been used for nano-sized micelles despite the fact that continuum models are obviously not suitable. For example, concentration gradients are difficult to be defined as a result of the inherent concentration fluctuations existing in such small systems [160].Regardless of the geometry of the delivery systems (micron-sized thin film or nano-sized micelles), such continuum models require the knowledge of the

diffusivity of the drug in the presence of water. Measurement of the mutual diffusivity of such systems, especially in the case of micelles, is not a trivial task. For instance, to measure diffusion coefficients of small molecules in polymers, the technique of pulsed-field gradient nuclear magnetic resonance (PFG-NMR) technique is commonly used [161]. However, the technique cannot be readily extended to micelles. Given the limitation of the current experimental techniques, molecular dynamics simulation offers a valuable alternative to study the dynamics of such nano-sized systems. Nonetheless, in order to simulate micelles at the atomistic level, it is computationally very expensive simply because a micelle normally contains more than hundred thousands of atoms (it contains tens of block copolymers, tens of drug molecules and tens of thousands of water molecules). Therefore, in the current study, instead of simulating the entire micelle, we considered only a small part of a micelle to mimic the micelle environment in the presence of water at various concentrations (i.e., different degrees of swelling). Figure 4-1illustrates such a system in which concentration of the drug is about 10 wt%, a concentration comparable to that of the corresponding experimental system.

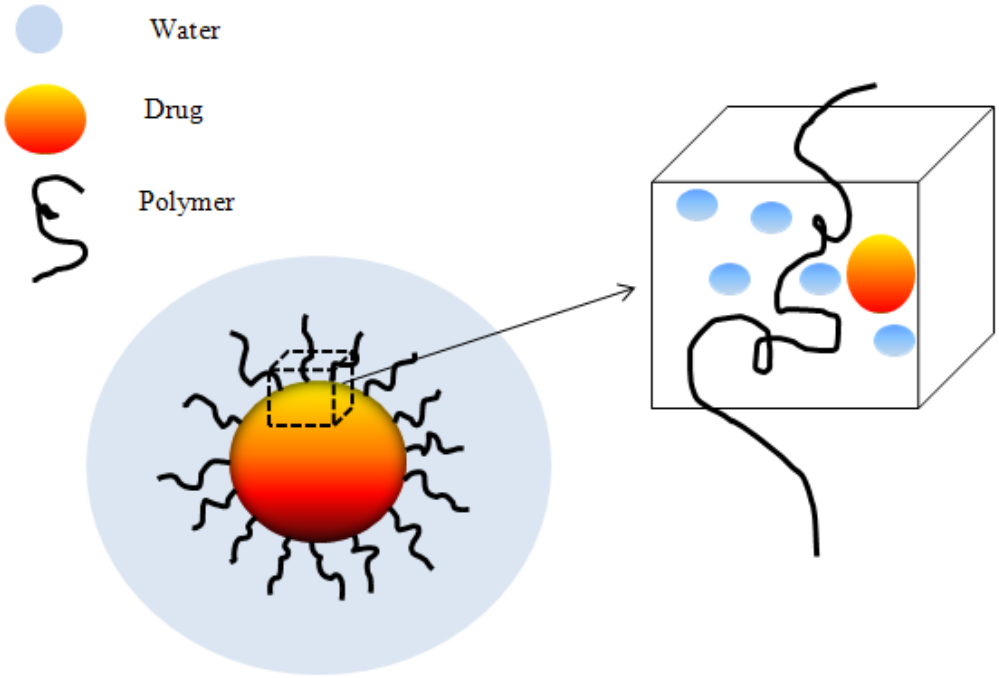

Figure 4-1 A schematic representation of a portion of a micelle using a simulation unit cell subjected to three-dimensional periodic boundary conditions.

In this work, we will study the diffusivity of a cancer drug namely Cucurbitacin B (CuB) in two pseudo micelle environments formed by two model block copolymers made up of blocks of polyethylene oxide (PEO) and polycaprolactone (PCL) but with different architectures. Different amounts of water were used to mimic different degrees of swelling induced by water.

4.2. Models and simulation method

As mentioned, two model block copolymers made up of PEO and PCL blocks were used. As shown in Figure 4-2, the first model contained a PEO block and a PCL block with each block having a molecular weight of 2,500 g/mol while the second one had a branched configuration in which three PCL blocks with approximately equal chain length were connected to one end of the PEO block, hereafter referred to as PEO-*b*-3PCL. In the case of PEO-*b*-3PCL, the PEO block had a molecular weight of 2,500 g/mol and the three PCL blocks had a total molecular weight of 2,500 g/mol. Cucurbitacin B (CuB), a hydrophobic cancer drug with a molecular weight of 558 g/mol, was used (see Figure 4-2).

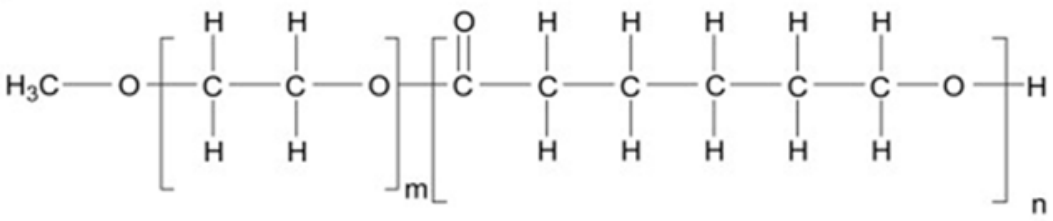

(A)

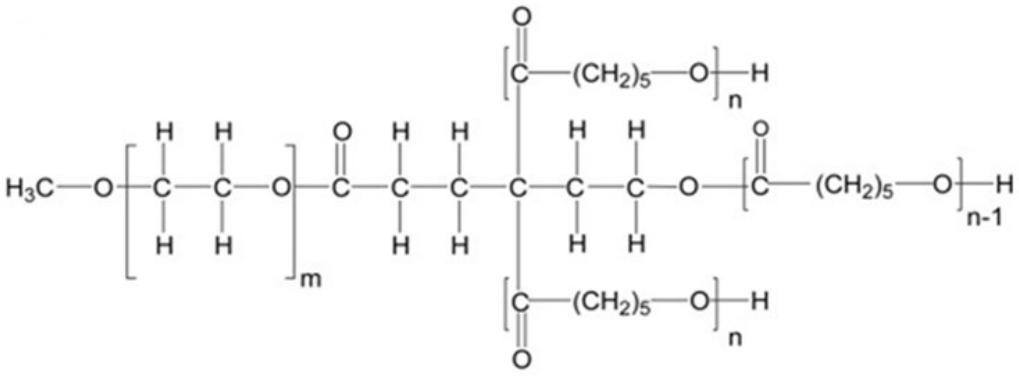

(B)

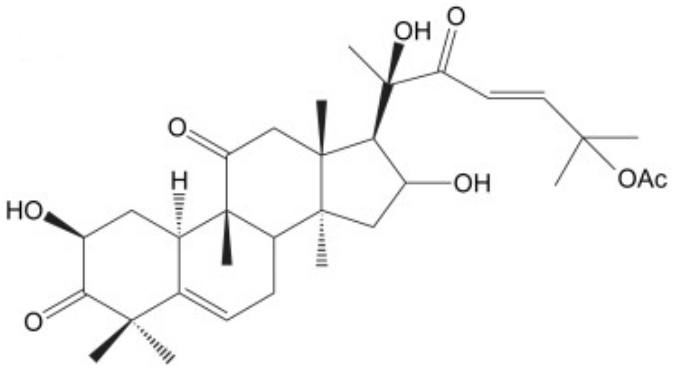

(C)

Figure 4-2 Chemical structures of PEO-*b*-PCL (A), PEO-*b*-3PCL (B), and Cucurbitacin B (CuB) (C)

The rationale for studying the CuB release kinetics in PEO-*b*-PCL and PEO-*b*-3PCL with the same total molecular weight was that our previous work showed that the branched configuration exhibits more favourable interactions with CuB (hydrogen bonds in particular) than the linear one, thereby encapsulating more CuB [160]. It is of interest to determine whether CuB would exhibit difference in its diffusivity in the two configurations.

As mentioned, simulation of the entire micelle is prohibitively expensive with the currently available computer resources. Therefore, we only modeled a portion of a micelle. In particular, we constructed an amorphous unit cell containing one block copolymer molecule and one CuB molecule and the unit cell was subjected to three-dimensional periodic boundary conditions. We constructed such models using commercial software (Materials Studio) according to the procedure described by Theodorou and Suter [162]. The method is particularly designed to generate bulk amorphous structure. However, owing to the amphiphilic nature of the copolymer, the resultant structure resembled somewhat the conformation of a block copolymer in a micelle. We refer this structure to as a pseudo micelle environment that would give us insight into how intermolecular interactions between various molecules affect the drug diffusivity. It is worth noting that there is experimental evidence showing that the PEO block is amorphous in the corona while the PCL block is crystalline in the core [163]. Given the procedure we used to generate the pseudo micelle environment, it was impossible to construct a crystalline core. As a result, the PCL block was also in the amorphous phase. However, as one can imagine, when

the water and drug molecules diffusing in and out of the core, respectively, some of the crystalline phase would turn into the amorphous phase to allow the penetrants to diffuse, as diffusion does not occur in the crystalline phase. Lack of crystallinity in our models might lead to the overestimation of the diffusivity of CuB and water. To introduce swelling to the systems, different amounts of water molecules were added. We used the simplest water model namely rigid simple point charge (SPC) model for the water molecules, as the concentration of water of interest was low [164].

The pseudo micelle unit cell was constructed in the following procedure. First, a cubic unit cell containing the block copolymer of interest that was subjected to three-dimensional periodic conditions was constructed. A single Cucurbitacin B molecule was then inserted into the unit cell at a random location. Sizes of the unit cells of PEO-*b*-PCL and PEO-*b*-3PCL were 1.95 nm × 1.95 nm ×1.95 nm and 2.17 nm × 2.17 nm × 2.17 nm, respectively, corresponding to the same density value of 1,000 kg/m^3. Once the pseudo micelle models were set up, energy minimization was carried out using the steepest descent method to remove high-energy overlaps. We then carried out isobaric-isothermal (NPT) molecular dynamics (MD) simulations at 310 K (body temperature) and 1 bar using GROMACS along with its GROMOS96 force field for about 5 ns to equilibrate the systems to the corrected density. GROMOS96 was chosen, as it is a condensed-phase force field and suitable for systems with organic liquids, solutions and crystals (more details below). The simulation temperature used was significantly higher than the glass transition temperatures of the PEO and PCL blocks (-60 ^oC). We used Nose-Hoover coupling

[165,166] to control the temperature and the Parrinello-Rahman [167] approach to control the pressure, respectively. The leap-frog Verlet algorithm along with a time step of 1 femtosecond (fs) was used to integrate the Newtonian equations of motion [168,169]. The data was stored every picosecond (ps). After the 5 ns NPT MD annealing, various amounts of water molecules were inserted into the system to create 6 systems for each block copolymer. The corresponding water concentrations were 0.32, 1.63, 3.26, 4.89, 6.53 and 8.16 wt%. Once again, energy minimization was carried out on the systems after the water insertion.

For each system, a total of 10 NPT MD simulations with different initial positions of CuB and water molecules were carried out to obtain better statistics. Each MD simulation, once again, was carried out at 310 K (body temperature) and 1 bar over a period of 100 ns, which should be long enough to obtain reliable diffusion data (see Results and Discussion). The simulation box size increased, on average, from 3.1 × 3.1 × 3.1 nm^3 (0.32 wt% water) to 4.5 × 4.5 × 4.5 nm^3 (8.16 wt% water).

In the GROMOS96 force field, there are two types of potentials describing the interaction between atoms. One is the bonded potential and the other is the non-bonded potential. The bonded potential is described by the following equation:

$$\boldsymbol{V(r) = \sum \frac{1}{4} K_1 [b_n^2 - b_{n0}^2]^2 + \sum \frac{1}{2} K_2 [\cos \theta_n - cos\theta_{n0}]^2 + \sum \frac{1}{2} K_3 [\xi_n - \xi_{n0}]^2 + \sum K_4 [1 + cos(\delta_n) \cos(m_n \varphi_n)]} \quad (4\text{-}1)$$

The bonded potential has four terms and K_1 to K_4 are the four force constants. The first term signifies the force associated with the change of the covalent bond length. The second term originates from the angle between two neighbouring bonds. The third term corresponds to the potential change of the dihedral angles while the fourth term improper dihedral angles. The non-bonded potential can be specified by the following equation:

$$\mathbf{V(r)} = \sum\{[\frac{\mathbf{C12_{ij}}}{\mathbf{r_{ij}^6}} - \mathbf{C6_{ij}}]\frac{\mathbf{1}}{\mathbf{r_{ij}^6}} + \frac{\mathbf{q_i q_j}}{\mathbf{4\pi\varepsilon_0\varepsilon_1}}\frac{\mathbf{1}}{\mathbf{r_{ij}}} + \mathbf{V^{RF}}(\mathbf{r_{ij}}, \mathbf{q_i}, \mathbf{q_j}, \mathbf{R_{RF}}, \boldsymbol{\varepsilon_1}, \boldsymbol{\varepsilon_2}, \mathbf{k})\} \qquad (4\text{-}2)$$

The non-bonded potential includes three terms. The first term denotes the van der Waals interaction. And $C12_{ij}$ and $C6_{ij}$ are the van der Waals interaction constants. The second term corresponds to the electrostatic potential and q_i and q_j are the partial atomic charges. The third term is the electrostatic interactions by Poisson-Boltzmann generalized reaction field term. For all types of interactions, a cut off distance of 1 nm was used to reduce computational efforts.

To quantify the diffusivity of CuB and water molecules in the pseudo micelle environment, we used the well-known Einstein's equation as shown below to calculate their self-diffusion coefficients.

$$\mathbf{D} = \frac{\mathbf{1}}{\mathbf{6}}\frac{\mathbf{d}\left(\langle\frac{\mathbf{1}}{\mathbf{N}}\sum(\vec{\mathbf{r}}_\mathbf{i}(\mathbf{t}) - \vec{\mathbf{r}}_\mathbf{i}(\mathbf{0}))^\mathbf{2}\rangle\right)}{\mathbf{dt}} \qquad (4\text{-}3)$$

Here $\langle\frac{1}{N}\sum(\vec{r_i}\,(t) - \vec{r_i}(0))^2\rangle$ is the mean square displacement (MSD) of the penetrant molecules.

4.3. Results and discussion

Diffusion coefficients of CuB and water were calculated based on the slope of the regressing lines fitted through the portion of the MSD plots in which the slope of log (MSD) vs. log t was equal to 1 (i.e., Einstein diffusion). The Einstein region started at around 60 ns for CuB. Obviously, the MSD values signify the distances that CuB and water molecules travel through the free volume holes formed by the block copolymers.

Table 4-1summarize the computed self-diffusion coefficients of CuB and water in PEO-*b*-PCL and PEO-*b*-3PCL, respectively, at various water concentrations. All data reported in the tables correspond to means of 10 MD simulations using different initial positions of CuB and water molecules. In Table 4-2 and Table 4-3, we also show the data on the mean numbers of hops per ns and mean hopping distances for the water molecules. This is because the water molecules were observed to exhibit a "hopping" diffusion mechanism while CuB did not.

Table 4-1 Computed self-diffusion coefficients of CuB in PEO-*b*-PCL and PEO-b-3PCL at 310 K at different water concentrations.

System	Water concentration wt%	self-diffusion coefficient of CuB in PEO-*b*-PCL $\times 10^8$ cm^2/s	self-diffusion Coefficient of CuB in PEO-*b*-3PCL $\times 10^8$ cm^2/s
1	0.32	2.5 ± 0.3	1.3 ± 0.3
2	1.63	2.0 ± 0.5	0.8 ± 0.1
3	3.26	2.2 ± 0.4	1.0 ± 0.5
4	4.89	2.3 ± 0.2	1.0 ± 0.1
5	6.53	2.0 ± 0.3	0.9 ± 0.1
6	8.16	2.4 ± 0.4	1.1 ± 0.3

Table 4-2 Computed self-diffusion coefficients, mean numbers of hops per 1 ns and mean hopping distances of water in PEO-*b*-PCL at 310 K at various water concentrations.

System	Water concentration wt%	self-diffusion coefficient of water in PEO-*b*-PCL $\times 10^5$ cm^2/s	Mean number of hops per 1 ns	Mean hopping distance Nm
1	0.32	3.2 ± 0.7	18.0 ± 0.3	1.5 ± 0.1
2	1.63	1.5 ± 0.8	10.0 ± 0.5	1.3 ± 0.3
3	3.26	1.2 ± 0.8	11.0 ± 0.5	1.3 ± 0.2
4	4.89	1.0 ± 0.6	10.0 ± 0.4	1.0 ± 0.1
5	6.53	1.0 ± 0.5	9.0 ± 0.5	1.4 ± 0.3
6	8.16	0.8 ± 0.3	9.0 ± 0.3	1.0 ± 0.1

Table 4-3 Computed self-diffusion coefficients, mean numbers of hops per 1 ns and mean hopping distances of water in PEO-*b*-3PCL at 310 K at various water concentrations.

System	Water concentration wt%	self-diffusion coefficient of water in PEO-*b*-3PCL $\times 10^5$ cm^2/s	Mean number of hops per 1 ns	Mean hopping distance Nm
1	0.32	1.5 ± 0.6	10 ± 0.3	1.5 ± 0.5
2	1.63	0.8 ± 0.5	7.0 ± 0.5	1.3 ± 0.2
3	3.26	0.8 ± 0.4	7.0 ± 0.7	1.3 ± 0.1
4	4.89	0.7 ± 0.4	6.0 ± 0.5	1.2 ± 0.1
5	6.53	0.7 ± 0.5	6.0 ± 0.5	1.3 ± 0.2
6	8.16	0.7 ± 0.3	5.0 ± 0.3	1.3 ± 0.1

In fact the diffusion of CuB depended on the wriggling motion of the block copolymer chains. This explains why the self-diffusion coefficients of CuB (10^{-8} cm^2/s) are three orders of magnitude lower than those of water (10^{-5} cm^2/s). The simulation results showed two obvious trends. First, diffusivity of CuB and water in PEO-*b*-3PCL is about 50% of that in PEO-*b*-PCL. Secondly, diffusivity of CuB is more or less independent of water concentration while that of water decreases with increasing water concentration. The above observation is probably attributed to a well-known fact in the polymer literature that a branched polymer diffuses through an arm retraction mechanism (slow) while their linear counterpart diffuses through a reptation mechanism (relatively faster) [170]. Therefore, mobility of the branched polymer is lower than that of the linear polymer with the same molecular weight. In

the context of the present work, the lower mobility of PEO-*b*-3PCL, compared to PEO-*b*-PCL, would slow down the rate of free volume redistribution, thereby decreasing the diffusivity of CuB and water (lowering the number of hops in the case of water). In fact, Table 4-2 and Table 4-3 show that the mean numbers of hops per ns for water in PEO-*b*-PCL are much higher than those of PEO-*b*-3PCL.

The above results on the water diffusivity are also consistent with those of Zhou and Choi [171]. In particular, they studied the effect of water concentration on its diffusivity in two types of polyurethanes of which one is swollen by water while the other is not. They found that the diffusivity of water in the polyurethane that can be swollen by water decreased with increasing water concentration and suggested that the observed trend was attributed to the intermolecular hydrogen bonds formed between water molecules and the polymer (higher activation energy for hopping). It seems that the intermolecular hydrogen bonds (see hydrogen bond data shown in Table 4-4 and Table 4-5) may be one of the factors contributing to the observed difference in the water diffusivity of the two block copolymers.

To quantify the effect of hydrogen bonds, we calculated mean numbers of hydrogen bonds that CuB and water formed with respective blocks of the two copolymers. Table 4-4 and Table 4-5 show the corresponding data. Here, the hydrogen bond is defined based upon a geometric criterion in which a hydrogen bond exists if the hydrogen bond donor-acceptor angel is greater than 135˚ and distance between the donor and acceptor is below 3Å. The results were obtained using the average of the last 5 ns of each simulation and that of the 10 MD simulations of the

same system. Table 4-4 shows that mean numbers of hydrogen bonds between CuB and the PCL block(s) are

Table 4-4 Computed mean numbers of hydrogen bonds per ns formed between CuB and PEO-*b*-PCL and PEO-*b*-3PCL, respectively, at various water concentrations at 310 K.

System	Water concentration wt%	Mean number of hydrogen bonds between CuB and PEO-*b*-PCL PCL block (top) PEO block (bottom)	Mean number of hydrogen bonds between CuB and PEO-*b*-3PCL PCL blocks (top) PEO block (bottom)
1	0.32	0.05 ± 0.005 0.02 ± 0.004	0.06 ± 0.003 0.03 ± 0.006
2	1.63	0.04 ± 0.005 0.03 ± 0.005	0.07 ± 0.006 0.04 ± 0.005
3	3.26	0.04 ± 0.003 0.02 ± 0.003	0.06 ± 0.004 0.04 ± 0.005
4	4.89	0.05 ± 0.006 0.04 ± 0.004	0.06 ± 0.005 0.04 ± 0.003
5	6.53	0.05 ± 0.005 0.04 ± 0.003	0.06 ± 0.005 0.05 ± 0.004
6	8.16	0.04 ± 0.004 0.04 ± 0.004	0.06 ± 0.005 0.05 ± 0.005

Table 4-5 Computed mean numbers of hydrogen bonds per ns formed between water and PEO-*b*-PCL and PEO-*b*-3PCL, respectively, at various water concentrations at 310 K.

System	Water concentration wt%	Mean number of hydrogen bonds between water and PEO-*b*-PCL PCL block (top) PEO block (bottom)	Mean number of hydrogen bonds between water and PEO-*b*-3PCL PCL blocks (top) PEO block (bottom)
1	0.32	0.01 ± 0.003 0.03 ± 0.003	0.02 ± 0.007 0.04 ± 0.003
2	1.63	0.03 ± 0.005 0.09 ± 0.005	0.06 ± 0.006 0.12 ± 0.05
3	3.26	0.04 ± 0.004 0.13 ± 0.05	0.07 ± 0.005 0.14 ± 0.02
4	4.89	0.04 ± 0.006 0.13 ± 0.05	0.07 ± 0.004 0.15 ± 0.03
5	6.53	0.05 ± 0.006 0.13 ± 0.04	0.08 ± 0.004 0.15 ± 0.02
6	8.16	0.05 ± 0.006 0.14 ± 0.04	0.08 ± 0.005 0.15 ± 0.02

higher than those between CuB and PEO block at all water concentrations, indicating that CuB preferred the PCL block(s). The total number of hydrogen bonds in the case of PEO-*b*-3PCL is higher than that of PEO-*b*-PCL which is consistent with the observation that diffusivity of CuB in PEO-*b*-PCL is higher. As Table 4-6 shows, the PEO block in both block copolymers was probably fully hydrated when water concentration was above 3.26 wt%, as the mean number of hydrogen bonds between

water and the PEO block leveled off at the aforementioned water concentration. Nevertheless, there were still water molecules hydrating the PCL block(s) even at water concentrations below 3.26 wt%, indicating that water molecules moved through both PEO and PCL phases. As mentioned earlier, the self-diffusion coefficients of CuB and water in PEO-*b*-3PCL are about 50% of those of PEO-*b*-PCL at the same water concentration. The data in Table 4-4 and Table 4-5 show, mean numbers of hydrogen bonds in the case of PEO-*b*-PCL are not 50% of those of PEO-*b*-3PCL. This confirms that the chain mobility, as discussed before, plays an important role in influencing the diffusivity of CuB and water.

In addition to the chain mobility and hydrogen bond effect, we further analyzed the data to check there were differences in the degrees of swelling of the block copolymers. In particular, we calculated their swelling factor that is defined as the ratio of the fractional volume change over the fractional mass change at a given water concentration. Table 4-6 shows the corresponding results. It is clear that both PEO-*b*-PCL and PEO-*b*-3PCL swell even at very low water concentrations and the swelling factor levels off at about 2 wt% water. Nevertheless, PEO-*b*-PCL swells about 20% more than PEO-*b*-3PCL. It seems that difference in the swelling factors also contribute to the difference in the diffusivity of CuB in PEO-*b*-PCL and PEO-*b*-3PCL.

Table 4-6 Degrees of swelling of PEO-*b*-PCL and PEO-*b*-3PCL at 310 K.

System	Water concentration wt%	Swelling factor of PEO-*b*-PCL	Swelling factor of PEO-*b*-3PCL
1	0.32%	2.5	2
2	1.63%	2	1.5
3	3.26%	1.6	1.4
4	4.89%	1.5	1.3
5	6.53%	1.5	1.2
6	8.16%	1.5	1.2

The radius of gyration (R_g) data of the PEO and PCL blocks as a function of time support the swelling data. Such data are shown in the Additional Information section. For clarity, we only provide data of two water concentrations (3.26 and 8.16 wt%) for both block co-polymer configurations (Figure A 1- Figure A 8). It is obvious from the figures that at both water concentrations, the PEO block of PEO-*b*-PCL exhibits a larger R_g than that of PEO-*b*-3PCL even though the PEO block is linear. This is consistent with the expectation that R_g of a branched polymer is smaller than that of a linear polymer with the same total molecular weight. At higher water concentration, the PEO block tends to have higher mobility. This is because water acts like a plasticizer helping the rotation of the skeletal bonds of the PEO block [172]. As expected, the R_g fluctuations of PEO-*b*-3PCL are smaller than those of PEO-*b*-PCL. The trend of the R_g of the PCL block is similar to that of the PEO block.

We also analyzed the normalized velocity autocorrelation functions (VACF) of CuB and water molecules, respectively, in PEO-*b*-PCL and PEO-*b*-3PCL over the last 1 ns of the 100 ns MD simulation. They are shown in the Additional Information Section (Figure A 9- Figure A 12). The reason that we only examine the VACF over a period of 1 ns out of a 100 ns MD simulation is that most of the time, velocities of CuB and water de-correlate (to approximately 0) within 1 ns. This is an indication that 100 ns MD simulation is long enough for the present systems. Also, at equilibrium, any 1 ns VACF within the 100 ns MD simulation, except those in the first few ns, resemble each other. Before analyzing the figures, it is worth noting that the fluctuations of the VACF (velocity sign reversal) signify the collision motion of the penetrant in the free volume holes (i.e., cages) formed by the block copolymers. According to the VACF results, CuB exhibited a much higher frequency collision motion in PEO-*b*-3PCL than in PEO-*b*-PCL suggesting that the cages formed by PEO-*b*-3PCL are more rigid than those by PEO-*b*-PCL. And the difference in the frequencies is rather insensitive to the water concentration. This is consistent to the diffusivity data discussed earlier. However, water concentration (i.e., degree of swelling) seems to affect the de-correlation time (longer de-correlation time in PEO-*b*-PCL). However, there exists somewhat opposite behavior for water. In particular, water at low concentrations exhibited higher frequency collision motion. This may be due to the fact that there exist higher numbers of hydrogen bonds at higher water concentrations as shown in previous tables.

One final comment is that swelling encountered in a block copolymer micelle is different from that of a polymer thin film. As one can conceive, correlating the diffusivity of a drug in a swelling micelle (such as the results obtained in the present work) to the macroscopically observed drug fractional release profile is not trivial. And such a correlation is yet to develop. Nevertheless, Mirzazadeh *et al* [173]. have carried out in-vitro release studies for naltrexone hydrochloride from block-copolymer micelles at 37 °C under perfect sink conditions and they observed that the fractional drug release is related to the square root of time and concluded that drug release from their system was "Fickian". On the other hand, Wang et al [174] observed another form of time dependency of the fractional drug release for micelles. Obviously, further research work is needed to determine the time dependence of drug release for micelles.

4.4. Conclusions

We used isobaric-isothermal molecular dynamics simulation to study the diffusivity of a hydrophobic drug namely Cucurbitacin B (CuB) in pseudo micelle environments that were made up of individual block copolymers containing PEO and PCL blocks with different configurations swollen by different amounts of water. Regardless of the configuration of the block copolymer, it was found that the diffusivity of CuB was insensitive to the water concentration while the water diffusivity decreased with increasing water concentration. However, the diffusivity of both CuB and water in

PEO-*b*-PCL is about twice of that in PEO-*b*-3PCL. The combined effect of slower chain dynamics, more intermolecular hydrogen bonds and lower degree of swelling explains the slower dynamics in PEO-*b*-3PCL. Velocity auto-correlation functions of CuB and water are consistent with the above findings. However, it is interesting to note that CuB exhibited higher frequency collision motion in PEO-*b*-3PCL than in PEO-*b*-PCL while water showed similar behavior at lower water concentrations. Finally, it should be pointed out that the diffusivity obtained from the present work is not suitable to be used for conventional continuum drug release models to determine the *in-vitro* fractional drug release curve.

4.5. Supporting Information for Publication

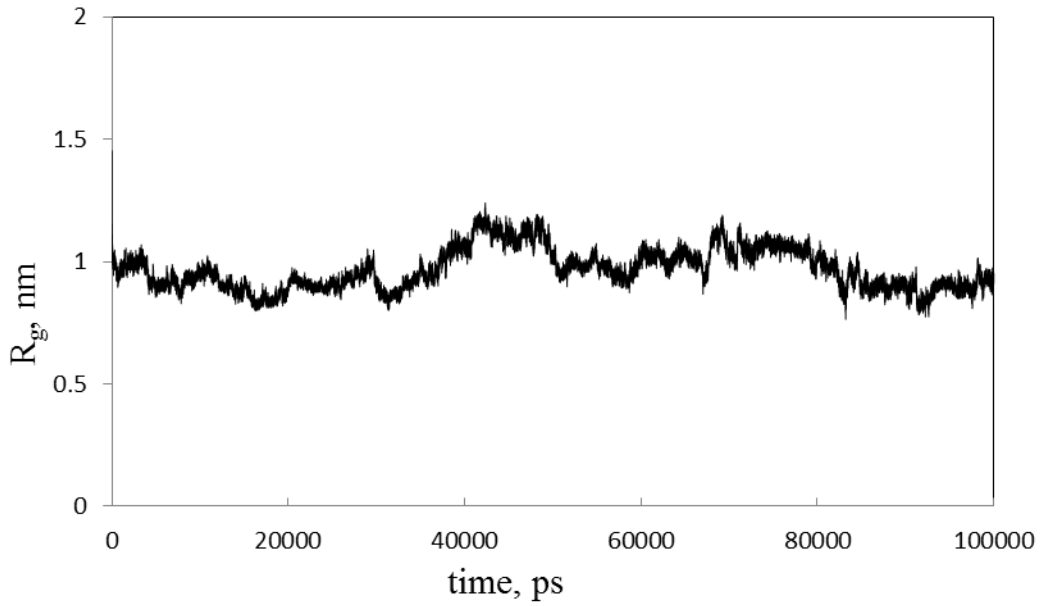

Figure A 1 Radius of gyration of the PEO block of PEO-*b*-PCL (3.26 wt% water).

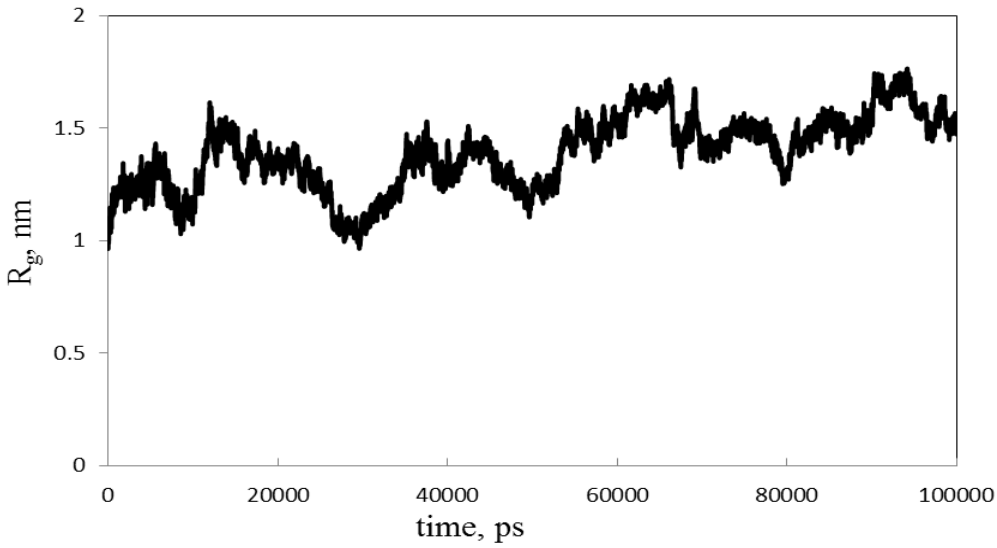

Figure A 2 Radius of gyration of the PEO block of PEO-*b*-PCL (8.16 wt% water)

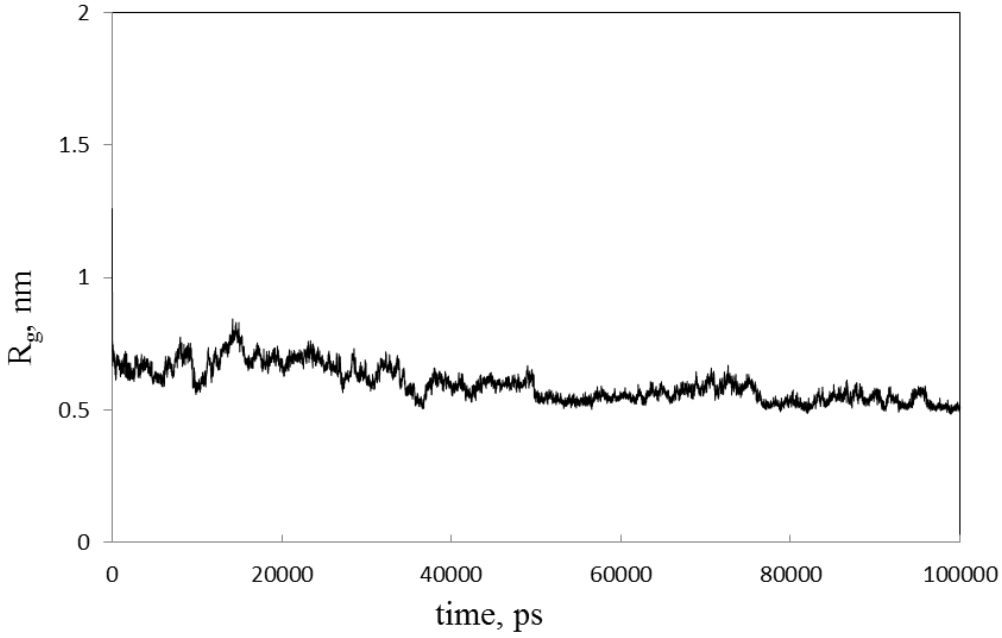

Figure A 3 Radius of gyration of the PEO block of PEO-*b*-3PCL (3.26 wt% water).

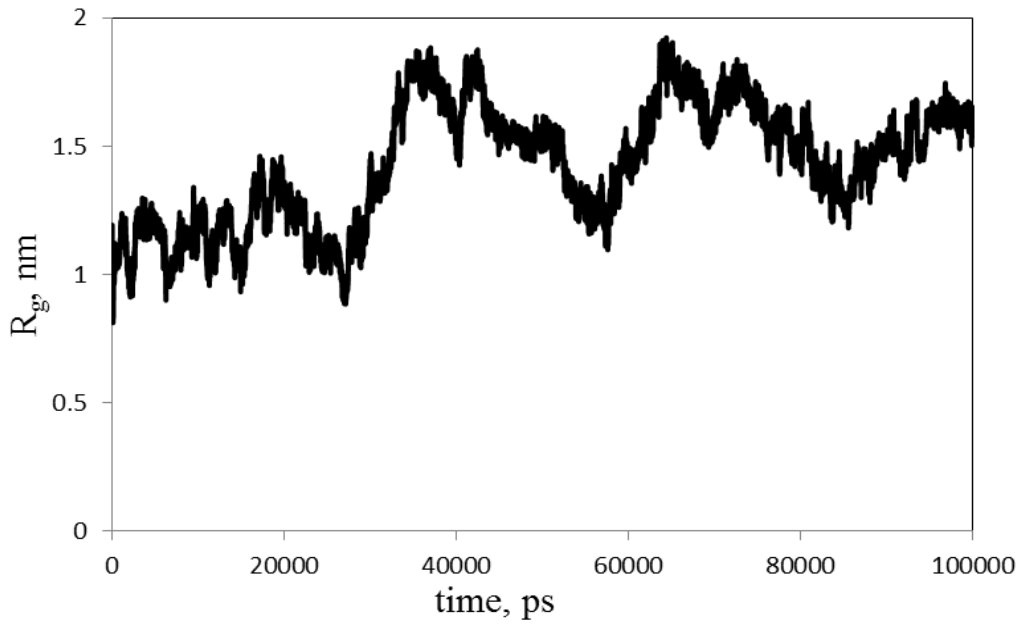

Figure A 4 Radius of gyration of the PEO block of PEO-*b*-3PCL (8.16 wt% water)

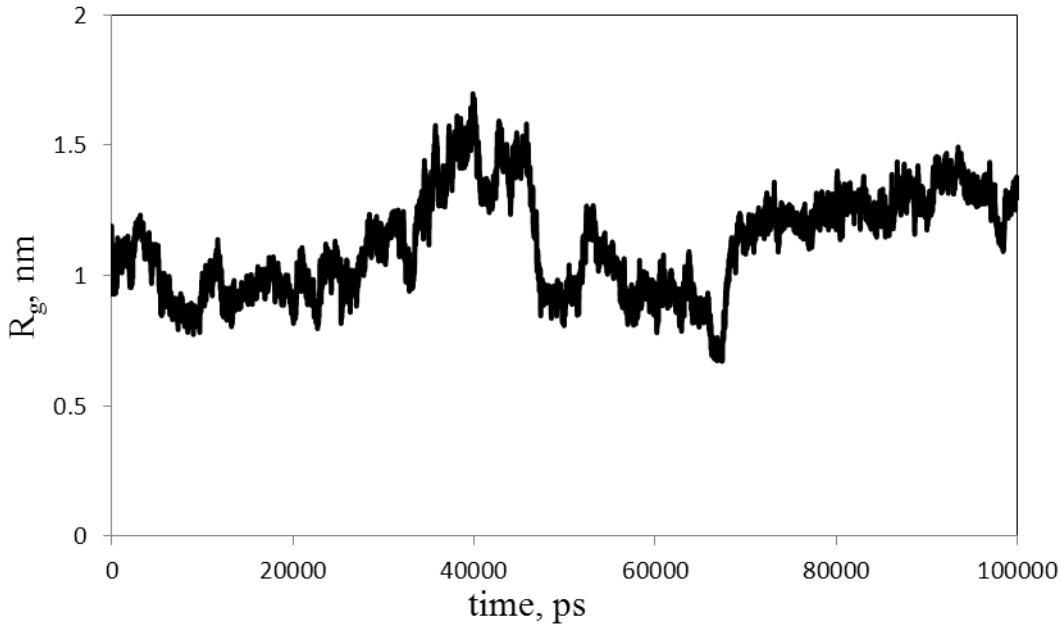

Figure A 5 Radius of gyration of the PCL block of PEO-*b*-PCL (3.26 wt% water).

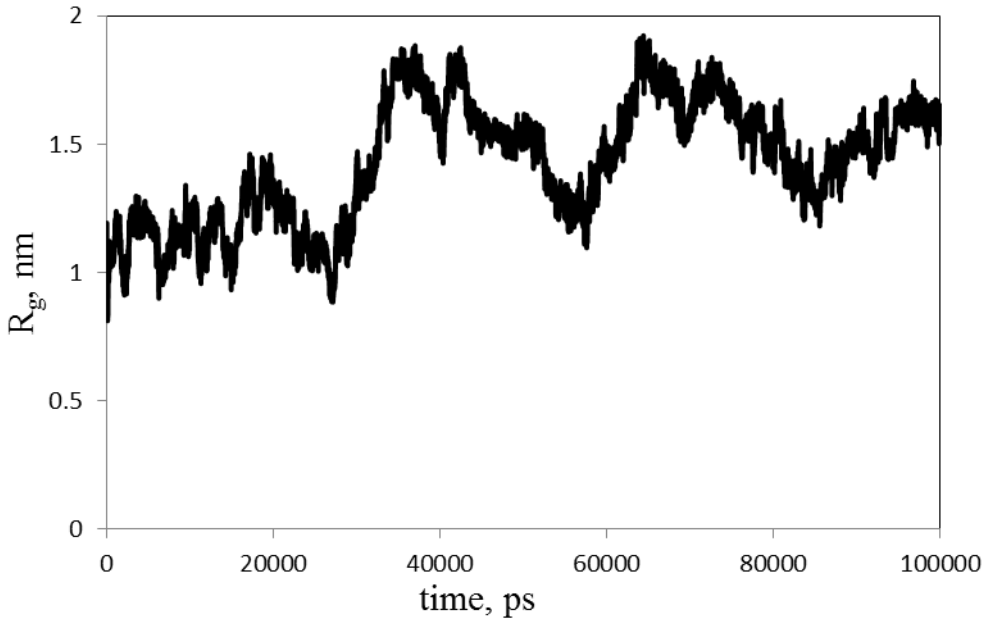

Figure A 6 Radius of gyration of the PCL block of PEO-*b*-PCL (8.16 wt% water).

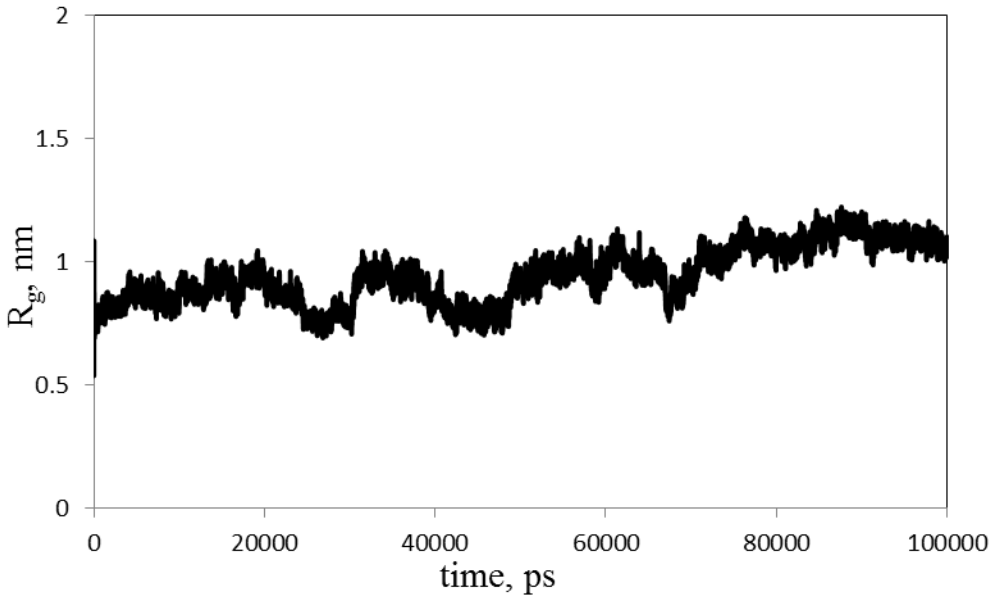

Figure A 7 Radius of gyration of the PCL blocks of PEO-*b*-3PCL (3.26 wt% water).

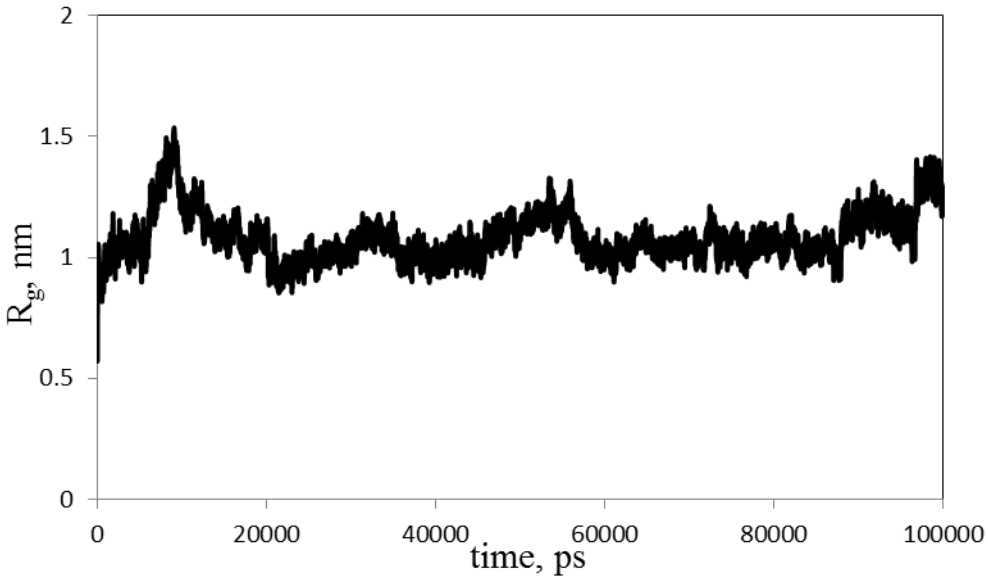

Figure A 8 Radius of gyration of the PCL blocks of PEO-*b*-3PCL (8.16 wt% water).

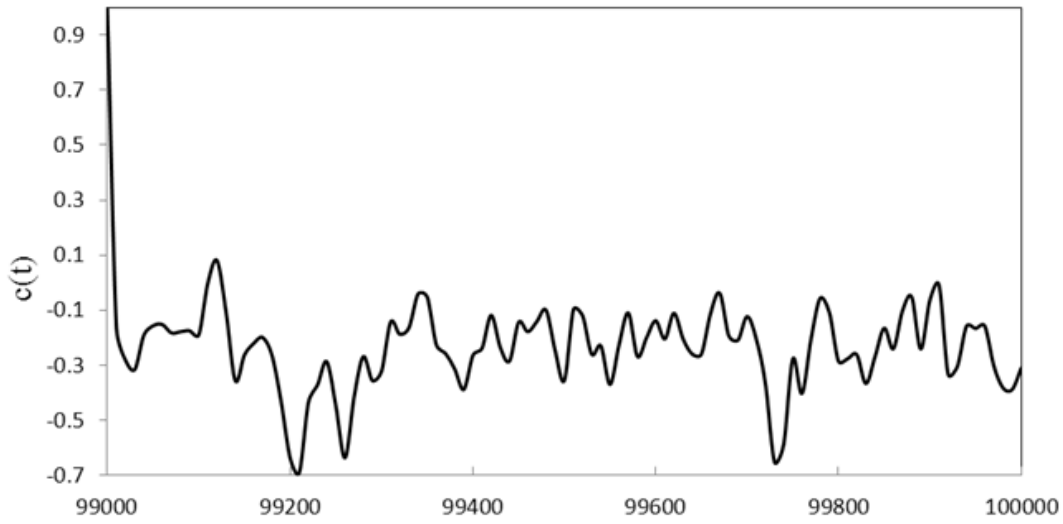

a)

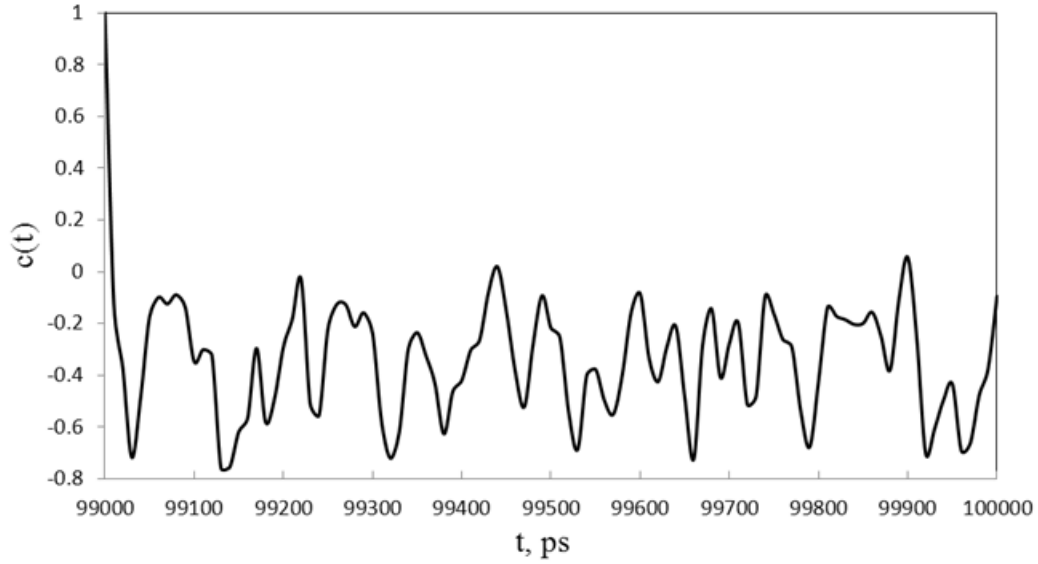

b)

Figure A 9 Velocity autocorrelation functions of CuB in PEO-*b*-PCL a) 1.63 wt% water b) 8.16 wt% water.

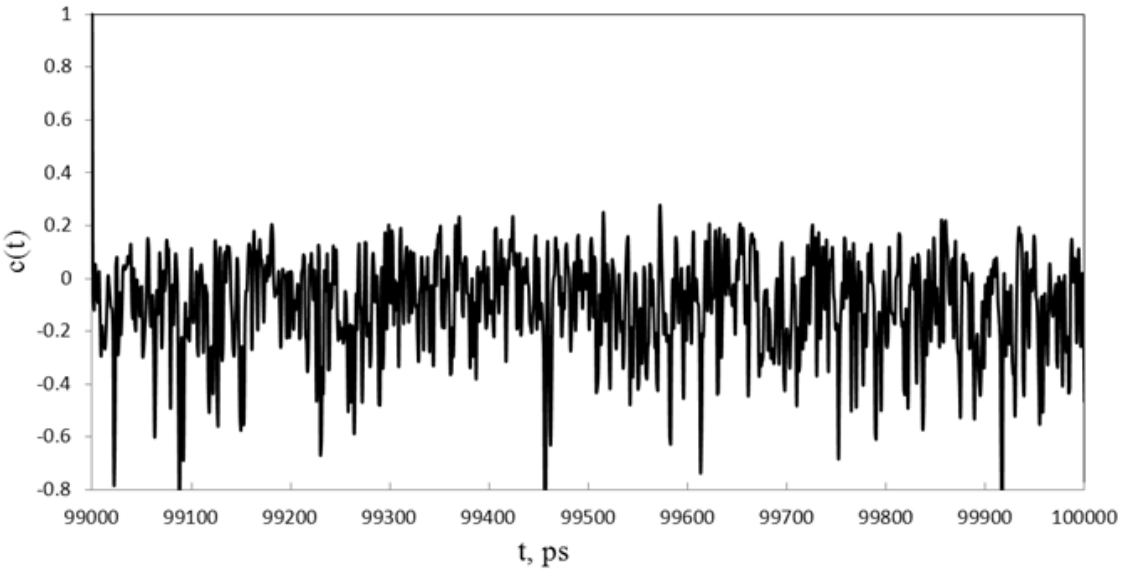

a)

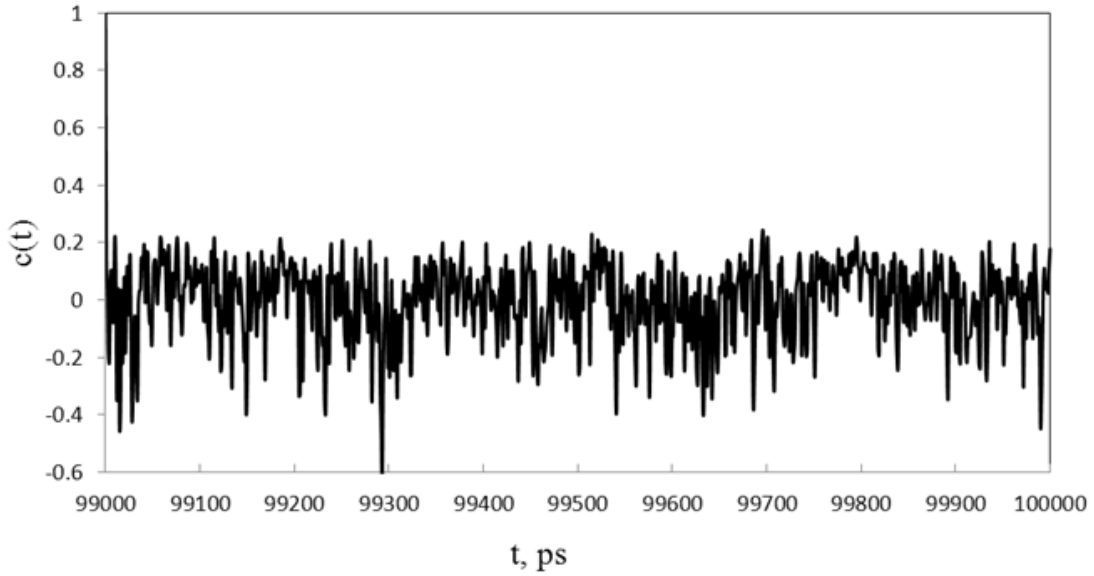

b)

Figure A 10 Velocity autocorrelation functions of CuB in PEO-*b*-3PCL a) 1.63 wt% water b) 8.16 wt% water.

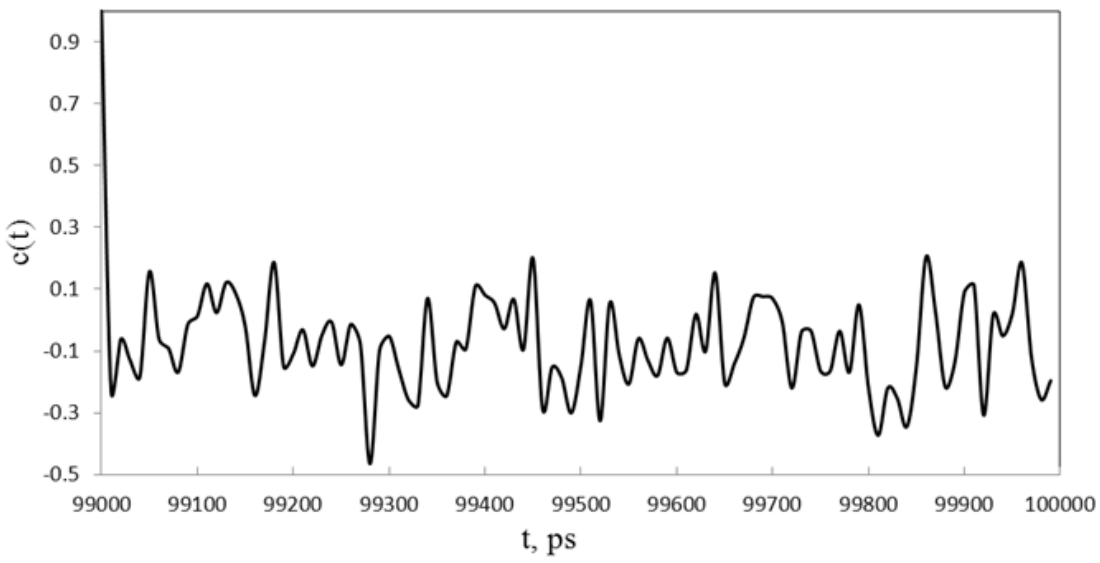

a)

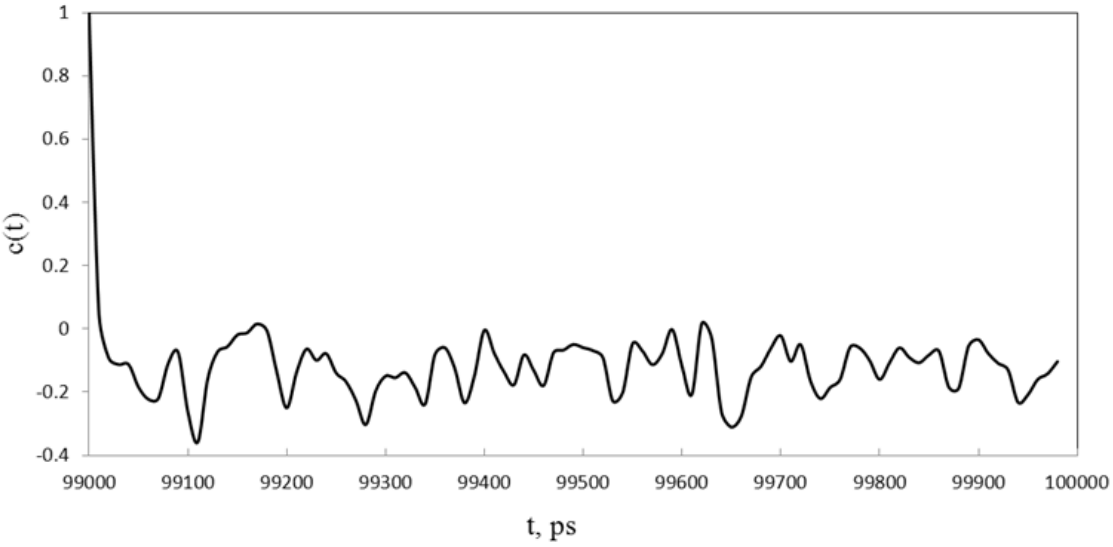

b)

Figure A 11 Velocity autocorrelation functions of water in PEO-*b*-PCL a) 1.63 wt% water b) 8.16 wt% water.

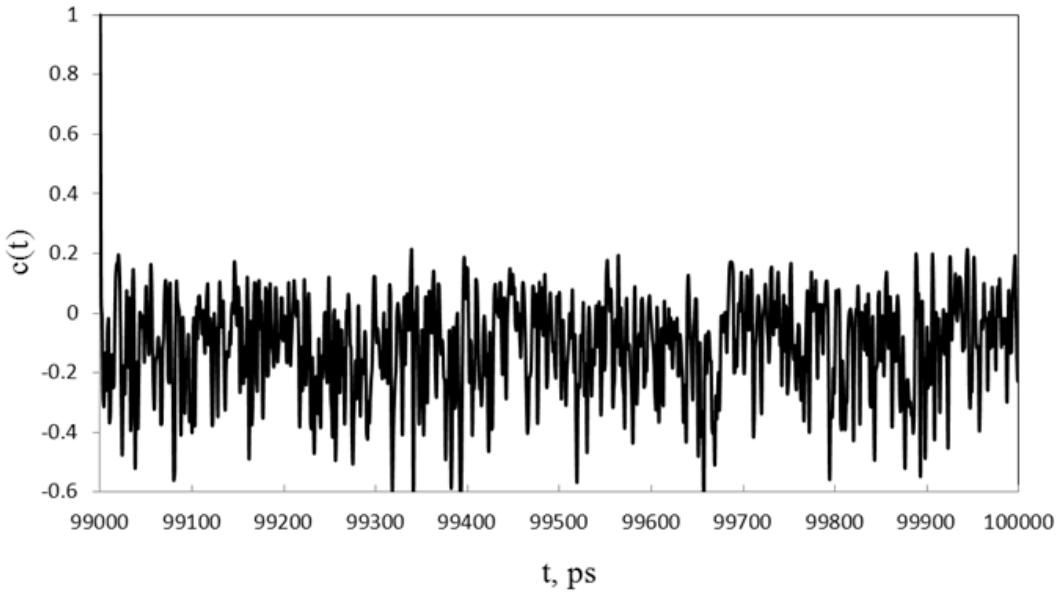

a)

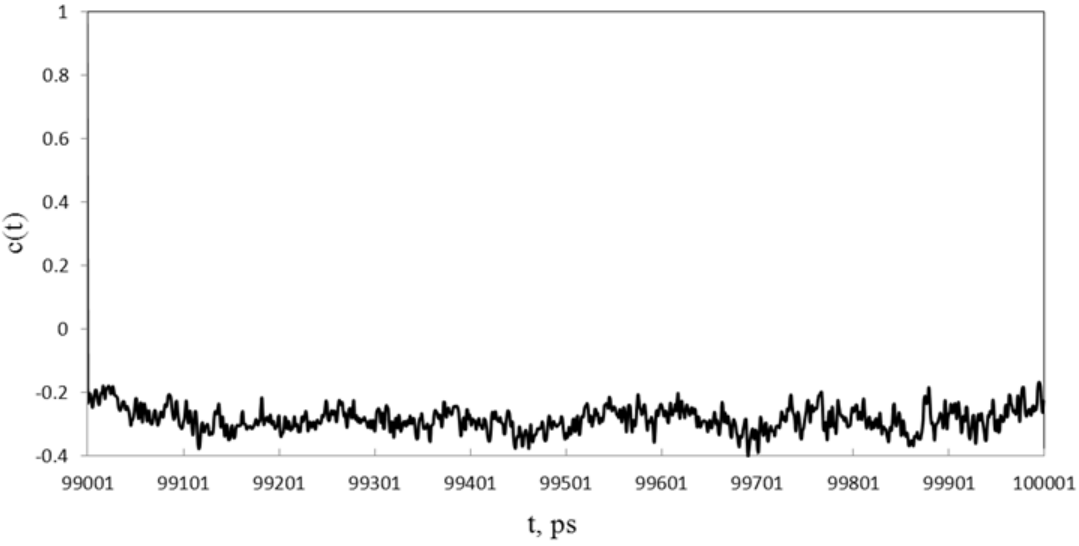

b)

Figure A 12 Velocity autocorrelation functions of water in PEO-*b*-3PCL a) 1.63 wt% water b) 8.16 wt% water.

5. Diffusivity of Cucurbitacin B in Water Swollen poly ethylene oxide-b-polycaprolactone Matrix with Different PCL/PEO Weight Ratios[3]

5.1. Introduction

In recent years, micelles made up of block copolymers have become the choice of nano-scale drug carriers. One major design criterion of such block copolymers is to balance their hydrophobicity and hydrophilicity for the drugs of interest so that maximum drug loadings and desired release kinetics are obtained. In fact, this has been the focus of many researchers over the past couple decades [175-184]. One

[3] A version of this chapter is being considered for publication.

approach to enhance drug loadings is to introduce chemical moieties that exhibit specific interactions (e.g., hydrogen bonds) into the block copolymers. However, many studies have shown that specific interactions would slow down the drug release kinetics, which may or may not be desirable [184-187]. In particular, Lee et al. [188] reported that the release rate of a drug papaverine encapsulated by micelles formed by polyethylene oxide-*b*-polylactic acid (PEO-*b*-PLA) was retarded when it was chemically modified with substituted carboxylic acid moieties. Interestingly, Molavi *et al*. observed that the cumulative release, expressed in terms of the percentage of encapsulated drug, of a hydrophobic drug Cucurbitacin B (CuB) encapsulated by polyethylene oxide-*b*-polycaprolactone) (PEO-*b*-PCL) micelles decreases by 37.5% when the PCL/PEO weight ratio increases from 1 to 4.8 [189]. In their work, the molecular weights of the two block copolymers used were PEO(5000)-b-PCL(5000) and PEO(5000)-b-PCL(24000). Here, the number in the bracket signifies the molecular weight of the block in g/mol. It is not clear that the decrease in the cumulative release is simply due to the increase in molecular weight of the block copolymer or its hydrophobicity or to both. If hydrophobicity does contribute to slowing down the release rate, why would hydrophobicity, mainly involving non-directional dispersion forces, increase the activation energy of the diffusion of CuB? In a recent study, Sarthak et al. [190] used molecular dynamics simulation to clearly demonstrate that increasing the PCL/PEO weight ratio of PEO-*b*-PCL from 0.5 to 2 (i.e., 4 times increase) decreases the corresponding Flory-Huggins interaction parameter significantly, thereby increasing the ability of the block copolymer to encapsulate more CuB. They found that molecular origin of the observation stems

from the hydrogen bonds formed between the oxygen atoms on CuB and the activated hydrogen atoms on the PCL block. The above finding explains the fact that increasing PCL/PEO weight ratio of PEO-*b*-PCL decreases the CuB release rate. However, in the experimental systems, water was present while this was not the case in the simulation models that Sarthak et al. used. According to S_w ratio (equation 2-30) introduced in chapter 2, swelling controls drug release in polymer micelles when S_w is greater than 1 which means micelle swelling will affect drug diffusion until all drug molecules diffuse out of the micelle. Therefore, in this work, we carried out molecular dynamics simulation to calculate the self-diffusion coefficients of CuB in PEO-*b*-PCL with PCL/PEO weight ratios at 0.5, 1 and 2 swollen by different amounts of water at body temperature (310 K) and ambient pressure (1 bar). We also studied a PEO-*b*-PCL model with a PCL/PEO weight ratio of 1 but with higher molecular weight to study the molecular weight effect. To compute the self-diffusion coefficients, we used an approach that was used in our recent work [191].

5.2. Molecular Models and Simulation Methodology

Figure 5-1 and Figure 5-2 show the ethylene oxide and caprolactone repeating units of the block copolymer PEO-*b*-PCL and the molecular structure of the anti-cancer drug Cucurbitacin B (CuB), respectively. Four models of PEO-*b*-PCL were used in which three models had the same total molecular weight of 3,750 g/mol but with three different PCL/PEO weight ratios of 1,250/2,500 (i.e., 0.5), 1,875/1,875 (i.e., 1)

and 2,500/1,250 (i.e., 2). The fourth model had a PCL/PEO weight ratio of 1 but the molecular weights of the PEO and PCL blocks are 2,500 g/mol, respectively. The molecular weight of CuB is 558 g/mol.

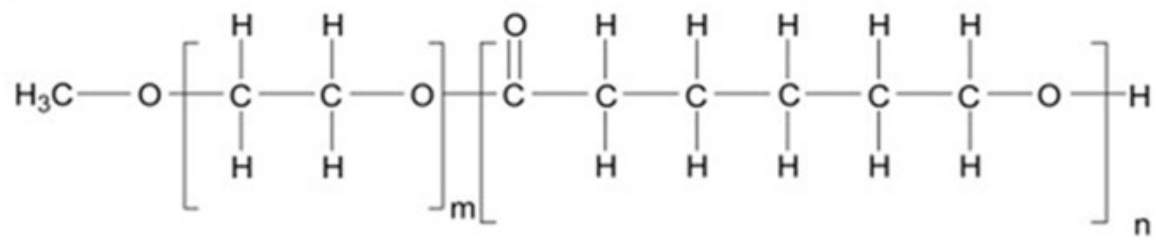

Figure 5-1 Chemical structure of polyethylene oxide-*b*-polycaprolactone (PEO-*b*-PCL)

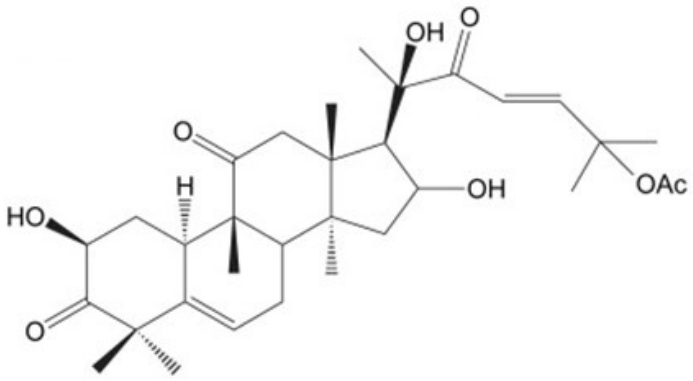

Figure 5-2 Chemical structure of the anti-cancer drug Cucurbitacin B (CuB)

Simulation of an entire micelle is computationally expensive with the currently available computer resources. Therefore, we modeled a small part of the micelle referred to as a pseudo micelle environment following a strategy that we used in our

previous work and the limitation of such an approach was discussed in reference [191]. In particular, we constructed an amorphous unit cell containing one block copolymer molecule and one CuB molecule. The weight ratios of CuB to the block copolymers were about 12-15% that are the drug loadings that can be achieved in practice. The unit cell was subjected to three-dimensional periodic boundary conditions. The procedure of Theodorou and Suter [192] was used to construct the unit cell. An initial density value of 1000 kg/m3 was used. It is worth noting that after the addition of CuB and water molecules, each system was annealed using isobaric-isothermal molecular dynamics simulation to obtain the correct density. The initial edge length of the cubic unit cell was about 3.0 nm. Then, a CuB molecule was inserted randomly into the cubic cell. Energy minimization was carried out with the steepest descent method to remove high-energy overlaps. After energy minimization, different numbers of water molecules were added to generate systems with different concentrations of water. Energy minimization was performed again on such systems and the resulting structures were then used for subsequent MD simulations. The corresponding water concentrations are shown in Table 5-1.

Table 5-1 Water concentrations of systems (1 – 12) containing various numbers of water molecules, one CuB molecule and one PEO-*b*-PCL block polymer with a total molecular weight of (a) 3,750 g/mol and (b) 5,000 g/mol.

(a)

System	Number of water molecules	Water concentration, wt%
1	1	0.40
2	5	2.35
3	10	4.70
4	15	7.05
5	20	9.40
6	25	11.75

(b)

System	Number of water molecules	Water concentration, wt%
7	1	0.32
8	5	1.63
9	10	3.26
10	15	4.89
11	20	6.53
12	25	8.16

The force field that we used for the energy minimization and the subsequent MD simulations was GROMOS96 and the detail of the force field used was given in our previous work [192]. The SPC water model was used, as the water concentrations considered in this work were low [192].

GROMACS version 3.3.1 was used to carry out isobaric-isothermal (NPT) molecular dynamics (MD) simulations at 310 K (body temperature) and 1 bar pressure. The simulation temperature used was significantly higher than the glass transition temperature of the PEO and PCL blocks (both at -60°C). The simulation temperature was controlled by the Nose-Hoover thermostat [165,166] and the pressure was controlled by the Parrinello-Rahman [167] approach. The leap-frog Verlet algorithm with a time step of 1 femtosecond (fs) was used to obtain positions of atoms at every time step [169]. The sampling time used was 1 picosecond (ps). For each system, a 5 ns NPT MD equilibration was performed before the 100 ns production simulation. The NPT MD simulation was repeated 10 times using different initial positions of CuB and water molecules. In other words, the results reported for each system correspond to the average of 10 simulations.

GROMACS software was also used to analyze the simulations results in order to obtain the self-diffusion coefficient for CuB. The well-known Einstein's equation as shown below was used for this purpose:

$$\mathbf{D} = \frac{\mathbf{1}}{\mathbf{6}} \frac{\mathbf{d}\left(\left\langle \frac{\mathbf{1}}{\mathbf{N}} \sum (\vec{\mathbf{r}}_\mathbf{i}(\mathbf{t}) - \vec{\mathbf{r}}_\mathbf{i}(\mathbf{0}))^\mathbf{2} \right\rangle\right)}{\mathbf{dt}} \qquad (5\text{-}1)$$

Here $\langle \frac{1}{N} \sum (\vec{r_i}(t) - \vec{r_i}(0))^2 \rangle$ is the mean square displacement (MSD) of the penetrant molecules of interest.

5.3. Results and Discussion

Figure 5-3 shows typical MSD plots for CuB in PEO(2500)-*b*-PCL(2500). Note that this system has a PCL/PEO weight ratio of 1. The corresponding self-diffusion coefficients of CuB in all systems were then calculated based on the slope of the regressing lines fitted through the portion of the MSD plots between the first and last 10% of the whole region. The diffusion coefficient for this system was then validated by obtaining the intercept of the line fitted through the linear portion of log (MSD) versus log (t) (i.e., Einstein diffusion) where the slope of this line was almost 1.0.

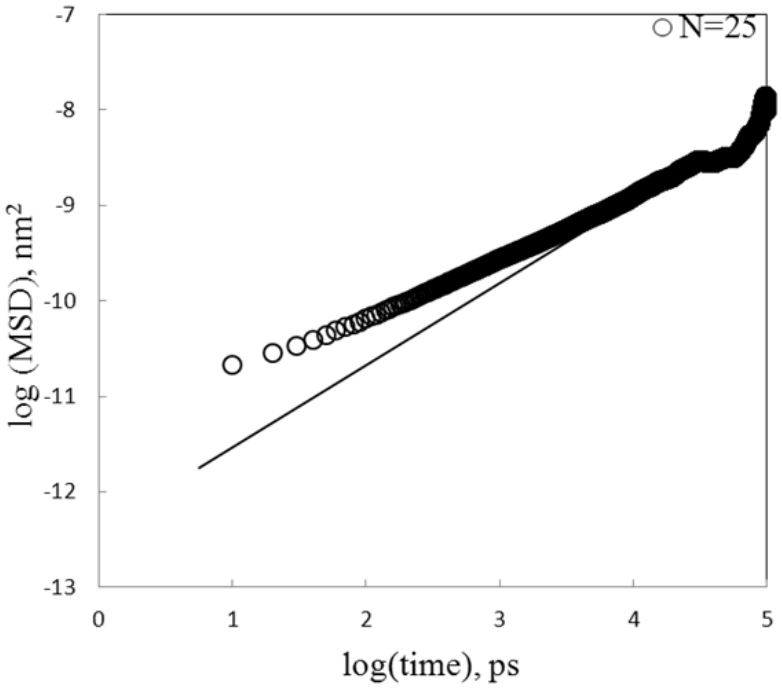

Figure 5-3 Mean square displacement versus time of CuB in PEO(2500)-*b*-PCL(2500) swollen by 25 numbers of water molecules at 310 K

Figure 5-4 shows the computed self-diffusion coefficients of CuB in the block copolymer models at six different water concentrations. Once again, each self-diffusion coefficient reported in the figure corresponds to an average of 10 MD simulations with different initial positions of CuB and water molecules. The uncertainties signify the corresponding standard errors. The simulation results show that the diffusivity of CuB is independent of the water concentration and that decreases with increasing PCL/PEO weight ratio for the block copolymers with the same total molecular weight of 3,750 g/mol. According to the classical free volume

theory for the diffusion of small molecules in a polymer matrix, the first observation suggests that the presence of water up to a concentration of about 12 wt% does not alter the free volume characteristics (i.e., the amount of free volume and its redistribution rate). In the following, we will have further discussion about this point. The second observation means that increasing hydrophobicity of the block copolymer significantly decreases the diffusivity of CuB. As mentioned in the introduction, decrease in the diffusivity of a penetrant is expected when the penetrant and the block copolymer interact favourably with each other through specific interaction. In this case, increasing the PCL/PEO weight ratio should decrease the ability of the block copolymer (i.e., decrease in the number of ethylene oxide units) to form hydrogen bonds with CuB. However, Patel et al. [193] showed that hydrogen atoms on the PCL block are activated due to the presence of the nearby carbonyl groups. As a result, such hydrogen atoms are able to form hydrogen bonds with the oxygen atoms present on the CuB molecules, thereby leading to the observed decrease in CuB diffusivity with increasing PCL/PEO weight ratio. According to the work of Patel et al. [193], the chance of the hydroxyl moieties on CuB to form hydrogen bonds is low. Comparing the results of PEO(1875)-*b*-PCL(1875) to those of PEO(2500)-*b*-PCL(2500) clearly shows the expected molecular weight effect as both systems have the PCL/PEO weight ratio of 1.

To show that increasing the PCL/PEO weight ratio would increase the number of hydrogen bonds formed between the PCL block and CuB, we determined the corresponding mean numbers of hydrogen bonds in all 12 systems. Table 5-2

summarizes the results. Here, the presence of a hydrogen bond is determined based upon a geometric criterion in which a hydrogen bond exists if the hydrogen donor-acceptor angle is greater than 135° and distance between the hydrogen donor and acceptor is below 3 Å. The number of H-bonds obtained for every nano second in Gromacs were summed over 100 ns and finally divided by 100 to obtain the average number of hydrogen bonds per 1 ns. The reproducibility of the results were then checked in 10 simulations with different initial conformations of the drug molecule in simulation box.

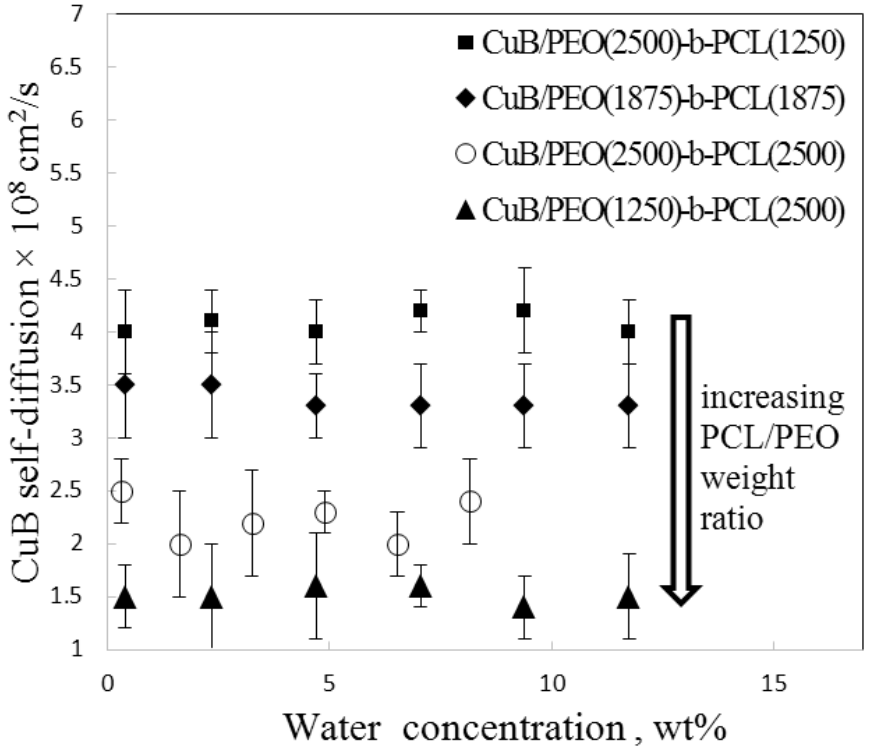

Figure 5-4 Computed self-diffusion coefficients of CuB in the four PEO-*b*-PCL models swollen by different amounts of water at 310 K

Table 5-2 Computed mean numbers of hydrogen bonds per ns formed between CuB and the PCL block in PEO-*b*-PCL with three different PCL/PEO ratios swollen by various amounts of water at 310 K (a) a total molecular weight of 3750 g/mol and (b) a total molecular weight of 5000.

(a)

System	Water concentration, wt%	Mean number of H-bonds between CuB and PCL in PEO(2500)-*b*-PCL(1250)	Mean number of H-bonds between CuB and PCL in PEO(1875)-*b*-PCL(1875)	Mean number of H-bonds between CuB and PCL in PEO(1250)-*b*-PCL(2500)
1	0.40	0.02 ± 0.005	0.03 ± 0.004	0.08 ± 0.003
2	2.35	0.02 ± 0.005	0.03 ± 0.005	0.07 ± 0.005
3	4.70	0.02 ± 0.007	0.04 ± 0.003	0.09 ± 0.005
4	7.05	0.03 ± 0.003	0.04 ± 0.005	0.07 ± 0.002
5	9.40	0.02 ± 0.005	0.04 ± 0.004	0.09 ± 0.002
6	11.75	0.03 ± 0.005	0.04 ± 0.006	0.09 ± 0.005

(b)

System	Water concentration, wt%	Mean number of H-bonds between CuB and PCL in PEO(2500)-*b*-PCL(2500)
7	0.32	0.04 ± 0.005
8	1.63	0.03 ± 0.003
9	3.26	0.04 ± 0.003
10	4.89	0.04 ± 0.003
11	6.53	0.05 ± 0.005
12	8.16	0.04 ± 0.002

It is obvious from Table 5-2 that the mean number of hydrogen bonds per ns between CuB and the PCL block increases almost 4 times when the PCL/PEO ratio in the polymer with a molecular weight of 3750 g/gmol increases 4 times. It is also interesting to note that the mean numbers of hydrogen bonds of two systems with the same PCL/PEO ratio but different molecular weights are comparable confirming that the difference in the CuB diffusivity in the two models are mainly attributed to their molecular weight difference, not the difference in the intermolecular interactions. Also, the mean number of hydrogen bonds seems to be insensitive to the water concentration. The amount of water does not affect the number of hydrogen bonds

formed between the PCL block and CuB. This may explain that the diffusivity of CuB is independent of water concentration.

It is expected that increasing water concentration would increase the swelling of the block polymer, thereby increasing the diffusivity of CuB. However, this was not observed (Figure 5-4). To determine whether there was swelling in the systems under constant temperature and pressure conditions, we calculated the polymer swelling factor that is defined as the ratio of the fractional volume change to the fractional mass change at a given water concentration. Results are shown in Figure 5-5 and it is clear from the table that all block copolymer models swell significantly even at very low water concentrations. However, the swelling factor decreases as the number of water molecules increases from 1 to 5 and levels off at about 5 water molecules. It is noteworthy that the swelling factor is insensitive to the PCL/PEO weight ratio from 0.5 to 1 but increases significantly from 1 to 2. The plots of radius of gyrations for the PCL block in all three polymers with PCL/PEO ratios of 0.5,1 and 2 all confirm the swelling factor plots shown in Figure 5-5. The radius of gyration for PCL block does not change significantly in polymers with PCL/PEO ratios from 0.5 to 1 as shown in Figure 5-6. As the PCL/PEO ratio increases from 1 to 2, the radius of gyration for the PCL block changes significantly as shown in Figure 5-6.

Given that systems with the highest PCL/PEO weight ratio exhibited the highest swelling factor but lowest diffusivity of CuB, the data suggest that hydrogen bonds dominate the diffusion process in these systems.

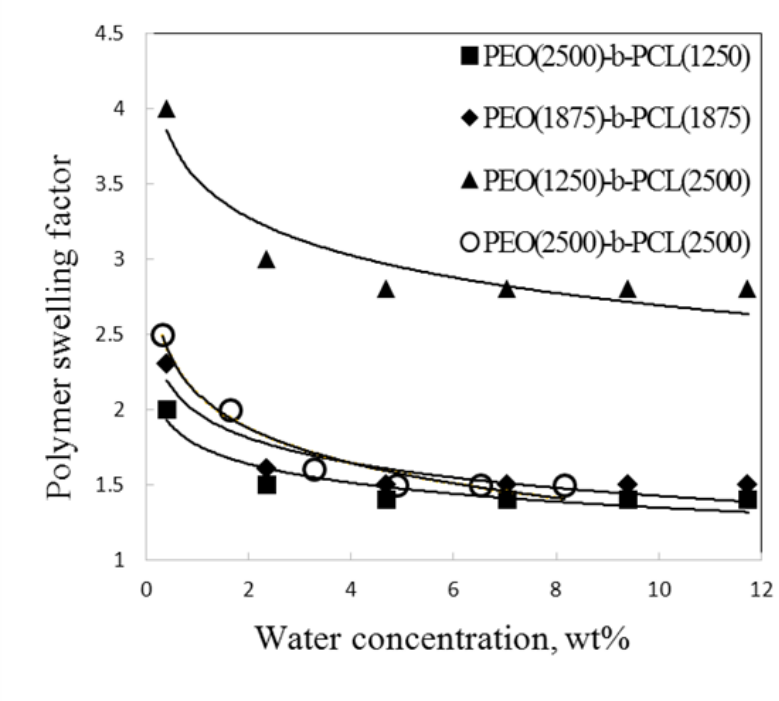

Figure 5-5 Swelling factors of different PEO-*b*-PCL block copolymers swollen by various amounts of water at 310 K

To determine the effect of the segmental mobility of the block copolymers on the diffusivity of CuB, we calculated the radii of gyration (R_gs) of the PEO and PCL blocks in the systems with the lowest and highest PCL/PEO weight ratios (0.5 and 2) as a function of time. We only show the results at the highest water concentration (i.e., 11.75 wt% and 8.16 wt%) as the PCL/PEO weight ratio is of main interest. Figure 5-6 to Figure 5-8 summarize the results. It is evident from the figures that the system with the highest PCL/PEO weight ratio exhibits larger amplitudes of the fluctuation of R_g, with those of the PCL block more pronounced than that of the PEO block, indicating that the mobility of the block copolymer increases with increasing

PCL/PEO weight ratio and that that of the PCL block is higher than that of the PEO block. This observation suggests that the increasing degree of the wriggling motion of the block copolymers (i.e., increasing the free volume redistribution rate) is not sufficient to increase the diffusion of CuB. Here, the radius of gyration of CuB at 310 K is about 0.45 nm which is insensitive to the water concentration.

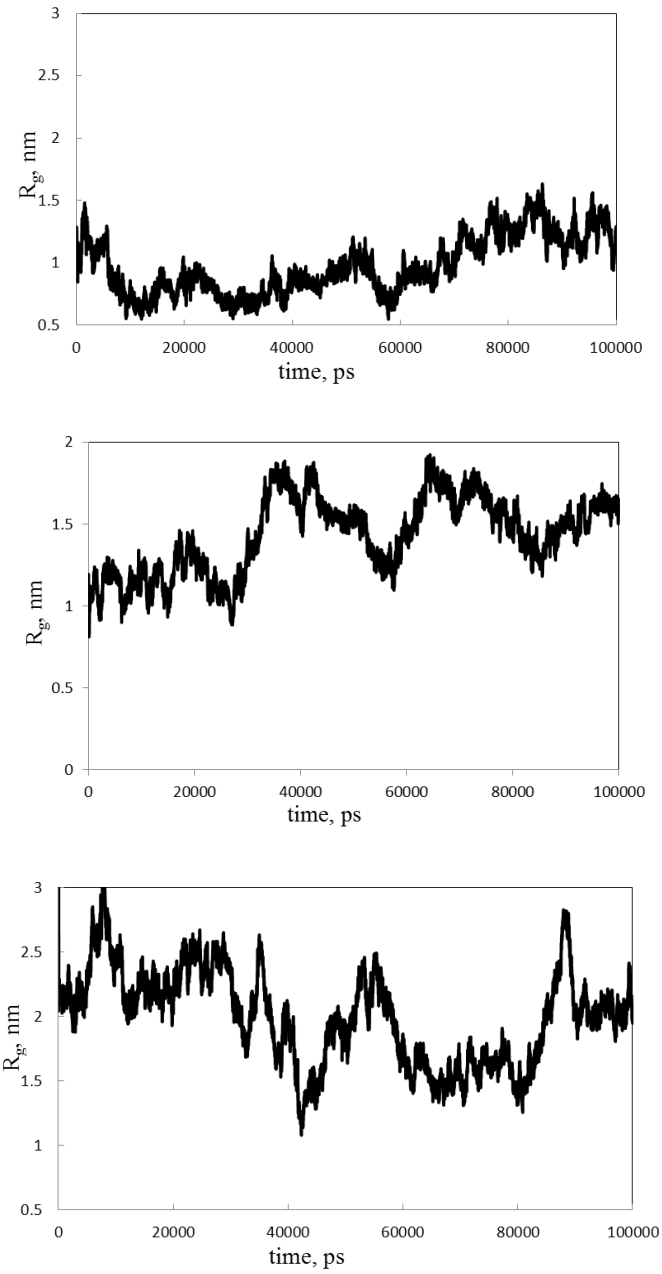

Figure 5-6 Radius of gyration of the PCL block of (from top to bottom) PEO(2500)-b-PCL(1250), PEO(2500)-b-PCL(2500) and PEO(1250)-*b*-PCL(2500) containing 11.75 wt%, 8.16 wt% and 11.75 wt% of water at 310 K. Second figure from top is taken from chapter 4.

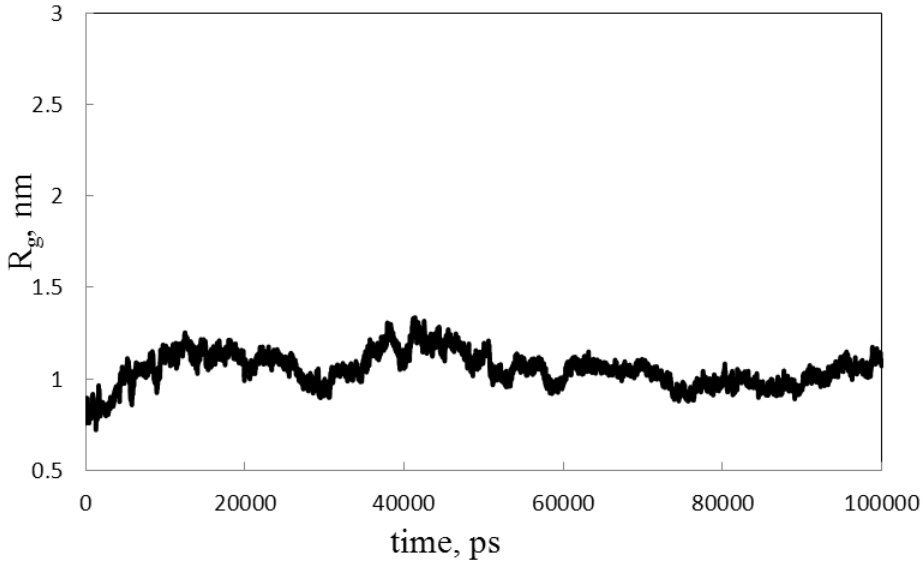

Figure 5-7 Radius of gyration of the PEO block of PEO(2500)-*b*-PCL(1250) containing 11.75 wt% of water at 310 K

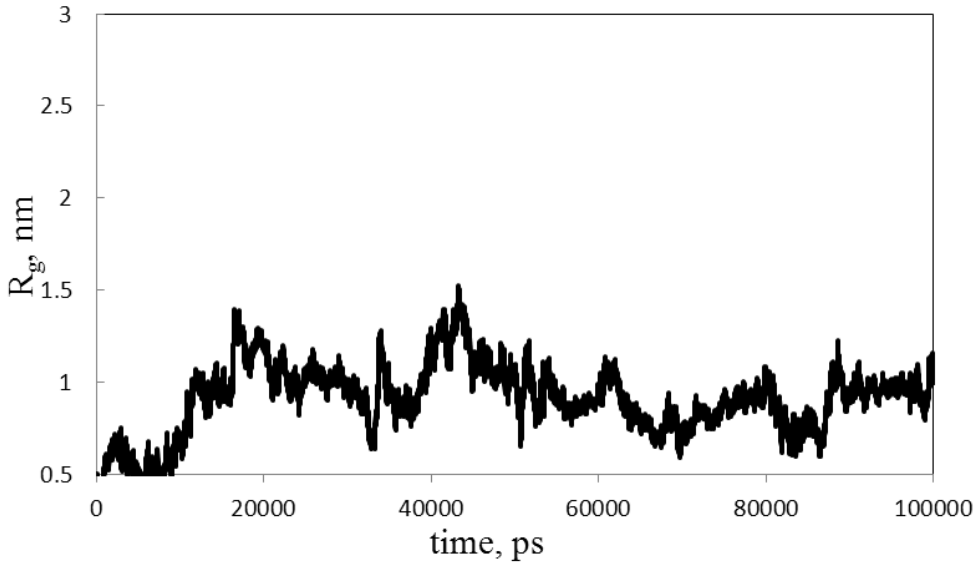

Figure 5-8 Radius of gyration of the PEO block of PEO(1250)-*b*-PCL(2500) containing 11.75 wt% of water at 310 K

5.4. Conclusions

Isobaric-isothermal (NPT) molecular dynamics (MD) simulation was used to study the self-diffusion of a hydrophobic drug namely Cucurbitacin B (CuB) in pseudo micelle environments made up of polyethylene oxide-*b*-polycaprolactone (PEO-*b*-PCL) and water at different concentrations up to about 12 wt%. PEO-*b*-PCL models with 3 different PCL/PEO weight ratios (0.5, 1 and 2) but with the same total molecular weight (3750 g/mol) were used. An additional model with a PCL/PEO weight ratio of 1 but with a total molecular weight of 5000 g/mol was used. It was found that the diffusivity of CuB decreased with increasing PCL/PEO weight ratio and that such observation was attributed to the increase in the number of hydrogen bonds formed between the oxygen atoms on CuB and the activated hydrogen atoms on the PCL block as its chain length increased. In addition, the swelling factor and mobility of both PEO and PCL blocks as quantified by their time variations of the radius of gyration increased with increasing PCL/PEO weight ratio. Since increase in the degree of swelling and mobility of the blocks should increase the diffusivity of CuB but the results show the opposite, it suggests that hydrogen bonds formed between CuB and the PCL block dominate the diffusion process. As a result, regardless of the PCL/PEO weight ratio, diffusivity of CuB was insensitive to the water concentration. The results of the two models with the same PCL/PEO weight ratio but different total molecular weights show that CuB in the higher molecular weight model exhibited lower diffusivity, as expected.

6. Calculation of CuB Activation Energies in Water Swollen polyethylene oxide-b-Polycaprolactone Matrix with Different PCL/PEO Ratios

6.1. Introduction

Self-diffusion of small and large molecules in polymers has been of interest for many years [194]. Diffusion in polymers is a complex process. It depends strongly on the thermal motion of the solvent molecules and on the structure of the polymer which dictates different polymer-solvent interactions. It remains a challenge to understand and predict the diffusion of small and large molecules in polymer systems. Some theories are available for the diffusion of small molecules with size comparable to that of polymer monomers diffusing in polymers. In some models, the polymer is

considered to be stationary compared to the solvent molecules [195-198]. However, these theories tend to estimate the diffusion coefficient inaccurately when the diffusing molecule size is large. For example, such models are not able to predict the diffusion of protein in gel or the diffusion of polystyrene in polyvinyl methyl ether gels [199-202]. In these cases, the interaction between the polymer and the penetrating molecules is even more important than the free volume or holes available. The importance of the polymer-solvent interaction on solvent diffusivity while the polymer is swollen by the solvent has been demonstrated in the literature before [203]. In order to better understand the effect of polymer-solvent interactions on the self-diffusion coefficient, we decided to calculate the drug molecule's activation energy in this chapter.

The Arrhenius activation energy model is the most popular one for obtaining the temperature dependence of diffusion coefficient [204-206] as shown in the following equation:

$$\mathbf{D} = \mathbf{D_0} \exp\left(-\frac{\mathbf{E_a}}{\mathbf{RT}}\right) \qquad \textbf{(6-1)}$$

where D_0 is a constant, R is the universal gas constant and E_a is the activation energy for the diffusion process. In some studies, it was shown that the drug release over the temperature range of 25ºC-60ºC showed an Arrhenius behaviour and the activation energy was about 14 kJ/mol [207]. An interesting observation in the aforementioned studies was that for a Fickian diffusion mechanism where the polymer relaxation rate

is much higher than the drug diffusion rate, very low activation energy is required for the drug to move into adjacent free volumes in the polymer network. Moreover, it was shown that much higher activation energy is required for diffusion of particles in polymer networks when the diffusion mechanism was "non-Fickian" or swelling controlled. The mentioned results are interesting and can help us better understand the effect of the polymer structure, chain rigidity, etc. on the diffusion of small molecules.

Brandt et al. [207] described a complete model to explain this energy activated motion of particles in different polymer chains. According to their model, once the density or the length of the whole chain or the length of a part of the polymer chain changes, the chain motion is affected which in turn could affect the motion of particles and their activation energy. Er. et al. [208], have shown that as the PEG content in the PEG-liposome incorporated polymer increases, the diffusion of the drug molecule was restricted in the lipid layer causing the activation energy to increase, thereby making it more difficult for the particle to move in the polymer network. In their work, structural differences between polymers were reflected in the differences obtained for the drug diffusion and activation energies.

In this study, five models of PEO-b-PCL were used in which three models had the same total molecular weight of 3,750 g/mol but with three different PCL/PEO weight ratios of 1,250/2,500 1,875/1,875 and 2,500/1,250 [209]. The fourth and fifth models had a PCL/PEO weight ratio of 1 but the molecular weights of the PEO and PCL blocks were 2,500 g/mol Table 6-1. One of the last two models was a linear block

copolymer while the other one was a branched one. The last 2 models were identical to the ones used in chapter 4 in which it was shown that the drug diffusion does not depend on water concentration. As the polymer total molecular weight increased from 3750 g/mol to 5000 g/mol, the drug diffusion coefficient decreased at fixed water concentrations. Also, as the PCL/PEO weight ratio increased from 0.5 to 2 for polymers with the same molecular weight of 3750 g/mol, the drug diffusion decreased by 60% at the same water concentrations.

In this Chapter, we calculated activation energies of diffusion of CuB in the aforementioned polymers at 4 different temperatures (27ºC, 37ºC, 47ºC and 57ºC) and at the same water concentration (25 water molecules).

6.2. Models and simulation methods

The model construction followed the procedures described in chapters 4 and 5. The isothermal-isobaric molecular dynamics simulation (NPT) was used at temperatures 27^{o}C, 37^{o}C, 47^{o}C, 57ºC and 1 bar pressure along with the force field described in chapter 4 and 5.

Table 6-1 Water concentrations of systems (1 – 12) containing various numbers of water molecules, one CuB molecule and one PEO-b-PCL block polymer with a total molecular weight of (a) 3,750 g/mol and (b) 5,000 g/mol.

a)

System	Number of water molecules	Water concentration, wt%
1	1	0.40
2	5	2.35
3	10	4.70
4	15	7.05
5	20	9.40
6	25	11.75

b)

System	Number of water molecules	Water concentration, wt%
7	1	0.32
8	5	1.63
9	10	3.26
10	15	4.89
11	20	6.53
12	25	8.16

6.3. Results and Discussion

The diffusion coefficients for CuB in all polymers at temperatures 27ºC, 37ºC, 47ºC and 57ºC were calculated based on the method described in chapters 4 and 5. The calculated self-diffusion values for the drug in all polymers with 25 water molecules in each system are shown in Table 6-2**.**

Table 6-2 Calculated self-diffusion coefficients of CuB diffusing in PEO-*b*-PCL models over the temperature range of 298 to 330 K. Each model contained 25 water molecules.

T, K	self-diffusion of CuB in PEO(1250)-b-PCL(2500) $\times 10^8$ cm^2/s	self-diffusion of CuB in PEO(2500)-b-PCL(1250)$\times 10^8$ cm^2/s	self-diffusion of CuB in PEO(1875)-b-PCL(1875)$\times 10^8$ cm^2/s	self-diffusion of CuB in PEO(2500)-b-PCL(2500)$\times 10^8$ cm^2/s	self-diffusion of CuB in PEO(2500)-b-3PCL(2500) $\times 10^8$ cm^2/s
298	1.0±0.5	3.2±0.5	2.0±0.5	1.5±0.6	0.6±0.04
310	1.5±0.3	4.0±0.3	3.3±0.4	2.4 ± 0.4	1.1 ± 0.3
320	2.5±0.4	4.6±0.4	4.0±0.3	3.5±0.5	2.0±0.5
330	3.8±0.4	6.0±0.5	5.5±0.3	4.8±0.5	3.0±0.3

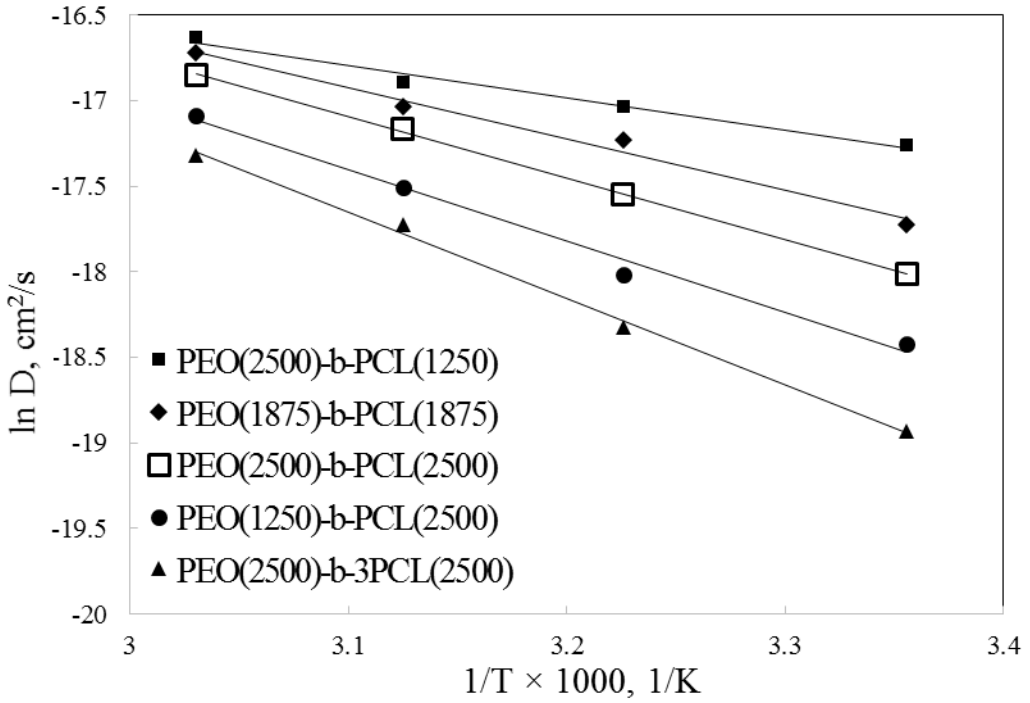

Figure 6-1 Plots of *ln* D vs. 1/T for CuB diffusing in the PEO-*b*-PCL models depicted in Table 6-2. Each model contained 25 water molecules.

The activation energy for the self-diffusion of CuB in the five PEO-*b*-PCL models depicted in Table 6-2 was directly calculated from the slope of the plot of *ln* D vs. 1/T. The values of the activation energy are shown in Table 6-3. Both Table 6-3 and Figure 6-2 clearly show that at a fixed molecular weight (3,750 g/mol) activation energy (i.e., slope) increases with increasing PCL/PEO weight ratio. This is expected as the self-diffusion coefficient decreases with increasing PCL/PEO weight ratio. As shown in Chapter 5, low self-diffusion coefficients of CuB in PEO-*b*-PCL models with high PCL/PEO weight ratios are attributed to higher numbers of hydrogen bonds formed between CuB and the PCL block of the block copolymer. And such short-range interactions increase the activation energy. A similar effect of

intermolecular interaction on polymer chain motion has been observed by Er et al. [208] which cause the drug's activation energy to increase. The same authors have also observed the effect of PEG molar ratio in liposomes on the drug's activation energy. They showed that the activation energy for guanosine release from liposomes is in the range 14–22 kJ/mol and increases with PEG coverage.

Table 6-3 Calculated activation energy of CuB diffusing in the block copolymer models depicted in Table 6-1. Each model contained 25 water molecules.

Block Copolymer Model	Activation Energy E_a (kJ/mol)
PEO(2500)-*b*-PCL(1250)	15.46
PEO(1875)-b-PCL(1875)	24.94
PEO(2500)-b-PCL(2500)	29.93
PEO(1250)-b-PCL(2500)	33.26
PEO(2500)-b-3PCL(2500)	41.57

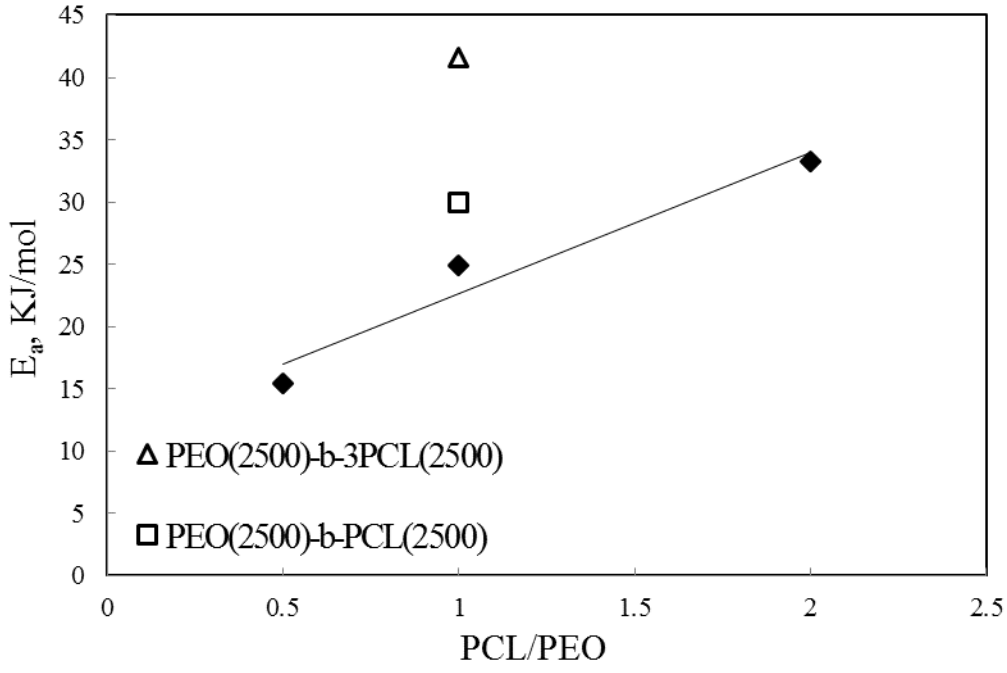

Figure 6-2 The PCL/PEO weight ration dependence of activation energy of CuB at a fixed molecular weight of 3,750 g/mol. Each model contained 25 water molecules.

At a fixed total molecular weight (5,000 g/mol), the activation energy for the branched structure is higher than the linear one. As mentioned in Chapter 4, this is because PEO-*b*-3PCL formed more hydrogen bonds with CuB than PEO-*b*-PCL. Given the finding in Chapter 4 that the self-diffusion coefficient is insensitive to water concentration, we did not expect that the calculated activation energy would depend on water concentration.

6.4. Conclusion

The diffusion coefficients for CuB in five PEO-b-PCL models at temperatures 27ºC, 37ºC, 47ºC and 57ºC were calculated. Three models had the same total molecular weight of 3,750 g/mol but with three different PCL/PEO weight ratios of 0.5, 1 and 2. The remaining two models had a PCL/PEO weight ratio of 1 but the molecular weights of the PEO and PCL blocks are 2,500 g/mol. One of such models had a linear architecture while the other with a linear PEO block connected to 3 PCL blocks. The diffusion coefficients for CuB in all block polymers increased as temperature increased from 298 K to 330 K. However, the block copolymers exhibit different temperature dependence on the diffusion coefficient. In particular, the diffusion coefficient for CuB in PEO(1250)-b-PCL(2500) is four times larger as the temperature increases from 298 K to 300 K while that in PEO(2500)-b-PCL(1250) is only two times larger over the same temperature range. As a result, the activation energy obtained for the branched block copolymer is higher than the linear one with the same molecular weight. The PCL block in the linear polymer interacts with the drug less than the PCL block in the branched polymer causing the drug to move easier and needing lower energy of activation. Finally, it was showed that the same activation energy was obtained for CuB in linear PEO-b-PCL at two different water concentrations. This means that diffusion of CuB is insensitive to the degree of swelling of the polymer and that the free volume redistribution does not affect the diffusion of CuB.

7. Conclusions

In this thesis, the MD approach was used to predict the hydrophobic drug self-diffusion coefficients at different water concentrations in drug-polymer systems. Different polymer structures were used to measure the drug (CuB) self-diffusion in polymer models. The effect of different polymer structures on drug-polymer interactions and drug self-diffusion in polymers was also studied by applying molecular dynamics simulations. Once the structures were designed and built the interaction effects on drug self-diffusion was measured which was a faster method than experimental methods. In addition to saving time, the molecular dynamics simulation approach provides very useful atomistic details to estimate the intermolecular interactions between drug and polymers as well as detailed understanding of the diffusion mechanism. This type of molecular information cannot be obtained in experiments and are even necessary to analyse experimental results. In Chapter 3, major drug release models in polymeric systems were discussed. The mechanism of drug release from non-degradable, swelling and degrading polymer matrices were explained. Drawbacks of different kinetic drug release models were discussed. It was evident from Chapter 3 that drug release

kinetics used for micron-sized drug delivery systems lacks the ability to correctly predict the drug release kinetics in nano-sized drug delivery systems and the usefulness of molecular dynamics simulation was discussed as well. In Chapters 4 and 5, molecular dynamics simulations effectively predicted the intermolecular interactions between drug and polymers at different water concentrations and different polymer structures. In our studies, it was confirmed that the intermolecular interactions or H- Bonds formed between the PCL block of copolymers and hydrophobic drug at different water concentrations play an important role in the calculation and prediction of drug diffusivity in different systems. It was shown however that the different water concentrations and polymer swelling do not affect the drug's diffusivity in the same polymer as discussed in Chapter 4. In other words, the interactions between polymer and drug molecules were more important than the free volumes available to drug during polymer swelling at different water concentrations. This could be due to the size of our drug molecule which is comparable to polymer's monomer or repeating unit. If the drug's size was small according to the free volume theory formation of larger vacant holes during polymer swelling would lead to faster motion and change drug diffusivity. Also, it was shown that the PCL block in the branched structure of PEO-b-PCL forms more hydrogen bonds with hydrophobic drug and water in comparison to the PCL block in the linear structure of PEO-b-PCL which affected both water and drug's diffusion in swelling polymers. The plots of radius of gyration for PCL block in different systems confirmed slower chain motions for the PCL block in branched polymer and therefore explained the different water diffusivities in linear and branched structures

of polymers. In other words, the diffusion of water molecules in the swelling polymers was affected by polymer- water interactions. Larger vacant holes created during swelling did not increase water diffusivity. Again as in the case for drug molecules, water-polymer interactions played a more important role in water diffusivity than the size of the vacant holes available for water molecules. Water molecules demonstrated a hopping mechanism whereas drug molecule (CuB) did not perform any hops in different systems. The hops were defined as jumps to neighbour holes or free volumes that are greater than the diffusant's size.

We extended this study in Chapter 5 and we used different PCL block lengths or different PCL/PEO ratios in polymers with the same molecular weight. The swelling factor was calculated based on the ratio of fractional volume changes over the fractional mass change at a given water concentration. Polymer swelling increased with increasing the hydrophobic block length, PCL, in polymers with the same molecular weight. However, the diffusion coefficient of drug molecule decreased as the PCL block length increased. The reason behind this was the larger inter molecular interactions between PCL block of polymers and hydrophobic drug due to more hydrogen bonds formed. The system with the highest PCL/PEO ratio exhibited the lowest diffusivity but highest swelling factor. It was suggested that hydrogen bonds dominate the diffusion process in these systems. Another interesting point was that the PCL block is considered a hydrophobic block which has low water solubility, however this block demonstrated higher number of H- Bonds with drug molecule (CuB) in comparison to the PEO block in the same polymer.

Finally, we calculated the activation energy of CuB diffusing in block copolymers with different PCL/PEO weight ratios. The activation energy of the drug molecule was calculated by estimating the slope of the semi-log plot of diffusion vs. absolute temperature of the systems. As the temperature increased, the self-diffusion of the drug molecule increased according to the Arrhenius equation. As the PCL/PEO weight ratio increased, the drug's activation energy increased due to stronger intermolecular interactions between polymer block and drug molecule or higher number of H-Bonds formed between drug and polymer.

7.1. Limitations

The molecular models used throughout the thesis were in a pseudo-micelle environment and are thermodynamically different from real micelles formed in human blood stream. Hence, ideally one would like to simulate di-block copolymer micelles to determine how block copolymer structures and its block lengths affect drug loadings and encapsulation efficiency for the drug of interest. Nevertheless, simulating such systems at the atomistic level is computationally expensive at the time being. Therefore, in the present work, we have focussed on investigating binary interactions between drugs and di-block copolymers of interest in their liquid state and in a pseudo-micelle environment. Additionally, simulating di-block copolymers, in amorphous state is relevant as such molecules have hydrophobic tails and

hydrophilic heads and would form micelles above critical micelle concentrations in the presence of water.

7.2. Implications and future work

The contributions of the analysis provided in this thesis can benefit both industrial and academic parties. The analysis of intermolecular interactions between drug and polymers provided in this thesis can provide an alternative to the time-consuming trial and error approach in experimental formulation studies. Based on the studies provided in this thesis we could extend this approach to other block copolymer and drug systems and choose the most suitable polymer candidates among a library of the synthetic polymers which already have been tested for drug loading capacity. In other words, we can discuss which polymer for a specific anti-cancer drug results in slower drug release to the target tissue based on the effect of inter-molecular interaction analysis on drug diffusion.

In the future, one could study polymeric micelles encapsulating anticancer hydrophobic drug molecules in the presence of much higher water concentrations. In such systems, we would have tens of drug molecules, tens of polymer chains and tens of thousands of water molecules which would result in system sizes much larger than the ones we have studied and explained in this thesis. Regarding the simulation of such systems, if we consider a coarse-grain model and treat several molecules as

one particle, an accurate force field which could describe the intra-molecular interactions, non-bonded and bonded potentials should be applied.

It would be interesting to study block copolymer micelles above their critical micelle concentrations (CMC) in water solutions. . When micelles are injected into the blood stream, they are subjected to perfect sink conditions and if they are kinetically stable, they could avoid dissociation in the blood stream for longer times. In this case, they would have a better chance to reach tumor sites without losing drug concentrations in the blood stream.

As mentioned in the introduction of this thesis, the thermodynamic stability of a polymeric micelle could be modified by changing the shell or core dimensions. Large molecular dimensions of the hydrophobic micelle core could lead to a higher tendency for aggregation in aqueous solutions and could in turn increase the thermodynamic stability of a polymeric micelle. The larger the hydrophobic core is, the stronger inter- molecular interactions in the core of polymer micelles would be which would result in much slower dissociation rates in water solutions. Therefore, larger hydrophobic core dimensions would also result in kinetic stability of the micelle.

Once the micelle is exposed to water two different degradation kinetics could occur. Bulk degradation and surface degradation. The PEO-*b*-PCL polymeric micelle core is made of crystalline PCL blocks while the corona is mainly hydrophilic and amorphous. When such micelles are present in biological systems, water molecules

diffuse much faster into the corona (shell) in comparison to hydrophobic drug molecules that are entrapped in the hydrophobic core. Depending on the distribution of the hydrolysing groups in the PEO block two types of degradation processes could take place:

1. The presence of Ester groups (hydrolysing groups) at the surface of the micelle results in surface degradation. Since the surface of the micelle is saturated with water molecules the hydrolysis reaction taking place on the surface of the micelle does not depend on the concentration of water molecules. In this type of degradation, surface erosion occurs before water diffuses completely into the micelle core. Water diffusion into the micelle core could affect and change the PCL crystalline structure which in turn could affect and facilitate drug diffusion out of the micelle core.
2. Bulk degradation occurs if water diffusion is much faster than polymer degradation rate. In tis case, the hydrolysis reaction depends on the concentration of water. Wherever enough water concentration is provided for hydrolysis reactions inside the micelle volume, degradation occurs. In this case degradation can take up to several weeks. This type of degradation could result in a heterogeneous micelle due to the existing amorphous and crystalline structures of PEO and PCL. The crystalline PCL degrades much slower than the amorphous phase. The micelle mass change during degradation could affect water and drug diffusivities in the micelle which would result in diffusion changes as a function of time. Understanding the

mechanism of drug release from polymeric micelles would enable us to better simulate such drug delivery systems.

One could study the kinetic and thermodynamic stability of polymer micelle drug delivery systems as a function of many parameters such as the dimensions of the hydrophobic or hydrophilic core and the space distribution of the hydrolysing groups (hydroxyl groups) in the hydrophilic shell of polymer micelles using molecular dynamics simulations. In such systems the effect of hydrolysing group distribution in the corona on drug and water diffusion coefficient would be very interesting.

It would also be interesting to study the effect of the pH in the aqueous solution surrounding the polymeric micelle on water and drug diffusion in the micelle. As mentioned before, lower pH in the aqueous environment could trigger micelle degradation and result in faster degradation and drug release kinetics.

Another interesting study would be combining the thermodynamic information about the polymer-drug-water systems in micelle environments with the kinetic data (self-diffusion coefficients of drug molecule in polymer micelles) in order to measure the diffusion of drug molecules in drug-polymer-water systems. The mentioned diffusion would also be a function of concentration gradient or the chemical potential gradient in the system under isobaric-isothermal conditions. The kinetics of drug release from degrading polymeric micelles as discussed in chapter 3 were only valid for micron-sized systems and as a result cannot be used for bulk or surface degrading polymeric micelles. Therefore, obtaining the concentration profile for anticancer

hydrophobic drugs in such systems is not possible using the current drug release models. For the purpose of estimating water and drug diffusivities in ternary systems, other thermodynamic parameters should be studied in order to determine and measure the diffusion coefficients of drug and water molecules in a ternary system (water+drug+polymer).Another challenge in this study would be constructing the structure files which give us information about the conformation of water, drug and polymer atoms along with their charges, bonded and non-bonded information between the atoms and molecules in the system. Finding an accurate force field that could predict the total potential of the system correctly could also be challenging task.

In order to obtain a density of the system that is very close to the experimental density of the polymeric micelle, one might need to modify the existing force fields in literature. In most cases the non-bonded potentials are very important and can affect the accuracy of the obtained density of the system after simulations. Therefore one might need to change the parameters in the Lenard-jones (LJ) potential term in order to achieve an accurate density and force field that could predict the system correctly. This step would involve several iterations to correctly predict the micelle and could take up to several months.

Once this stage is done, the thermodynamic and kinetic information of the systems could be obtained relatively quickly avoiding the long experimental kinetic studies. In addition, a molecular level understanding could be provided very quickly by molecular dynamics simulations of such systems.

References

[1] Chen, X., Bao, J., Guo, J., Ding, Q., Lu, J., Huang, M., Wang, Y. Biological activities and potential molecular targets of cucurbitacins: a focus on cancer. Anticancer Drugs. 2012, (23) 777–87.

[2] Lang, K.L., Silva, I.T., Zimmermann, L.A., Machado, V.R., Teixeira, M.R., Lapuh, M.I., Galetti, M.A., Palermo, J.A., Cabrera, G.M., Bernardes, L.S., Simões, C.M., Schenkel, E.P., Caro, M.S., Durán, F.J. Synthesis and cytotoxic activity evaluation of dihydrocucurbitacin B and cucurbitacin B derivatives. Bioorg Med Chem. 2012, (20) 3016–30.

[3] Ríos, J.L., Andújar, I., Escandell, J.M., Giner, R.M., Recio, M.C. Cucurbitacins as inducers of cell death and a rich source of potential anticancer compounds. Curr Pharm Des. 2012, (18) 1663–76.

[4] Pan, L., Yong, Y,. Deng, Y., Lantvit, D.D., Ninh, T.N., Chai, H., Carcache de Blanco, E.J., Soejarto, D.D., Swanson, S.M., Kinghorn, A.D. Isolation, structure

elucidation, and biological evaluation of 16, 23-epoxycucurbitacin constituents from Eleaocarpus chinensis. J Nat Prod. 2012, (75) 444–52.

[5] DeVita, V.T.Jr., Chu, E., Lawrence, T.S., Rosenberg, S.A., DePinho, R.A., Weinberg, R.A. Hellman, and Rosenberg's Cancer: Principles and Practice of Oncology. 9th edition. Lippincott Williams & Wilkins, NY, Part III: Principles of cancer treatment: Medical Oncology, 2011.

[6] Gry, J., Søborg, I., Andersson, H.C. Cucurbitacins in plant food. Tema Nord Nordic Council of Ministers, Ekspressen Tryk & Kopicenter, Copenhagen. Identity physical and chemical properties and analytical methods, 2006, 17–22.

[7] Aliabadi, H.M., Lavasanifar, A. Polymeric micelles for drug delivery. Expert Opin Drug Deliv. 2006, (3) 139–62.

[8] Kwon, G.K., Forrest, M.L. Amphiphilic block copolymer micelles for nanoscale drug delivery. Drug Dev Res. 2006, (67) 15–22.

[9] Matsumura, Y., Maeda, H. A new concept for macromolecular therapeutics in cancer chemotherapy: mechanism of tumoritropic accumulation of proteins and the antitumor agent smancs. Cancer Res. (1986) 46(12 Pt 1):6387-6392.

[10] Wakebayashi, D., Nishiyama, N., Yamasaki, Y. Lactose-conjugated polyion complex micelles incorporating plasmid DNA as a targetable gene vector system: their preparation and gene transfecting efficiency against cultured HepG2 cells. J. Control. Release (2004)95(3):653-664.

[11] Nagasaki, Y., Yasugi, K., Yamamoto, Y., Harada, A., Kataoka, K. Sugar-installed block copolymer micelles: Their preparation and specific interaction with lectin molecules. Biomacromolecules (2001) 2(4):1067-1070.

[12] Yamamoto, Y., Nagasaki, Y., Kato, M., Kataoka, K. Surface charge modulation of poly(ethylene glycol)- poly(D,L-lactide) block copolymer micelles: conjugation of charged peptides. Colloids Surf. B. Biointerfaces (1999) 16(1-4):135-146.

[13] Zhang, X., Burt, H.M., Von hoff, D. An investigation of the antitumour activity and bio distribution of polymeric micellar paclitaxel. Cancer Chemother. Pharmacol. (1997) 40(1):81-86.

[14] Zhang, X., Jackson, J.K., Burt, H.M. Development of amphiphilic diblock copolymers as micellar carriers of taxol. Int. J. Pharm. (1996) 132(1-2):195-206.

[15] Zhang, X., Burt, H.M., Mangold, G. Anti-tumor efficacy and bio distribution of intravenous polymeric micellar paclitaxel. Anticancer Drugs (1997) 8(7):696-701.

[16] Leung, S.Y., Jackson, J., Miyake, H., Burt, H., Gleave, M.E. Polymeric micellar paclitaxel phosphorylates Bcl-2 and induces apoptotic regression of androgen independent LNCaP prostate tumors. Prostate (2000) 44(2):156-163.

[17] Piskin, E., Kaitian, X., Denkbas, E.B., Kucukyavuz, Z. Novel PDLLA/PEG copolymer micelles as drug carriers.J. Biomater. Sci. Polym. Ed. (1995) 7(4):359-373.

[18] Yokoyama, M., Okano, T., Sakurai, Y., Kataoka, K. Improved synthesis of adriamycin-conjugated poly(ethylene oxide)-poly(aspartic acid) block copolymer and formation of unimodal micellar structure with controlled amount of physically entrapped adriamycin. J. Control. Release (1994) 32:269-277.

[19] Lavasanifar A., Samuel, J., Kwon, G.S. The effect of fatty acid substitution on the in vitro release of amphotericin B from micelles composed of poly(ethylene oxide)-block-poly(N-hexyl stearate-L-aspartamide). J. Control. Release (2002) 79(1-3):165-172.

[20] Nishiyama, N., Okazaki, S., Cabral, H. Novel cisplatin incorporated polymeric micelles can eradicate solid tumors in mice. Cancer Res. (2003) 63(24):8977-8983.

[21] Li, Y., Kwon, G.S. Methotrexate esters of poly(ethylene oxide)-block-poly(2-hydroxyethyl-L-aspartamide). Part I: Effects of the level of methotrexate conjugation on the stability of micelles and on drug release. Pharm. Res. (2000) 17(5):607-611.

[22] Nishiyama, N., Koizumi, F., Okazaki, S. Differential gene expression profile between PC-14 cells treated with free cisplatin and cisplatin incorporated polymeric micelles. Bioconjug. Chem. (2003) 14(2):449-457.

[23] Shuai, X., Merdan, T., Schaper, A.K., Xi, F., Kissel, T. Core-cross-linked polymeric micelles as paclitaxel carriers. Bioconjug. Chem. (2004) 15(3):441-448.

[24] Yuan, X., Harada, A., Yamasaki, Y., Kataoka, K. Stabilization of lysozyme incorporated polyion complex micelles by the omega-end derivatization of poly(ethylene glycol)-poly(alpha,betaaspartic acid) block copolymers with hydrophobic groups. Langmuir (2005)21(7):2668-2674.

[25] Matsuya, T., Tashiro, S., Hoshino, N. A core-shell-type fluorescent nanosphere possessing reactive poly(ethylene glycol) tethered chains on the surface for zeptomole detection of protein in time-resolved fluorometric immunoassay.Anal. Chem. (2003) 75(22):6124-6132.

[26] Lee, J., Cho, E.C., Cho, K. Incorporation and release behavior of hydrophobic drug in functionalized poly(D,L lactide)-blockpoly(ethylene oxide) micelles. J. Control.Release (2004) 94(2-3):323-335.

[27] Rapoport, N. Stabilization and activation of pluronic micelles for tumortargeted drug delivery. Colloids Surf. B. Biointerfaces (1999) 16(1-4):93-111.

[28] Kwon, G.S., Suwa, S. Enhanced tumor accumulation and prolonged circulation times for micelle-forming poly(ethylene oxide-aspartate) block copolymer-adriamycin conjugates. J. Control. Release (1994) 29:17-23.

[29] Yokoyama, M., Miyauchi, M., Yamada, N. Characterization and anticancer activity of the micelle-forming polymeric anticancer drug adriamycinconjugated

poly(ethylene glycol)- poly(aspartic acid) block copolymer. Cancer. Res. (1990) 50(6):1693-1700.

[30] Yokoyama, M., Okano, T., Sakurai, Y. Toxicity and antitumor activity against solid tumors of micelle-forming polymeric anticancer drug and its extremely long circulation in blood. Cancer Res. (1991) 51(12):3229-3236.

[31] Lee, J., Cho, E.C., Cho, K. Incorporation and release behavior of hydrophobic drug in functionalized poly(D,L lactide)-blockpoly(ethylene oxide) micelles. J. Control. Release (2004) 94(2-3):323-335.

[32] Yuan, X., Harada, A., Yamasaki, Y., Kataoka, K. Stabilization of lysozyme incorporated polyion complex micelles by the omega-end derivatization of poly(ethylene glycol)-poly(alpha,betaaspartic acid) block copolymers with hydrophobic groups. Langmuir (2005)21(7):2668-2674.

[33] Yokoyama, M., Satoh, A., Sakurai, Y. Incorporation of water-insoluble anticancer drug into polymeric micelles and control of their particle size. J. Control. Release (1998) 55(2-3):219-229.

[34] Nakanishi, T., Fukushima, S., Okamoto, K. Development of the polymer micelle carrier system for doxorubicin. J. Control. Release (2001) 74(1-3):295-302.

[35] Kakizawa, Y., Harada, A., Kataoka, K. Glutathione-sensitive stabilization of block copolymer micelles composed of antisense DNA and thiolated poly(ethylene

glycol)-block-poly(L-lysine): a potential carrier for systemic delivery of antisense DNA. Biomacromolecules (2001) 2(2):491-497.

[36] Gao, T., Uludag, H. Effect of molecular weight of thermoreversible polymer on in vivo retention of rhBMP-2. J. Biomed. Mater. Res. (2001) 57(1):92-100.

[37] Kang, N., Perron, M.E., Prud'homme, R.E. Stereocomplex block copolymer micelles: core-shell nanostructures with enhanced stability. Nano Letters (2005) 5(2):315-319.

[38] Onyuksel, H., Ikezaki, H., Patel, M., Gao, X.P., Rubinstein, I. A novel formulation of VIP in sterically stabilized micelles amplifies vasodilation in vivo. Pharm. Res. (1999) 16(1):155-160.

[39] Gandhi, S., Tsueshita, T., Onyuksel, H., Chandiwala, R., Rubinstein, I. Interactions of human secretin with sterically stabilized phospholipid micelles amplify peptide induced vasodilation in vivo. Peptides (2002) 23(8):1433-1439.

[40] Rubinstein, I., Ashok, B., Tsueshita, T., Onyuksel, H. All DVIP mitigates vasodilation elicited by L-VIP, micellar L-VIP and micellar PACAP1-38, but not PACAP1-38, in vivo. Peptides (2005) 26(3):509-515.

[41] Torchilin, Y.P., Lukyanov, A.N., Gao, Z., papahadjopoulos-sternberg, B. Immuno micelles: targeted pharmaceutical carriers for poorly soluble drugs. Proc. Natl Acad. Sci. USA (2003) 100(10):6039-6044.

[42] Wakebayashi, D., Nishiyama, N., Yamasaki, Y. Lactose-conjugated polyion complex micelles incorporating plasmid DNA as a targetable gene vector system: their preparation and gene transfecting efficiency against cultured HepG2 cells. J. Control. Release (2004) 95(3):653-664.

[43] Oishi, M., Nagatsugi, F., Sasaki, S., Nagasaki, Y., Kataoka, K. Smart polyion complex micelles for targeted intracellular delivery of PEGylated antisense oligonucleotides containing acid-labile linkages. Chembiochem. (2005) 6(4):718-725.

[44] Dufresne, M.H., Gauthier, M.A, Leroux, J.C. Thiol-functionalized polymeric micelles: From molecular recognition to improved mucoadhesion. Bioconjug. Chem. (2005) 16(4):1027-1033.

[45] Vinogradov, S., Batrakova, E., Li, S., Kabanov, A. Polyion complex micelles with protein-modified corona for receptormediated delivery of oligonucleotides into cells. Bioconjug. Chem. (1999) 10(5):851-860.

[46] Oishi, M., Nagasaki, Y., Itaka, K., Nishiyama, N., Kataoka, K. Lactosylated (ethylene glycol)-siRNA conjugate through acid-labile betathiopropionate linkage to construct pH sensitive polyion complex micelles achieving enhanced gene silencing in hepatoma cells. J. Am. Chem. Soc. (2005) 127(6):1624-1625.

[47] Jule, E., Nagasaki, Y., Kataoka, K. Lactose-installed poly(ethylene glycol)-poly(D,L-lactide) block copolymer micelles exhibit fast-rate binding and high

affinity toward a protein bed simulating a cell surface. A surface plasmon resonance study. Bioconjug. Chem. (2003) 14(1):177-186.

[48] Francis, M.F., Piredda, M., Winnik, F.M. Solubilization of poorly water soluble drugs in micelles of hydrophobically modified hydroxypropylcellulose copolymers. J. Control. Release (2003) 93(1):59-68.

[49] Francis, M.F., Lavoie, L., Winnik, F.M., Leroux, J.C. Solubilization of cyclosporin A in dextran-g-polyethylene glycol alkyl ether polymeric micelles. Eur. J. Pharm. Biopharm. (2003) 56(3):337-346.

[50] Francis, M.F., Cristea, M., Yang, Y., Winnik, F.M. Engineering polysaccharide based polymeric micelles to enhance permeability of cyclosporin A across Caco-2 cells. Pharm. Res. (2005) 22(2):209-219.

[51] Lee, E.S., Na, K., Bae, Y.H. Polymeric micelle for tumor pH and folate-mediated targeting. J. Control. Release (2003) 91(1-2):103-113.

[52] Taillefer, J., Jones, M.C., Brasseur, N., Van lier, J.E., Leroux, J.C. Preparation and characterization of pH-responsive polymeric micelles for the delivery of photosensitizing anticancer drugs. J. Pharm. Sci. (2000) 89(1):52-62.

[53] Jones, M.C., Ranger, M., Leroux, J.C. pH-sensitive unimolecular polymeric micelles: synthesis of a novel drug carrier. Bioconjug. Chem. (2003) 14(4):774-781.

[54] Allen, C., Maysinger, D., Eisenberg, A. Colloids Surf , B Biointerfaces, 1999, (16) 3-27.

[55] Liu, J., Xiao, Y., Allen, C. J. Pharm. Sci. 2004, (93) 132-143.

[56] Lavasanifar, A., Samuel, J., Kwon, G. S. Adv. Drug Deliv. Rev. 2002, (54) 169-190.

[57] Soo, P. L., Luo, L., Maysinger, D., Eisenberg, A. Langmuir 2002, (18) 9996-10004.

[58] Liu, H., Finn, N., Yates, M. Z. Langmuir 2005, (21) 379-385.

[59] Letchford, K., Liggins, R., Burt, H. J. Pharm. Sci. 2008, (97) 1179-1190.

[60] Mahmud, A., Patel, S., Molavi, O., Choi, P., Samuel, J., Lavasanifar, A. Biomacromolecules, 2009, (9) 471-478.

[61] Patel, S.K., Lavasanifar, A., Choi, P. Biomacromolecules. 2009, 10(9) 2584-91.

[62] Bruck, S.D. Problems and artifacts in the evaluation of polymeric materials for medical uses, Biomaterials, 1 (1980) 103-107.

[63] Chien,Y.W., Cabana, B.E., Mares, S.E. Novel drug delivery systems: fundamentals, developmental concepts, biomedical assessments,14 (1982) 633.

[64] Langer, R., Implantable controlled release systems, Pharm Ther, 1983, 21-35.

[65]Langer, R., Invited Review Polymeric Delivery Systems For Controlled Drug Release, Chemical Engineering Communications, 1980, (6) 1-48.

[66] Langer, R. Medical Applications of Controlled Release, CRC Press, FL, (2) 1986.

[67] Kwon,G.S. Polymeric micelles for delivery of poorly water soluble compounds, Drug Carrier Systems, 2003, (20) 357-403.

[68]Allen, M.D.,Eisenberg, A. Nano-engineering block copolymer aggregates for drug delivery, Colloids Surf., B Biointerfaces, 1999, (16) 3-27.

[69] Lavasanifar, A., Kwon, G.S. Poly(ethylene oxide)-block-poly(-amino acid) micelles for drug delivery, Adv Drug Deliv Rev. , 2002, (54) 169-190.

[70] Kataoka,H.A., Nagasaki,Y. Block copolymer micelles for drug delivery: design, characterization and biological significance, Adv Drug Deliv Rev. , 2001, (47) 113-131.

[71] Aerts, S.N.H., Meier, M.A.R., Staal, B.B.P., Rasa, M., Schubert, U.S. Detailed Characterization and Selected Micellar Drug Encapsulation Behavior, Macromolecules, 2005 (26) 1918-1924.

[72] Fick, A., On liquid diffusion, Membr Sci., 1995, (100) 33–38.

[73] Higuchi, T. Rate of release of medicaments from ointment bases containing drugs in suspensions, Pharm Sci., 1961, (50) 874-875.

[74] Higuchi, W.I., Roseman, T.J. Release of medroxyprogesterone acetate from a silicone polymer, Pharm Sci. , 1970, (59) 353–357.

[75] Roseman, T.J. Release of steroids from a silicone polymer, Pharm Sci. ,1972, (61) 46–50.

[76] Lee, P. Diffusional release of a solute from a polymeric matrix-approximate analytical solutions, Membr Sci. , 1980, (7) 255-275.

[77] Crank, J. The mathematics of diffusion, Oxford University Press Inc., New York, 1956, 1-32.

[78] D'Aurizio, P.S.E., Cerasa, L.S., Vacca, M., Brunetti, L., Orlando, G., Chiavaroli, A., Kok, R.J., Hennink, W.E., Di Stefano, A. Biodegradable microspheres loaded with an anti-parkinson prodrug: an in vivo pharmacokinetic study, Mol Pharmaceutics, 2011, 8(6) 2408–2415.

[79] Siepmann, J. Modeling of diffusion controlled drug delivery, Controlled Release, 2012, (161) 351-362.

[80] Sinclair, G.W., Peppas, N.A. Analysis of non-Fickian transport in polymers using simplified exponential expressions, Membr Sci., 1984, (17) 329-331.

[81] Alfrey, G.E., Lloyd, W.G. Diffusion in glassy polymers, Polym Sci C.,1966, (12) 249–261.

[82] Ritger, P.L., Peppas, N.A., A simple equation for decription of solute release:Fickian and non-Fickian release from non-swellable devices in the form of slabs spheres,cylinders or discs, Controlled Release, 1987, (5) 23-26.

[83] Beker, R. Controlled Release of Biologically Active Agents, John Wiley & Sons, New York, (2) 1987.

[84] Lu, W.C.Z., Hamman, J.H. Chitosan-polycarbophil interpolyelectrolyte complex as a matrix former for controlled release of poorly water-soluble drugs I in vitro evaluation, Drug Development and Industrial Pharmacy, 2010, 36(5) 539-546.

[85] Peppas, N.A. Analysis of Fickian and non-Fickian drug release from polymers, Pharm Acta Helv, (60) 1985.

[86] Lu, W.C.Z., Hamman, J.H. Chitosan-polycarbophil interpolyelectrolyte complex as a matrix former for controlled release of poorly water-soluble drugs I: in vitro evaluation, Drug Development and Industrial Pharmacy, 2010, 36(5) 539-546.

[87] Lee, P.I. Diffusional release of a solute from a polymeric matrix—approximate analytical solutions, Membr Sci., 1980 (7) 255–275.

[88] Lee, P.I. Interpretation of drug-release kinetics from hydrogel matrices in terms of time-dependent diffusion coefficients, American Chemical Society, Washington DC, 1987 (348) 71-83.

[89] Siepmann, J., Bodmeier, R., Peppas, N.A. HPMC-matrices for controlled drug delivery: a new model combining diff usion, swelling and dissolution mechanisms and predicting the release kinetics, Pharm Res., 1999 (16) 1748–1756.

[90] Siepmann, J., Sriwongjanya, M., Peppas, N.A., Bodmeier, R. A new model describing the swelling and drug release kinetics from hydroxypropyl methylcellulose tablets, Pharm Sci., 1999, (88) 65–72.

[91] Siepmann, J. Hydrophilic matrices for controlled drug delivery: an improved mathematical model to predict the resulting drug release kinetics (the "sequential layer" model), Pharm Res., 2000 (17) 1290–1298.

[92] Siepmann, J., Peppas, N.A. Understanding and predicting drug delivery from hydrophilic matrix tablets using the "sequential layer" model, Pharm Res., 2002, (19) 306–314.

[93] Narasimhan, B., Peppas, N.A. On the importance of chain reptation in models of dissolution of glassy polymers, Macromolecules, 1996 (29) 3283–3291.

[94] Siepmann, J. Modeling of drug release from delivery systems based on hydroxypropyl methylcellulose (HPMC), Adv Drug Del Rev., 2001,(48) 139–157.

[95] Narasimhan, B. Mathematical models describing polymer dissolution: consequences for drug delivery, Adv Drug Deliv Rev., 2001, (48) 195–210.

[96] Hopfenberg. H.B, Controlled release from erodible slabs, cylinders, and spheres, American Chemical Society, Washington DC, ACS Symposium series 33, 1976.

[97] Panomsuk.S.P., Koizumi,T. Release of medicaments from spherical matrices containing drug in suspension: theoritical aspects, Int J Pharm., 1995,(116) 45–49.

[98] Himmelstein, K.J., Joshi, A. Dynamics of controlled release from bioerodible matrices, Controlled Release, 1991, (15) 95-104.

[99] Himmelstein, K.J., Thombre, A.G. A simultaneous transport-reaction model for controlled drug delivery from catalyzed bioerodible polymer matrices, AICHE., 1985, (31) 759-766.

[100] Thombre, A.G. Theoritical aspects of polymer biodegradation: mathematical modeling of drug release and acid-catalyzed poly(ortho-ester)biodegradation, Vert, M., Feijen, J., Albertsson, A., Scott, G., Cheillini, E. Biodegradable polymers and plastics, Redwood Press, 1992, 214-228.

[101] Lederc, B., Charlier, A., Couarraze, G. Release of mifepristone from biodegradable matrices: experimental and theoretical evaluations, Int J Pharm., 2000, (200) 115–120.

[102] Baker, R.W., Heller, J. Theory and practice of controlled drug delivery from bioerodible polymers, R.W.Baker, Controlled release of bioactive materials, Academic Press, New York, 1980 1-18.

[103] Frank, A. Factors affecting the degradation and drug-release mechanism of poly (lactic acid) and poly [(lactic acid)-co-(glycolic acid)], Polym Int., 2005, (54) 36–46.

[104] Shen, Z.R., Zhu, J.H., Wu, L.T., Yang, S.L. In vitro degradation of polylactide and poly (lactide-co-glycolide) microspheres, Appl Polym Sci., 1991, (43) 2099–2106.

[105] Kim, S.Y., Kim, J.H. Drug-release kinetics of MPEG/PLLA block copolymer micelles with different PLLA block lengths, Appl Polym Sci., 2001, (82) 2599-2605.

[106] Mirzazadeh, F.S., Khodaverdi, E., Mohajeri, S.A., Ganji, F., Zohuri, G., Hadizadeh, F. Preparation and investigation of sustained drug delivery systems using an injectable, thermosensitive, in situ forming hydrogel composed of PLGA–PEG–PLGA, Pharm SciTech., 2012, (13) 590-600.

[107] Wang, S., Sutton, D., Nasongkla, N., Gao, J., Dormidontova, E.E. Doxorubicin and b-lapachone release and interaction with micellar core materials: experiment and modeling, Experimental Biology and Medicine, 2007, (232), 1090-1099.

[108] Allen, M. P., Tildesly, D. J. Computer Simulation of Liquids, Oxford University Press, New York, 1987.

[109] Frenkel, D., Smit, B. Understanding Molecular Simulation, Academic Press, New York, 2002.

[110] Lin, J., Zhu, J., Chen, T., Lin, S., Cai, C., Zhang, L., Zhuang, Y., Wang, X., Drug releasing behavior of hybrid micelles containing polypeptide triblock copolymer. , J. Biomaterials, 2009, (30) 108-117

[111] Guo, X.D., Tan, J.P.K., Kim, S.H., Zhang, L.J., Zhang, Y., Hedrick, J. H., Yang, Y.Y., Qian, Y., Computational studies on self-assembled paclitaxel structures: Templates for hierarchical block copolymer assemblies and sustained drug release. , J. Biomaterials, 2009, (30) 6556-6563.

[112] Shelley, J.C.S., Reeder, M. Y., Bandyopadhyay, R. C., Klein, M. L. J. Phys. Chem., (105) 2001.

[113] Nielsen, S.O., Klein, M. L. In Bridging time scales: Molecular simulations for the next decade, Berlin, Germany, 2002.

[114] Nielsen, S.O., Lopez. C.F., Srinivas, G., Klein, M. L. A coarse-grain model for n-alkanes parameterized from surface tension data. J. Chem. Phys., 119 (2003).

[115] Goetz, R., Lipowsky, R. Computer simulations of bilayer membranes: Self-assembly and interfacial tension. J. Chem. Phys., 1998, (108) 7397-7409.

[116] Berhane, N.H., Nyquist, C., Haghighi, K., Corvalan, C., Keshavarzian, A., Campanella, O., Rickus, J., Farhadi, A. A multi-scale stochastic drug release model for polymer-coated targeted drug delivery systems, Journal of Controlled Release, 2006, (110) 314-322.

[117] Holy, C.E., Davies, J.E., Shoichet, M.S. In vitro degradation of a novel poly(lactide-co-glycolide) 75/25 foam, Biomaterials, 1999, (20) 1177–1185.

[118] Encyclopedia of biopharmaceutical statistics, Informa Health Care, New York, 2003.

[119] Dutta, R.C., Rai, B. Molecular Dynamics Study of Drug Diffusion In Hydrogels : Effect of Cross-Linking, in: AICHE, 2011.

[120] Allen, M. P., Tildesley, D. J. Computer Simulation of Liquids, Oxford, 1987.

[121] Chandler, D. Introduction to Modern Statistical Mechanics, Oxford, 1987.

[122] Mcquarrie, D. A. Statistical Mechanics, Harper & Row, New York, 1976.

[123] Frenkel, D., Smit, B. Understanding Molecular Simulation, Academic Press, 1996.

[124] Ermer, O. Calculations of molecular properties using force fields. Applications in organic chemistry. Structure and Bonding, 1976, (27) 161-211.

[125] Sun, H. Force field for computation of conformational energies, structures, and vibrational frequencies of aromatic polyesters. J. Comp. Chem., 1994, 15(7), 752-768.

[126] Sun, H. Ab initio calculations and force field development for computer simulation of poly silanes. Macromolecules, 1995, (28) 701-712.

[127] Sun, H. J. Computer simulations of poly (ethylene oxide): force field, PVT diagram and cyclization behavior. Phys. Chem. B, 1998, 102(3), 7338-7364.

[128] Rigby, D. Fluid density predictions using the COMPASS force field. Fluid Phase Equilib, 2004, 217(1), 77-87.

[129] Wilson, E. B., Decius, J. C., Cross, P. C. DNA topoisomerases: enzymes that catalyse the concerted breaking and rejoining of DNA back bone bonds, in Molecular Genetics. Molecular Vibrations, Dover, New York, 1980.

[130] Waldman, M., Hagler, A. T. J. New combining rules for rare gas van der Waals parameters. Comp. Chem., 1993, (14) 1077-1084.

[131] Verlet, L. Computer experiments on classical fluids. I. Thermodynamical properties of Lennard-Jones molecules. Phys. Rev., 1967, (159) 98-103.

[132] Andersen, H.C. Molecular dynamics simulations at constant pressure and/or temperature. Journal of Chemical Physics, 1980, (72) 2384-2393.

[133] Nose, S. J. A unified formulation of the constant temperature molecular dynamics methods. Chem. Phys., 1984, (81) 511-519.

[134] Nose, S. A molecular dynamics method for simulations in the canonical ensemble. Molec. Phys., 1984, (52) 255-268.

[135] Hoover, W. G. Canonical dynamics: Equilibrium phase-space distributions. Phys. Rev. A, 1985, (31) 1695-1697.

[136] Parrinello, M., Rahman, A. Polymorphic transitions in single crystals: A new molecular dynamics method. J. Appl. Phys., 1981, (52) 7182–7190,.

[137] Ewald, P. Die Berechnung optischer und elektrostatischer Gitterpotentiale. Ann. Phys. 1921, (64) 253-287.

[138] Allen, C., Eisenberg, A., Maysinger, D. Nano-engineering block copolymer aggregates for drug Delivery. Colloids Surf., B. 1999, (16) 3-27.

[139] Lavasanifar, A., Samuel, J., Kwon, G. S. Poly(ethylene oxide)-*block*-poly(L-amino acid) micelles for drug delivery. Adv. Drug. Deliv. Rev., 2002, (54) 169-190.

[140] Mahmud, A., Patel, S. K., Molavi, O., Choi, P., Samuel J., Lavasanifar, A. Self-Associating Poly(ethylene oxide)-*b*-poly(r-cholesteryl carboxylate-*ε*-caprolactone) Block Copolymer for the Solubilization of STAT-3 Inhibitor Cucurbitacin I. Biomacromolecules, 2009, (10) 471-478.

[141] Jones, M. C., Leroux, J. C. Polymeric micelles - a new generation of colloidal drug carriers. Eur. J. Pharm. Biopharm., 1999, (48) 101-111.

[142] Patel, S. K., Lavasanifar A., Choi, P. Application of Molecular Dynamics Simulation To Predict the Compatability between Water-Insoluble Drugs and Self-Associating Poly(ethylene oxide)-*b*-poly(*ε*-caprolactone) Block Copolymers. Biomacromolecules, 2008, (9) 3014-3023.

[143] Lukyanov, A. N., Torchilin, V. P. Micelles from lipid derivatives of water-soluble polymers as delivery systems for poorly soluble drugs. Adv. Drug Deliv. Rev., 2004, (56) 1273-1289.

[144] Ahmed, F., Discher, D. E. Self-porating polymersomes of PEG-PLA and PEG-PCL: hydrolysis-triggered controlled release vesicles. J. Controlled Release, 2004, (96) 37-53.

[145] Djordjevic, J., Barch, M., Uhrich, K. E. Polymeric Micelles Based on Amphiphilic Scorpion-like Macromolecules: Novel Carriers for Water-Insoluble. Drugs. Pharm. Res., 2005, (22) 24-32.

[146] Bhattarai, N., Ramay, H. R., Gunn, J., Matsen, F. A., Zhang, M. Q. PEG-grafted chitosan as an injectable thermosensitive hydrogel for sustained protein release. J. Controlled Release, 2005, (103) 609-624.

[147] Zhang, J. X., Qiu, L. Y., Zhu, K. J., Jin, Y. Physicochemical characterization of polymeric micelles constructed from novel amphiphilic polyphosphazene with poly(*N* isopropylacrylamide) and ethyl 4-aminobenzoate as side groups. Colloids Surf., B, 2005, (43) 123-270.

[148] Wang, F., Bronich, T. K., Kabanov, A. V., Rauh, R. D., Roovers. J. Synthesis and Evaluation of a Star Amphiphilic Block Copolymer from Poly(E-caprolactone) and Poly(ethylene glycol) as a Potential Drug Delivery Carrier. Bioconjugate Chem., 2005, (16) 397-405.

[149] Vandamme, T. F., Brobeck, L. Poly(amidoamine) dendrimers as ophthalmic vehicles for ocular delivery of pilocarpine nitrate and tropicamide. J. Controlled Release, 2005, (102) 23-38.

[150] Bhadra, D., Yadav, A. K., Bhadra, S., Jain, N. K. Glycodendrimeric nanoparticulate carriers of primaquine phosphate for liver targeting. Int. J. Pharm., 2005, (295) 221-223.

[151] Gillies, E. R., Fre´chet, J. M. Dendrimers and dendritic polymers in drug delivery. Drug Discovery Today, 2005, (10) 35-43.

[152] Qiu, L. Y., Bae, Y. H. Polymer Architecture and Drug Delivery. Pharm. Res., 2006, (23) 1-30.

[153] Patel, S. K., Lavasanifar, A., Choi, P. Molecular dynamics study of the encapsulation capability of a PCL–PEO based block copolymer for hydrophobic drugs with different spatial distributions of hydrogen bond donors and acceptors. Biomaterials, 2010, (31) 1780-1786.

[154] Shim, W. S., Kim, S. W., Choi, E. K, Park, H. J., Kim, J. S., Lee, D. S. Novel pH Sensitive Block Copolymer Micelles for Solvent Free Drug Loading. Macromol. Biosci., 2006, (6) 179-86.

[155] Zhang, J., Wang, L. Q., Wang, H., Tu, K. Micellization Phenomena of Amphiphilic Block Copolymers Based on Methoxy Poly(ethylene glycol) and Either Crystalline or Amorphous Poly(caprolactone-b-lactide). Biomacromolecules, 2006, (7) 2492-2500.

[156] Glavas, L., Olsen, P., Odelius, K., Albertson, A. C. Achieving Micelle Control through Core Crystallinity. Biomacromolecules, 2013, (14) 4150-4156.

[157] Ahmed, I., Monzurul, A.R., Kibria, G., Muhammad, R.I., Jalil, R. *In vitro* Release Kinetics Study of Ambroxol Hydrochloride Pellets Developed by Extrusion Spheronization Technique Followed by Acrylic Polymer Coating. J. Pharm. Sci., 2008, (7) 75-81.

[158] Shoaib, M Harris, Tazeen, Jaweria, Merchant, Hamid A,Yousuf, Rabia Ismail. Evaluation of drug release kinetics from ibuprofen matrix tablets using HPMC. Pak. J. Pharm. Sci., 2006, (19) 119-124.

[159] Siepmann, J., Peppas, N. A., Modeling of drug release from delivery systems based on hydroxypropyl methylcellulose (HPMC). Adv. Drug Delivery Rev., 2001, (48) 139-157.

[160] Razavilar, N., Choi, P. In-vitro modelling of the release kinetics of micron and nano sized polymer drug carriers, Int. J. Drug Delivery, 2013, (5) 362-378.

[161] Stejkal, E. O., Tanner, J. E. Spin diffusion measurements: spin echoes in the presence of a time-dependent field gradient. J. Chem. Phys., 1965, (42) 288-292.

[162] Suter, U. W., Theodorou, D. N. Detailed molecular structure of a vinyl polymer glass. Macromolecules, 1985, (18) 1467-1478.

[163] Du, Z. X., Xu, J. T., Fan Z. Q. Micellar morphologies of poly-caprolactone-b-polyethylene oxide block copolymers in water with a crystalline core. Macromolecules, 2007, (40) 7633-7637.

[164] Berendsen, H. J. C., Postma, J. P. M., van Gunsteren, W. F., Hermans, J. Interaction models for water in relation to protein hydration, Intermol. Forces, B. Pullman, Ed., The Netherlands. 1981, 331-342.

[165] Nose, S. A molecular dynamics method for simulations in the canonical ensemble. Molecular Physics, 1984, (52) 255-268.

[166] Hoover, W. G. Canonical dynamics: equilibrium phase space ditributions. Phys. Rev., 1985, (31) 1965-1967.

[167] Rahman, A., Parrinello, M. Polymorphic transitions in single-crystals—a new molecular-dynamics method. J. Appl. Phys., 1981, (52) 7182-7190.

[168] Klein, M. L., Nose, S. Constant pressure molecular dynamics for molecular systems. Molecular Physics, 1983, (50) 1055-1076.

[169] Allen, M. P., Tildesley, D. J. Computer Simulation of Liquids, Clarendon Press, Oxford, 1989.

[170] Teraok, I. Polymer Solutions: An Introduction to Physical Properties, John Wily & Sons, Inc, 2002.

[171] Zhou, D., Choi, P. Molecular dynamics study of water diffusivity at low concentrations in non-swollen polyurethans. Polymer, 2012, (53) 3253-3260.

[172] Trotzig, C., Abrahmsen-Alami, S., Maurer, F. H. Structure and mobility in water plasticized poly (ethylene oxide). Polymer, 2007, (48) 3294-3305.

[173] Mirzazadeh, F. S., Khodaverdi, E., Mohajeri, S.A., Ganji, F., Zohuri, G., Hadizadeh, F. Preparation and Investigation of Sustained Drug Delivery Systems Using an Injectable, Thermosensitive, In Situ Forming Hydrogel Composed of PLGA–PEG–PLGA. AAPS PharmSciTech, 2012, (13) 590-600.

[174] Wang, S., Sutton, D., Nasongkla, N., Gao, J., Dormidontova, E. E. Doxorubicin and β-Lapachone Release and Interaction with Micellar Core Materials: Experiment and Modeling. Exp. Biol. Med., 2007, (232) 1090-1099.

[175]Cui, W., Li, X., Zhu, X., Yu, G., Zhou, S., Weng, J. Investigation of drug release and matrix degradation of electrospun poly (DL-lactide) fibers with paracetanol inoculation. Biomacromolecules. 2006, 7(5) 1623-1629.

[176] Xie, Z., Buschle-Diller, G. Electrospun poly(D, L)-lactide fibers for drug delivery: the influence of cosolvent and the mechanism of drug release, J. Appl. Polym. Sci. 2010, 115(1) 1-8.

[177] Zamani, M., Morshed, M., Varshosaz, J., Jannesari, M. Controlled release of metronidazole benzoate from poly-caprolactone electrospun nanofibers for periodontal diseases. Eur. J. Pharm. Biopharm. 2010, 75 (2) 179-185.

[178] Zeng, J., Aigner, A., Czubayko, F., Kissel, T., Wendorff, J. H., Greiner, A. Poly(vinyl alcohol) nanofibers by electrospinning as a protein delivery system and the retardation of enzyme release by additional polymer coatings. Biomacromolecules. 2005, 6(3) 1484-1488.

[179] Taepaiboon, P., Rungsardthong, U., Supaphol, P. Drug loaded electrospun mats of poly vinyl alcohol fibers and their release characteristics of four model drugs. Nanotechnology. 2006

(17) 2317-2329.

[180]Chew, S.Y., Wen, J., Yim, E. K. F., Leong. K. W. Sustained release of proteins from electrospun biodegradable fibers. Biomacromolecules. 2005, 6(4) 2017-2024.

[181] Zeng, j., Yang, l., Liang, Q., Zhang, X., Guan, H., Xu, X., Chen, X., Jin, X. Influence of the drug compatibility with polymer solution on the release kinetics of electrospun fibers formulation. J. Controlled Release. 2005**,** 105(1-2) 43-51.

[182] Yu, D., Shen, X., White, C., White, K., Zhu, L., Bligh, S.W. Oral fast-dissolving drug delivery membranes prepared from electrospun polyvinylpyrrolidone ultrafine fibers. Nanotechnology**.** 2009, 20(5) 1-9.

[183] Tsuji, H., Ikada, Y. Blends of aliphatic polyesters. II. Hydrolysis of solution-cast blends from poly (L-lactide) and poly (ε-caprolactone) in phosphate-buffered solution. J. Appl. Polym. Sci. 1998, 67(3) 405-415.

[184] Hglund, A., Hakkarainen, M., Albertsson, A. C. Degradation profile of poly caprolactone- the influence of macroscopic and macromolecular biomaterial design. J. Macromol. Sci. Part A. 2007, (44) 1041-1046.

[185] Kim, S. H., Tan, J. P., Nederberg, F., Fukushima, K., Colson, J., Yang, C., Nelson, A., Yang, Y. Y., Hedrick, J. L. Hydrogen bonding-enhanced micelle assemblies for drug delivery. Biomaterials. 2010, 31(31) 8063-8071.

[186] Yan, J., Ye, Z., Chen, M., Liu, Z., Xiao, Y., Zhang, Y., Zhou, Y., Tan, W., Lang, M. Fine tuning micellar core-forming block of poly(ethylene glycol)-block-poly(εcaprolactone) amphiphilic copolymers based on chemical modification for the solubilization and delivery of doxorubicin. Biomacromolecules. 2011, 12(7) 2562-2572.

[187] Wang, D., Su, Y., Jin, C., Zhu, B., Pang, Y., Zhu, L., Liu, J., Tu, C., Yan, D., Zhu, X. Supramolecular copolymer micelles based on the complementary multiple hydrogen bonds of nucleobases for drug delivery. Biomacromolecules. 2011, 12 (4) 1370-1379.

[188] Lee, J., Cho, E. C., Cho, K. Incorporation and release behavior of hydrophobic drug in functionalized poly(D,L-lactide)-block-poly(ethylene oxide) micelles. J. Controlled Release. 2004, 94(2-3) 323-335.

[189] Molavi, O., Ma, Z., Mahmud, A., Alshamsan, A., Samuel, J., Lai, R., Kwon, G. S., Lavasanifar, A. Development of a poly(D,L-lactic-co-glycolic acid) (PLGA) nanoparticle formulation of STAT3 inhibitor JSI-124: Implication for cancer immunotherapy A. Int. J. Pharm. 2008, 7(2) 364-374.

[190] Patel S. K., Lavasanifar, A., Choi, P. Application of molecular dynamics simulation to predict the compatability between water-insoluble drugs and self-associating poly(ethylene oxide)-b poly(epsilon-caprolactone) block copolymers. Biomacromolecules. 2008, 9(11) 3014-3023.

[191] Razavilar, N.; Choi, P. Molecular Dynamics Study of the Diffusivity of a Hydrophobic Drug Cucurbitacin B in Pseudo-poly(ethylene oxide-b-caprolactone) Micelle Environments. Langmuir. 2014, (30) 7798-7803.

[192] Suter, U. W., Theodorou, D.N. Atomistic modeling of mechanical properties of polymeric glasses. Macromolecules.1986, 19(1) 139-154.

[193] Patel, S. K.; Lavasanifar, A.; Choi, P. Roles of Nonpolar and Polar Intermolecular Interactions in the Improvement of the Drug Loading Capacity of PEO-b-PCL with Increasing PCL Content for Two Hydrophobic Cucurbitacin Drugs. Biomacromolecules. **2009,** 10(9), 2584-2591.

[194] Crank, J. The mathematics of diffusion, 2nd ed. Oxford: Clarendon Press, 1975.

[195] Fricke, H. A mathematical treatment of the electric conductivity and capacity of disperse systems, Phys Rev 1924, (24) 575-587.

[196] Mackie, J.S, Meares, P. The diffusion of electrolytes in a cation- exchange resin membrane, Proc. R. Soc. London A, 1955, (232) 498

[197] Ogston, A.G., Preston, B.N., Wells, J.D. On the transport of compact particles through solutions of chain-polymers, Proc. R. Soc. London A, 1973, (333) 297-316.

[198] Johansson, L., Elvingson, C., Lo¨froth, J.E. Diffusion and interactions in gels and solutions. 3. theoretical results on the obstruction effect, Macromolecules, 1991, (24) 6024-6029.

[199] Park, I.H., Johnson Jr, C.S, Gabriel, D.A. Probe diffusion in polyacrylamide gels as observed by means of holographic relaxation methods: Search for a universal equation. Macromolecules 1990, (23) 1548-1553.

[200] Rotstein, N.A., Lodge, T.P. Tracer diffusion of linear polystyrene in poly (vinyl methyl ether) gels. Macromolecules, 1992 (25) 1316-1325.

[201] Won, J., Lodge, T.P. Tracer diffusion of star-branched polystyrenes in poly (vinyl methyl ether) gels, J Polym Sci: Part B, 1993 (31) 1897-1907.

[202] Lofroth J.E, Elvingson C, Johansson L. Proc Int Symp Control Rel Bioact Mater 1991, 18, 146.

[203] Razavilar, N., Choi, P. Molecular Dynamics Study of the Diffusivity of a Hydrophobic Drug Cucurbitacin B in Pseudo-poly(ethylene oxide-b-caprolactone) Micelle Environments. Langmuir, 2014, (30) 7798-7803.

[204] Chi, S. C., Jun, H. W. Release rates of ketoprofen from poloxamer gels in a membraneless diffusion cell. J Pharm Sci, 1991, (80) 280–283.

[205] Emara, L.H. Thermodynamic of niclosamide diffusion from elastomeric matrices. Egyptian J. Pharm. Sci., 1994, (35) 663–673.

[206] Muranushi N., Nakajima Y. Mechanism for the inducement of the intestinal absorption of poorly absorbed drugs by mixed micelles. II. Effect of the incorporation of various lipids on the permeability of liposomal membranes. Int J Pharm, 1980, 4, 281–290.

[207] Brandt, W.W. Model calculation of the temperature dependence of small molecule diffusion in high polymers, 1959, (63) 1080–1058.

[208] Er,Y., Barnes, T.J., Fornasiero, D., Prestidge, C.A. The encapsulation and release of guanosine from PEGylated liposomes. Journal of Liposome Research, 2009, 19(1), 29–36.

[209] Razavila, N., Choi, P. Diffusivity of Cucurbitacin B in Water Swollen Poly(ethylene oxide-b-carpolactone) Matrix with Different PCL/PEO Weight Ratios. Molecular Pharmaceutics.

Appendix A: Velocity Autocorrelation Function

Let us consider a series of measurements of a quantity of a random nature at different times as depicted in Figure A1.

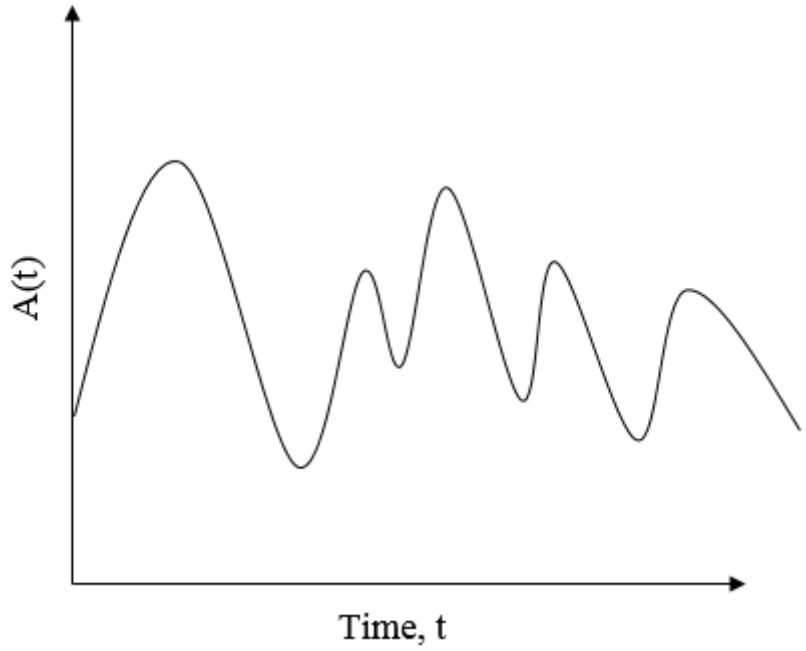

Figure A1 Fluctuation of property A as a function of time

For two measurements taken at times t' and t" that are close to each other, there are good chances that properties A(t') and A(t") have similar values which means that their values are correlated.

If two measurements taken at times t' and t" that are far apart, there is no relationship between values of properties A(t') and A(t") which means that the values are uncorrelated. According to the two scenarios mentioned here, the "level of correlation" plotted against time would start at some value and then decay to a low value.

If we shift the data by time t_{corr} and multiply the values in new data set to the values of the original data set, after averaging over the whole time range, we obtain a single number G (t_{corr}) Figure A2.

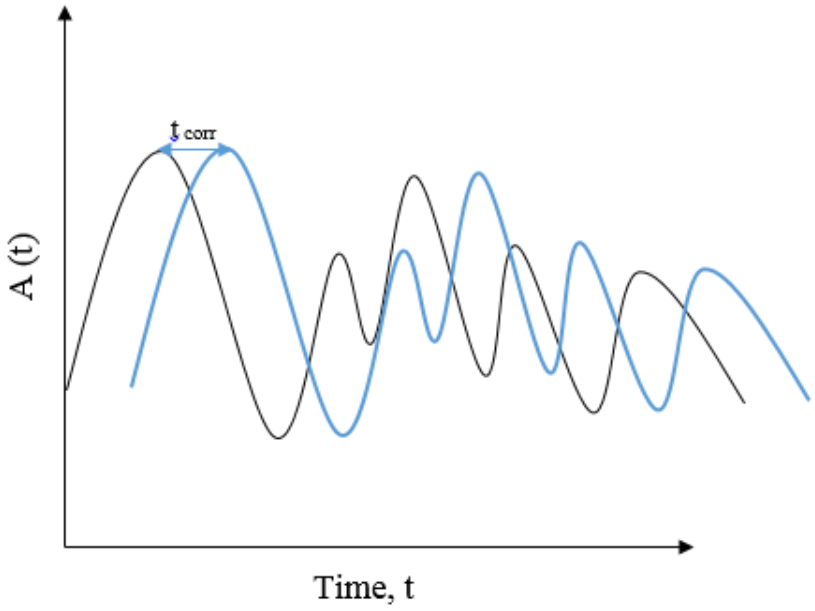

Figure A2 Curve of the fluctuation of property A is shifted by the correlation time

At small correlation times the peaks and troughs are aligned and we will obtain a big value from this operation. As we increase the correlation time value, the G (t_{corr}) declines to a constant value. The operation of multiplying two curves together and integrating them over the x-axis is called an overlap integral, since it gives a big value if the curves both have high and low values in the same places.

The overlap integral is also called the Auto Correlation Function where:

$$\boldsymbol{G(t_{corr}) = \langle A(t_0).A(t_0 + t_{corr})\rangle} \quad \text{(A-1)}$$

The value of the overlap integral is not a function of time (since we already integrated over time), this is function of the shift in time or correlation time.

For an ensemble of N particles we can calculate velocity auto correlation function is as the following:

$$\mathbf{G(\tau) = \langle \vec{v_i}(t_0).\vec{v_i}(t_0 + \tau)\rangle = \frac{1}{N}\sum_{i=1}^{N}\frac{1}{t_{max}}\sum_{t_0=1}^{N}\vec{v_i}(t_0).\vec{v_i}(t_0 + \tau)} \quad \text{(A-2)}$$

In the liquid phase atoms "lose memory" of their past within one/several periods of vibration. This "short memory" is reflected in the velocity autocorrelation function and therefore their auto correlation plots vs. time would decay much faster than the velocity auto correlation plots vs. time obtained for crystals or solid material.